nature chemistry

SUPPLEMENTARY INFORMATION

https://doi.org/10.1038/s41557-019-0337-3

In the format provided by the authors and unedited.

Electronic landscape of the P-cluster of nitrogenase as revealed through many-electron quantum wavefunction simulations

Zhendong Li*, Sheng Guo, Qiming Sun and Garnet Kin-Lic Chan*

Division of Chemistry and Chemical Engineering, California Institute of Technology, Pasadena, CA, USA. *e-mail: zhendongli2008@gmail.com; gkc1000@gmail.com

Electronic landscape of the P-cluster of nitrogenase as revealed through quantum many-electron wavefunction simulations

Zhendong Li[1*], Sheng Guo[1], Qiming Sun[1], Garnet Kin-Lic Chan[1*]
Division of Chemistry and Chemical Engineering, California Institute of Technology,
Pasadena, CA 91125, USA
*To whom correspondence should be addressed;
E-mail: zhendongli2008@gmail.com, gkc1000@gmail.com

Contents

1 Background on the electronic structure of the P-cluster

We briefly summarize some representative experimental and theoretical data on the electronic structure of the P-cluster. In the P^N ground-state, EPR and Mössbauer spectra are consistent with a diamagnetic (S=0) ground-state, with all ferrous irons[1]. The P^{OX} ground-state was first assigned to be paramagnetic with non-integer total spin due to an incorrect nuclearity assumption [2, 3], however, subsequent studies support a ground state with S=3 or S=4 [4]. The P^{1+} ground-state EPR spectrum has been associated with a mixed-spin system with S=1/2 and S=5/2 [5]. The sites of oxidation in P^{1+} and P^{OX} have not been established experimentally, but recent MCD measurements argued that in P^{1+}, the unpaired electron localizes to a single cubane based on similar spectral features of P^{1+} and the $[Fe_4S_4]^+$ cubane[6]. On the theoretical front, pioneering work by Mouesca et al. [7] tried to shed light on the spin-couplings in P^{OX} which cannot be directly accessed experimentally. They suggested that the ground-state most likely consists of a left cubane in an $S_L = 7/2$ state (cubane II in [7]), and a right cubane in an $S_R = 1/2$ state (cubane I), recoupling to an $S = 4$ state. However, this analysis used a simplified model where the ground state was assigned to a single spin-coupled configuration, and further assumed that P^{OX} was composed of two $[Fe_4S_4]^+$ cubanes, based on the low-resolution P-cluster structure available at the time[8, 9], now known to be far from the P^{OX} structure[10].

2 Computational details

2.1 Electronic models for P-clusters

Since a full QM solution of the Schrödinger equation for the entire P-cluster and protein is clearly not feasible, we need to simplify the problem. Constructing such a model requires making a structural model (i.e. choosing which atoms and residues to include) as well as an electronic model (choosing the basis set, active space, treatment of electron correlation, and

influence of geometry on the electronic structure). In this section we will be concerned with the approximations introduced in our electronic model (the structural model is discussed in more detail in Supplementary Sec. 2.2). We will try to estimate the error introduced by the simplifications in our electronic treatment, but necessarily such estimates can only be made with assumptions, which we highlight.

2.1.1 Basis set and geometry

To investigate the sensitivity of our results to basis set and geometry, we used broken-symmetry DFT (BS-DFT) as a proxy. Although we are eventually performing valence CAS DMRG calculations, the basis set requirement to converge valence CAS (and CASSCF) is typically more similar to that of mean-field methods[11] as such methods do not need to accurately model the correlation associated with the electron-electron cusp. Thus, we will assume that the impact of basis set and geometry on the relative energies of spin states is similar for BS-DFT and valence CAS DMRG. This assumption would be poor for charge-transfer excited states, which are sensitive to dynamic correlation, but these states do not appear in the low energy spectrum.

Supplementary Figure 1 displays the obtained relative energies (in kcal/mol) for different broken-symmetry spin isomers for P^{N} ($M_S = 0$ with 4 spin-up and 4 spin-down Fe ions, in total 70 BS configurations), P^{1+} ($M_S = 1/2$ with 4 spin-up and 4 spin-down Fe ions, in total 70 BS configurations), and P^{OX} ($M_S = 4$ with 5 spin-up and 3 spin-down Fe ions, in total 56 BS configurations) using ZORA/TPSSh-D3BJ[12, 13] with two different basis sets (def2-SVP and def2-TZVP[14]) and two different geometries (crystal geometries and optimized high-spin geometries with the positions of Fe and S relaxed at the ZORA/TPSSh-D3BJ/def2-SVP level) using the ORCA package[15]. The conductor like screening model (COSMO)[16] with a dielectric constant $\epsilon = 4.0$ was used in all these calculations to mimic the rest of the protein environment. We found that the effect of basis sets on relative energies is about 1-2 kcal/mol,

except in a few cases where the BS-DFT calculations with different basis sets converge to qualitatively different states, and thus unusually large differences (>15 kcal/mol) are observed. Similar findings were also obtained recently for the spin states of FeMoco[17], where the effect of basis set was also shown to be relatively small, up to 2.6 kcal/mol in relative energies, when going from def2-SV(P) to def2-TZVPD. While given unlimited computational resources, larger basis set calculations are naturally desirable, based on the above analysis we have chosen to carry out our calculations in the def2-SVP basis, to reduce the computational cost of integral transformations in this work.

As might be expected, geometries have a much larger impact on relative energies, since different geometries may favor different spin states. To estimate the impact, we considered the difference between energies computed at optimized high-spin geometries and the crystal geometry for different broken-symmetry spin isomers. The RMSD (root-mean-square deviation) between the crystal geometries and optimized geometries (see Supplementary Fig. 2) for the Fe and S atoms was 0.214Å for P^N, 0.244Å for P^{OX}, and 0.332Å for P^{1+}, respectively. As shown in Supplementary Fig. 1(a), the spin states of P^N with relative energies above 20kcal/mol are systematically further disfavored by about 10 kcal/mol at the optimized high-spin geometry, whereas those within 20 kcal/mol are less affected, with the difference in relative energies being about 5 kcal/mol. For P^{OX}, we observed that the trends of relative stabilities are quite parallel between the crystal and optimized structures, thus the relative energies are weakly affected. For both P^N and P^{OX}, the lowest spin isomers are found to be the same at two different geometries.

For P^{1+}, the relative energies at different geometries are much less correlated, due to the large structural difference between the crystal structure and optimized structure. As shown in Supplementary Fig. 2(b), at the optimized structure, the right cubane is clearly expanded compared with the very recently resolved crystal structure of P^{1+}[18]. Clearly, more thorough experimental and theoretical work is needed to resolve this structural discrepancy. In both cases,

however, the P^{1+} electronic landscape appears intermediate between that of P^{N} (with two deep wells) and that of P^{OX} (with a large amount of degeneracy). The primary difference is that at the crystal structure, P^{1+} looks closer to P^{OX}, while at the optimized P^{1+} geometry, it looks closer to P^{N}.

Together, the results indicate that the qualitative features of the low-energy landscape obtained with either the crystal or optimized geometry are representative for P^{N} and P^{OX}, while that of P^{1+} is more uncertain, although it can be viewed as intermediate between the two. In this work, we have chosen to use crystal structures for all P-clusters, although there is much scope for future work to examine the dependence of the electronic landscape on these geometric fluctuations.

2.1.2 Active space and dynamic correlation

The choices of active space and correlation treatment in this work are necessarily limited by what is feasible computationally. As we describe in detail in Supplementary Sec. 2.3, we carry out DMRG calculations in the full valence space of the Fe $3d$, S $3p$, and bonding ligand orbitals around each iron.

The remaining correlation errors can be then be divided into a few sources (i) the DMRG error in our chosen active space (due to finite bond dimension D) (ii) errors due to insufficiency of the active space (iii) errors due to lack of correlation outside of the active space (dynamic correlation). Error (i) is discussed in section 2.6 but is typically smaller than that arising from (ii) and (iii), due to the ability to perform extrapolation of DMRG energies to the complete bond dimension limit. Errors (ii) and (iii) are overlapping, since increasing the active space captures some of the dynamic correlation. We note that the performance of our chosen valence space has previously been benchmarked in our earlier work on FeS clusters [19].

Double d shells It is common in valence CAS calculations of smaller transition metal

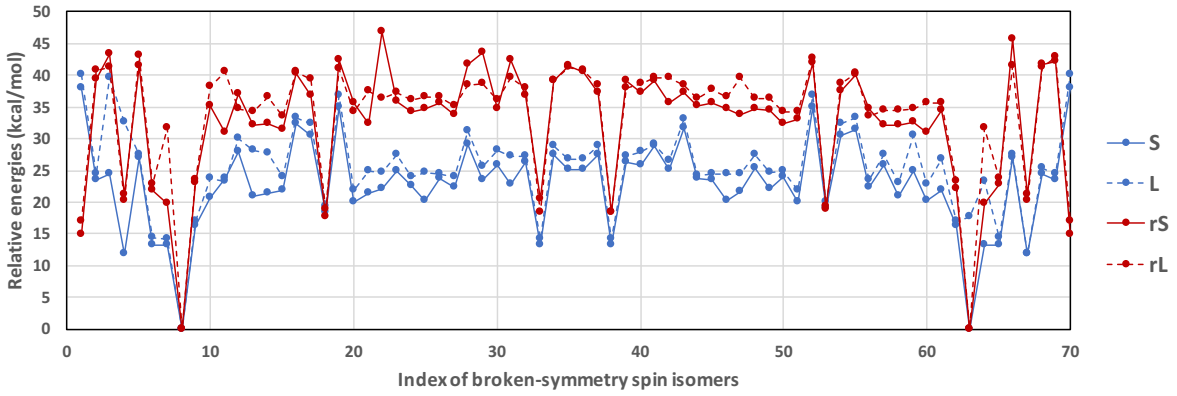

(a) P^N

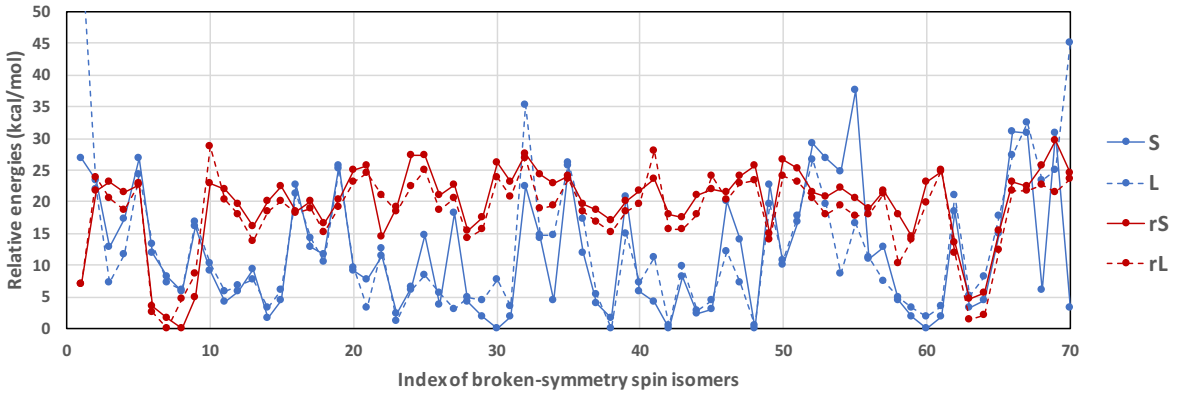

(b) P^{1+}

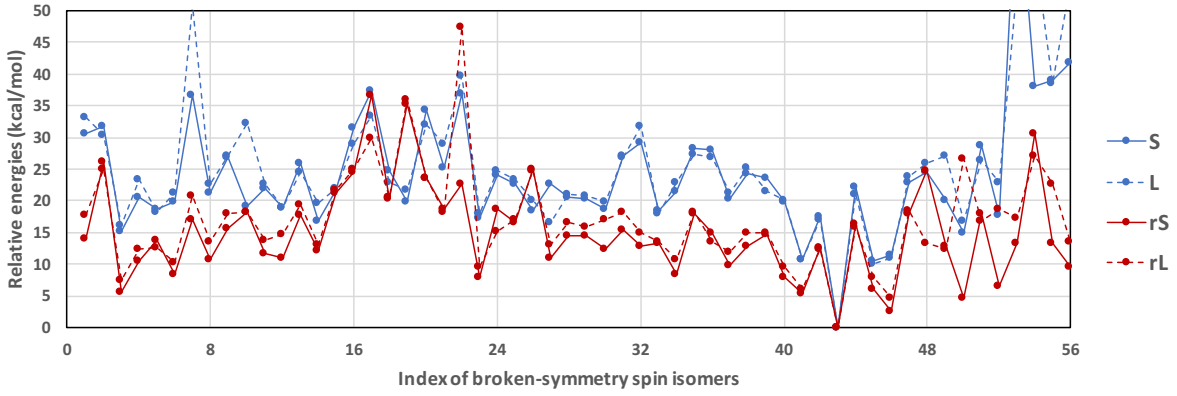

(c) P^{OX}

Supplementary Figure 1: Effect of basis set and geometry on computational models for P-clusters: (a) P^N; (b) P^{1+}; (c) P^{OX}. Relative energies (in kcal/mol) of different broken-symmetry spin isomers are shown for P^N ($M_S = 0$), P^{1+} ($M_S = 1/2$), and P^{OX} ($M_S = 4$). The legends are: 'S' - def2-SVP with crystal structures; 'L' - def2-TZVP with crystal structures; 'rS' - def2-SVP with optimized high-spin structures; 'rL'- def2-TZVP with optimized high-spin structures.

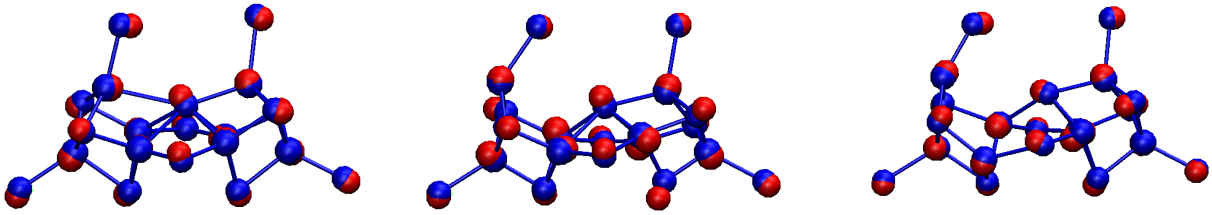

(a) P^N (RMSD=0.214Å) (b) P^{1+} (RMSD=0.332Å) (c) P^{OX} (RMSD=0.244Å)

Supplementary Figure 2: Comparison of crystal structures (blue) and optimized high-spin geometries (red) for P^N, P^{1+}, and P^{OX}.

complexes [20] to include a second (double) d-shell into the active space, which allows the d-electrons to relax. Including such a double d shell would increase our active space by an additional 40 orbitals which would be very challenging to handle. However, we note that in our previous experience [19] the need for such a double d-shell is reduced in bridged transition metal complexes (such as the FeS clusters) if one includes the bridging and terminal bonding ligand p orbitals into the active space. Qualitatively, this can be understood because diffuse $4d$-like metal orbitals can be mimicked by a linear combination of the ligand p orbitals. (Note that the discussion of necessity of the double d shell in conventional CAS is usually in the context of a single transition metal complex, where the ligand orbitals do not enter the active space). In CASSCF calculations we find that the $4d$ orbitals are often rotated out of the active space once the ligand p orbitals are included.

To verify the above arguments and to quantitatively estimate the effects of double d-shell and dynamic correlation beyond our chosen valence active space on the relative energies of spin states, we use the [2Fe-2S] cluster studied in our previous work[19] (since DMRG calculations of P-clusters including double d-shell and dynamical correlation effects are currently too expensive). We estimate the maximum effect of double d-shell correlations for P-clusters as roughly 4 times (since there are 4 times as many Fe pairs) the contribution of the double d-shell to the single-triplet (S-T) gap of the [2Fe(III,III)-2S] cluster (S-T gap of 0.94 kcal/mol

with CAS(30e,20o) versus 1.32 kcal/mol with CAS(30e,32o) at the DMRGCI/def2-SVP level, see Supplementary Table 4 of Ref. [19]). This gives an uncertainty in the energy difference of about 1.5 kcal/mol, although this is almost certainly an overestimate since the singlet-triplet transition in the P-cluster does not flip 4 times the number of spins as in the [2Fe-2S] cluster.

Dynamic correlation As a second estimate of dynamic correlation beyond our active space, we computed the S-T gap for the same [2Fe(III,III)-2S] model complex using DMRG-CI (0.68 kcal/mol) within the active space CAS(30e,20o) and DMRG-SC-NEVPT2 [21, 22] (0.97 kcal/mol) with dynamic correlation beyond the active space using a large triple-zeta basis set (TZP-DKH[23]), and again multiplied this difference by 4 to obtain an estimate of the uncertainty in the P-cluster of 1.2 kcal/mol. This estimate is similar to the number obtained above. Thus we believe a reasonable error bar for the uncertainty in energy differences arising from remaining untreated correlations (from the double d-shell and beyond) is ~ 1 kcal/mol. The inclusion of the dynamic correlation for [8Fe-7S] complexes remains a challenge for the state-of-the-art methodologies, although some economic treatments have been proposed recently[24].

2.1.3 Summary

In summary, while there is uncertainty in the precise relative energies of different states due to the truncations in our electronic model, this is unlikely to affect the structure of the low-energy landscape (for example, the states that appear within 10 kcal/mol of the ground state). Uncertainties in the relative energies of the spin states are less than 3 kcal/mol in most cases, coming from the uncertainties from the basis set and correlation treatments (ca. 2 kcal/mol) as well as that of the DMRG solutions (<0.8 kcal/mol, see the extrapolated results for relative energies in the following sections, except for the uncertainty of the energy difference between the lowest $S = 3$ and $S = 4$ states of P^{OX}, which is about 2.8 kcal/mol). Although in the present work, the electronic structure is discussed at the level of spin-free spin states, including

the spin-orbit coupling (SOC) may lead to a strong mixing of some very close-lying states in the oxidized P-clusters. However, the gross picture of the low-lying *energy* landscape is expected to be unchanged. Because SOC is relatively small for first-row transition metals and usually quenched in the compounds, and hence the size of splittings of energy levels may not be too large to alter the qualitative pictures of low-lying energy landscape. For instance, while the magnitude of SOC is on the order of 400 cm^{-1} in Fe atom[25], for the [2Fe-2S] complex its magnitude is on the order of 30 cm^{-1}[26].

Note that the relatively high accuracy achieved in energy differences stems in part from the fortunate lack of charge-transfer type excitations in this energy window. The largest factor controlling the relative energies of states is the geometry of the cluster. Nonetheless, generic features of the electronic landscape of P^N and P^{OX} appear to be the same at either the crystal structure or the nearby optimized structure, and while that of P^{1+} is more sensitive, the electronic features can be viewed as intermediate between P^N and P^{OX} at both geometries.

2.2 Structural models of P-clusters

The truncated structural models for the P-clusters were built from their respective crystal structures: P^N (PDB ID: 3MIN[10]), P^{OX} (PDB ID: 2MIN[10]), and P^{1+} (PDB ID: 6CDK[18]). The $[Fe_8S_7]$ core was augmented with the closest residues, and the resulting models contain about 100 atoms. The rest of the protein environment was mimicked using COSMO[16] with a dielectric constant $\epsilon = 4.0$. The positions of added hydrogen atoms were optimized at the ZORA/TPSSh-D3BJ/def2-SVP level[12, 13] within the solvation model using the ORCA package[15]. For the synthetic $[Fe_8S_7]$ complex ($[\{N(SiMe_3)_2\}\{SC(NMe_2)_2\}Fe_4S_3]_2(\mu_6\text{-}S)\{\mu\text{-}N(SiNMe_3)_2\}_2$), its coordinates were obtained from its crystal structure reported in Ref. [27].

For fixed geometries, unlike properties like redox potentials, we expect the relative energies of spin states to be less sensitive to the surroundings beyond the first solvation shell, since dif-

ferent spin states share very similar charge densities and the interactions with surroundings are mainly electrostatic in nature. This can be demonstrated by the insensitivity of the dielectric energy (see Supplementary Sec. (2.7)) with respect to the variation of the spin states. Similarly, the influence of electrostatics of the surroundings in FeMoco was found to be less than 1 kcal/mol on average for the relative energies of spin states[17]. However, it is important to note that the surroundings far away from the active center may affect the relative energies of spin states indirectly by affecting the geometry of the core. The sensitivity of our models and results with respect to the variation of the cluster geometry has been discussed in the previous section.

2.3 Construction of active spaces for iron-sulfur clusters

As described in the main text, we used DMRG to solve for the electronic structure of iron-sulfur clusters within the active space defined for each complex. The active space was chosen as the full valence space. At minimum, this includes the $3d_{\mathrm{Fe}}$ and $3p_{\mathrm{S}}$ orbitals for the [Fe_8S_7] core, which amounts to $8 \times 5 + 7 \times 3 = 61$ orbitals. The orbitals on the bridging S atom provide the exchange and superexchange pathways and also help provide dynamic correlation for the $3d_{\mathrm{Fe}}$ electrons, as mentioned in Supplementary Sec. 2.1. In addition, to provide a full ligand field for each iron in the correlated calculation, the bonding orbitals with other "terminal" ligands were also included in the active space. The remaining error due to the truncation to this active space is described in detail in Supplementary Sec. 2.1.

To improve convergence in DMRG, the active orbitals should be spatially local, while also preserving as much energetic locality as possible. To this end, we employed the following three-step split localization strategy to prepare the active orbitals for the DMRG calculations:

1. An unrestricted Kohn-Sham (UKS) calculation was carried out for the given complex in a *high-spin* state, with scalar relativistic effects taken into account by the spin-free exact two-component (sf-X2C) Hamiltonian[28, 29, 30]. The resulting total density ma-

trix $\mathbf{P}_\alpha + \mathbf{P}_\beta$ was used to produce the unrestricted natural orbitals (UNOs). The UNOs were further classified into "core", "active", and "virtual" UNOs based on the occupation numbers of UNOs, viz., any orbital with an occupation number in the range 0.05-1.95 was defined as active, while orbitals with occupation numbers above 1.95 (or below 0.05) were regarded as "core" (or "virtual").

2. To construct the active space with valence orbitals (e.g., $3d_{\mathrm{Fe}}$ and $3p_{\mathrm{S}}$), the Pipek-Mezey (PM) localization[31] was used to localize the "core" and "active" , respectively. For high-spin states of the P-cluster and its synthetic complex, the "virtual" spaces do not contain any valence orbitals, thus these are not be considered.

3. In addition to the full set of localized "active" orbitals, which are basically singly occupied $3d_{\mathrm{Fe}}$ orbitals, the final active orbitals were defined by further selecting the relevant localized "core" orbitals, which typically include the doubly occupied $3d_{\mathrm{Fe}}$ orbitals in Fe(II), the bonding orbitals to the irons, and the lone pairs of sulfur. This set of split-localized orbitals were further localized together to increase their locality, which can help to lower the bond dimension required in accurate DMRG calculations.

The resulting localized orbitals with well-defined $3d_{\mathrm{Fe}}$ character were later used in population analysis to analyze the local states of the irons. The specific computational details for each complex are given in the sections below. All of these steps were carried out with the PySCF[32] quantum chemistry package.

2.4 Summary of initial guesses

A summary of the classes of initial product states for each complex is given in Supplementary Table 1.

Supplementary Table 1: Summary of the classes of initial product states for each complex. The notation CAS(me,no) denotes a complete active space with m electrons distributed in n orbitals in all possible ways.

				classes of initial guesses[b]		
model	spin	CAS(me,no)	dim(FCI)[a]	states of eight Fe ions in the [Fe_8S_7] core	M^c	no.[d]
synthetic [Fe_8S_7]	$S=0$	(108e,71o)	1.1×10^{32}	{Fe(III)↑, Fe(III)↓, 3Fe(II)↑, 3Fe(II)↓}	0	20[e]
P^N	$S=0$	(114e,73o)	2.8×10^{31}	{4Fe(II)↑, 4Fe(II)↓}	0	35[f]
P^{1+}	$S=1/2$	(117e,75o)	2.5×10^{32}	{Fe(III)↑,3Fe(II)↑,4Fe(II)↓}	1/2	35[g]
	$S=5/2$	(117e,75o)	1.6×10^{32}	{Fe(III)↑,3Fe(II)↑,4Fe(II)↓}	1/2	35[g]
P^{OX}	$S=3$	(120e,77o)	1.2×10^{33}	(a) {2Fe(III)↓, 5Fe(II)↑, Fe(II)↓}	3	6[h]
				(b) {2Fe(III)↓, 4Fe(II)↑, 2Fe(II)↓}	-1	15[h]
				(c) {Fe(III)↑, Fe(III)↓, 3Fe(II)↑, 3Fe(II)↓}	0	40[h]
	$S=4$	(120e,77o)	7.3×10^{32}	(a) {2Fe(III)↓, 5Fe(II)↑, Fe(II)↓}	3	6[h]
				(b) {2Fe(III)↓, 4Fe(II)↑, 2Fe(II)↓}	-1	15[h]
				(c) {Fe(III)↑, Fe(III)↓, 3Fe(II)↑, 3Fe(II)↓}	0	40[h]
				(d) {Fe(III)↑, Fe(III)↓, 4Fe(II)↑, 2Fe(II)↓}	4	30[h]

[a] Dimension of the underlying FCI space with m electrons distributed in n orbitals for the high spin ($M_S = S$) case.
[b] Possible combinations of charges and spin projections compatible with the number of electrons and total spin S.
[c] Spin projection of the initial product state M_S.
[d] Number of initial product states for performing the SP-MPS optimizations.
[e] Reduced by time-reversal symmetry and assuming that irons 1 and 8 are Fe(III).
[f] Reduced by time-reversal symmetry.
[g] Reduced by assuming that iron 4 is Fe(III).
[h] Reduced by assuming that irons 2 and 4 are Fe(III).

2.5 Total energies

The DMRG calculations were performed using the following Hamiltonian defined for the active orbitals,

$$\hat{H}_{\rm act} = f_{xy}a^\dagger_{x\sigma}a_{y\sigma} + \frac{1}{2}\langle wx|yz\rangle a^\dagger_{w\sigma}a^\dagger_{x\tau}a_{z\tau}a_{y\sigma} + E_{\rm core}, \quad (1)$$

where

$$E_{\rm core} = 2h_{ii} + 2\langle ij|ij\rangle - \langle ij|ji\rangle + E_{\rm nuc}, \quad (2)$$

$$f_{xy} = h_{xy} + 2\langle xi|yi\rangle - \langle xi|iy\rangle. \quad (3)$$

The Einstein summation convention has been used. The indices i, j, k, l denote doubly occupied core orbitals, w, x, y, z denote active orbitals, and the Greek indices σ and τ denote spins $\{\alpha, \beta\}$. The core energy $E_{\rm core}$ is defined as the total energy of the doubly occupied core orbitals plus the nuclear repulsion energy $E_{\rm nuc}$. The final total energy of the system is given by

$$E_{\rm tot} = \langle\Psi_{\rm DMRG}|\hat{H}_{\rm act}|\Psi_{\rm DMRG}\rangle, \quad (4)$$

where $|\Psi_{\mathrm{DMRG}}\rangle$ is variationally optimized for the Hamiltonian $\hat{H}_{\mathrm{act}}$ within the matrix product state (MPS) ansatz. This can be written in the occupation number representation as[33],

$$|\Psi_{\mathrm{DMRG}}\rangle = \sum_{\{\alpha_k\}} A^{n_1}_{\alpha_1}[1] A^{n_2}_{\alpha_1\alpha_2}[2] \cdots A^{n_K}_{\alpha_{K-1}}[K] |n_1 n_2 \cdots n_K\rangle, \tag{5}$$

where n_k indexes the local configurations $\{|vac\rangle, |k_\beta\rangle, |k_\alpha\rangle, |k_\alpha k_\beta\rangle\}$. The dimensionality of the underlying Hilbert space is 4^K, and hence is exponential in the number of orbitals K. The indices $\{\alpha_k\}$ are usually called virtual or bond indices, and in practice, their maximal value is fixed at a given value D called the *bond dimension*. Once all the site tensors $A[k]$ are obtained variationally, one can use $|\Psi_{\mathrm{DMRG}}\rangle$ to compute properties such as the electron density $\rho(\vec{r})$, spin density $\rho_S(\vec{r})$, and spin-spin correlation functions $\langle \vec{S}_A \cdot \vec{S}_B \rangle$ (see section 2.8).

2.6 DMRG protocol

In this section, we provide a detailed explanation of our optimization procedure outlined in Supplementary Fig. 3 that allows us to converge DMRG calculations to different kinds of states. To map out the low-energy landscape of each complex, our DMRG calculation protocol involves four steps. The basic idea is to seed the calculation from a broken-symmetry determinant, convert that into a MPS and spin-project to obtain a spin-projected MPS (SP-MPS) with the correct spin symmetry, and eventually convert this into a spin-adapted MPS (SA-MPS) which allows for the most efficient computation at large bond dimension. The detailed steps are below:

Initialization For each initial BS product state ($D_{\mathrm{SP}} = 1$) in Supplementary Table 1, a very crude spin-projected MPS (SP-MPS) [34] calculation with a small bond dimension (and 10^{-4} noise in the decimation step in DMRG) is performed to obtain a better, correlated initial guess in subsequent spin-adapted MPS (SA-MPS) calculations. This initial spin-projected MPS calculation is only needed to generate some initial quantum numbers such that we are sure to start in the chosen spin isomer electronic basin. We find that the choice of $D_{\mathrm{SP}} = 50$ is

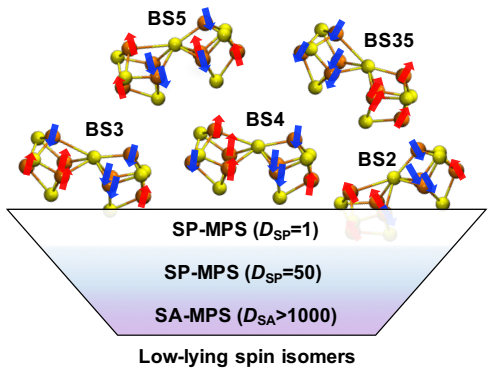

(a)

cluster	spin	class of initial guesses	no.
P^N	0	{4Fe^{2+}↑, 4Fe^{2+}↓}	35
Syn	0	{Fe^{3+}↑, Fe^{3+}↓, 3Fe^{2+}↑, 3Fe^{2+}↓}	20
P^{1+}	1/2	{Fe^{3+}↑, 3Fe^{2+}↑, 4Fe^{2+}↓}	35
	5/2	{Fe^{3+}↑, 3Fe^{2+}↑, 4Fe^{2+}↓}	35
P^{OX}	3	(a) {2Fe^{3+}↓, 5Fe^{2+}↑, Fe^{2+}↓}	6
		(b) {2Fe^{3+}↓, 4Fe^{2+}↑, 2Fe^{2+}↓}	15
		(c) {Fe^{3+}↑, Fe^{3+}↓, 3Fe^{2+}↑, 3Fe^{2+}↓}	40
	4	(a) {2Fe^{3+}↓, 5Fe^{2+}↑, Fe^{2+}↓}	6
		(b) {2Fe^{3+}↓, 4Fe^{2+}↑, 2Fe^{2+}↓}	15
		(c) {Fe^{3+}↑, Fe^{3+}↓, 3Fe^{2+}↑, 3Fe^{2+}↓}	40
		(d) {Fe^{3+}↑, Fe^{3+}↓, 4Fe^{2+}↑, 2Fe^{2+}↓}	30

(b)

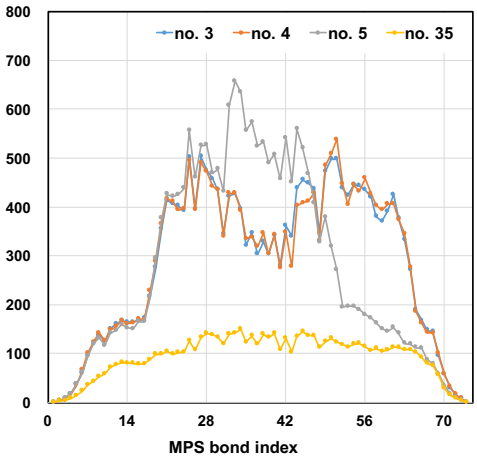

(c)

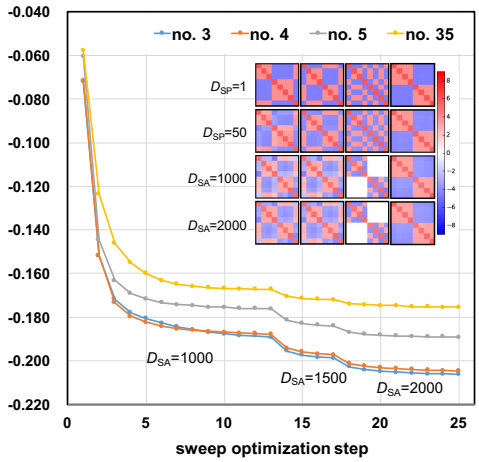

(d)

Supplementary Figure 3: Methods for mapping out the low-lying electronic states. (a) Optimization procedure starting from broken-symmetry (BS) product states with different spin-up (↑ in red) and spin-down (↓ in blue) configurations, followed by spin-projection and SP-MPS optimization, and finally SA-MPS optimization with large bond dimensions. (b) Initial guesses obtained by distributing different iron states across the eight Fe atoms. (c) Distribution of bond dimensions D_{SA} of SA-MPS converted from SP-MPS with $D_{\mathrm{SP}} = 50$ for four different initial guesses. (d) Energy convergence ($E + 17492$ in Hartree) of SA-MPS versus optimization step with inset showing convergence of the spin-spin correlation functions $\langle \vec{S}_A \cdot \vec{S}_B \rangle$ (red: positive, blue: negative) among the eight irons for the four states versus bond dimensions.

sufficient for the purpose of stabilizing the initial spin-spin correlation pattern, as can be seen in the comparison of spin-spin correlation functions between $D_{\mathrm{SP}} = 1$ and $D_{\mathrm{SP}} = 50$ for each complex in later steps, while providing a large enough set of quantum numbers for rapid energy convergence when converted to SA-MPS. As shown in Supplementary Fig. 2(c), typically, the bond dimension D_{SA} of the converted SA-MPS is $O(100)$.

Optimizations Starting from the obtained SA-MPS converted from SP-MPS for each initial guess, spin-adapted DMRG calculations[35] are carried out with gradually increasing bond dimensions D_{SA} from 1000 to 2000, as shown in Supplementary Fig. 2(d). The decrease of DMRG energies and the evolution of spin-spin correlation functions $\langle \vec{S}_A \cdot \vec{S}_B \rangle$ among the irons as a function of optimization step are monitored in this step to monitor convergence. We found that the correlation patterns $\langle \vec{S}_A \cdot \vec{S}_B \rangle$ are almost converged at $D_{\mathrm{SA}} = 2000$. [In fact, further increasing D_{SA} to 3000 in the next step does not lead to any visible change of the spin-spin correlation pattern, e.g., see Supplementary Fig. 9 for the synthetic cluster, indicating that the qualitative structure of the state has been established.]

Screening and refined optimizations Since calculations with larger D_{SA} are quite expensive for our large active spaces, we cannot afford to further increase D_{SA} for all the states obtained from the different initial guesses. Thus, in this step, we carefully screen out high-lying states, in order to eventually map out the low-lying energy landscape for each complex. This is done by continuing DMRG calculations only for the lowest few states obtained at $D_{\mathrm{SA}} = 2000$. For these, we do further calculations with larger bond dimension D_{SA} (3000, 3500, and 4000) and monitor the change of relative energies during this process. Note that already at $D_{\mathrm{SA}} = 2000$, we find that some of the states obtained from different initial BS-DFT guesses converge to the same state, which can be identified by the very similar energies and correlation functions $\langle \vec{S}_A \cdot \vec{S}_B \rangle$, e.g., see states obtained from the 3rd and 4th initial guesses in Supplementary Fig. 2(d). In this case, only one of them is selected for further DMRG

optimization with large D_{SA}, in order to save computational time.

Extrapolations After step 3, the lowest few states can be identified. To obtain a better relative energy, the total energy for each state can be extrapolated to the exact $D = \infty$ limit (also corresponding to zero discarded weight in DMRG calculations) following the standard procedures described in Refs. [36, 37]. (Note as is well established, the error in DMRG calculations depends linearly on the discarded weight at large D (it is bounded by $cw||H||$ where w is the discarded weight and $||H||$ is the norm of the Hamiltonian and c is a constant) because of the relationship between the density matrix truncation and the SVD decomposition of the wavefunction, see e.g. [38]. This linear relationship thus constitutes the standard functional form for DMRG energy extrapolation).

To obtain the best extrapolation (i.e. from well-converged DMRG calculations at each D) we performed a reverse sweep from $D = 4000$ back to $D = 3000$. Three energies (D =4000, 3500, and 3000) and their associated discarded weights obtained during the DMRG sweeps were then used to perform a linear fit (reweighted by 1.0, 0.1, and 0.01) to extrapolate the total energy to the limit of zero discarded weight. To obtain an error bar (given the small number of data points) we used the empirical error bar $(E_{D=4000} - E_{D=\infty})/5$ often used to estimate extrapolation errors in DMRG calculations [36, 37]. For relative energies ΔE of spin isomers, we expect smaller error bars than in the total energy, due to error cancellations between similar states of the same compound. To estimate the error bar in the relative energies, we used twice the absolute value of the difference between the error bars for the two total energies. In almost all cases, this relative energy error bar was less than 0.8 kcal/mol.

2.7 Solvation and environment effects

For the P-cluster models, we employed a simple treatment of solvation/environment effects, viz., an interaction potential $V_{xy}^{\mathrm{COSMO}}[\rho_{\mathrm{KS}}]$ generated from the Kohn-Sham density ρ_{KS} using

COSMO was added to f_{xy} (1). The corresponding modified total energy formula reads as

$$\begin{aligned} E_{\rm tot} &= \langle\Psi_{\rm DMRG}|\hat{H}_{\rm act}|\Psi_{\rm DMRG}\rangle - V_{xy}^{\rm COSMO}[\rho_{KS}]\gamma_{xy} + E_{\rm diel}^{\rm COSMO}[\rho_{\rm KS}], \\ \gamma_{xy} &= \langle\Psi_{\rm DMRG}|a_{x\sigma}^{\dagger}a_{y\sigma}|\Psi_{\rm DMRG}\rangle, \end{aligned} \tag{6}$$

where in this treatment the dielectric energy $E_{\rm diel}^{\rm COSMO}[\rho_{\rm KS}]$ is a constant, just like $E_{\rm core}$, for different $|\Psi_{\rm DMRG}\rangle$ corresponding to different states. The theoretical justification for this simplified treatment without self-consistency is that the interaction between the active cluster and the solvent/surroundings is mainly electrostatic in nature, and the different low-lying excited states do not change the total charge density significantly. Thus, when comparing relative energies, it is safe to assume $E_{\rm diel}^{\rm COSMO}$ is constant. It is also cheap to update $E_{\rm diel}^{\rm COSMO}$ once by using the density constructed from $|\Psi_{\rm DMRG}\rangle$ and the core orbitals. We found that indeed in almost all cases, the *relative* energies computed from Eq. (6) with $E_{\rm diel}^{\rm COSMO}$ updated by $|\Psi_{\rm DMRG}\rangle$, and those computed with $\langle\Psi_{\rm DMRG}|\hat{H}_{\rm act}|\Psi_{\rm DMRG}\rangle$, differ by less than 0.1kcal/mol, e.g., see Supplementary Table 5 for the P^N cluster. Therefore, in our discussion of the relative energies in the main text, we only use ΔE computed from $\langle\Psi_{\rm DMRG}|\hat{H}_{\rm act}|\Psi_{\rm DMRG}\rangle$ for simplicity.

2.8 Wavefunction analysis

For the [Fe_8S_7] clusters we studied, there are no strongly dominant electronic configurations due to the near degeneracy of the many d orbitals. To understand the electronic structure, the expectation values of the following local operators were evaluated using the computed DMRG

wavefunctions,

$$\hat{N}_A = \sum_{p\in A} \hat{n}_p, \quad \hat{n}_p = a^\dagger_{p\alpha} a_{p\alpha} + a^\dagger_{p\beta} a_{p\beta}, \tag{7}$$

$$\hat{S}^z_A = \sum_{p\in A} \hat{s}^z_p, \quad \hat{s}^z_p = \frac{1}{2}(a^\dagger_{p\alpha} a_{p\alpha} - a^\dagger_{p\beta} a_{p\beta}), \tag{8}$$

$$\vec{S}_A \cdot \vec{S}_B = \sum_{\mu\in\{x,y,z\}} \hat{S}^\mu_A \hat{S}^\mu_B, \quad \hat{S}^\mu_A = \sum_{p\in A} \hat{s}^\mu_p, \tag{9}$$

$$\hat{s}^x_p = \frac{1}{2}(a^\dagger_{p\alpha} a_{p\beta} + a^\dagger_{p\beta} a_{p\alpha}), \tag{10}$$

$$\hat{s}^y_p = \frac{1}{2i}(a^\dagger_{p\alpha} a_{p\beta} - a^\dagger_{p\beta} a_{p\alpha}), \tag{11}$$

which measure the local charge (population) $N_A \equiv \langle \hat{N}_A \rangle$, spin projection $S^z_A \equiv \langle \hat{S}^z_A \rangle$ on the center A, and the spin-spin correlation function $\langle \vec{S}_A \cdot \vec{S}_B \rangle$ between A and B, respectively. The notation $p \in A$ denotes that the localized active orbital p belongs to atom A. The charge fluctuations $\langle \Delta\hat{N}_A \Delta\hat{N}_B \rangle$ ($A \neq B$) between different irons defined via

$$\langle \Delta\hat{N}_A \Delta\hat{N}_B \rangle \equiv \langle (\hat{N}_A - N_A)(\hat{N}_B - N_B) \rangle = \langle \hat{N}_A \hat{N}_B \rangle - N_A N_B \tag{12}$$

and the spin fluctuations $\langle \vec{S}_A \cdot \vec{S}_B \rangle - S^z_A S^z_B$ were also investigated for different complexes.

Although oxidation state is not a uniquely defined theoretical concept, in practice it may provide some basic understanding of the charge distribution and reactivity. To assign the oxidation state for irons in the [Fe_8S_7] core, we used the local charge N_A with A=Fe as an indicator. However, its value should not be directly compared with the formal number of d electrons, 5 for Fe(III) and 6 for Fe(II), since the irons in a complex are not isolated. In addition, care must be taken with population analysis which may partition charge contributions from atoms in unphysical ways. We found that population analysis based on localized active orbitals gave quite consistent results across all the investigated iron-sulfur clusters. Specifically, taking the values for the synthetic complex and the P^N cluster as references, see Supplementary Tables 4 and 7, we found that $N_{\mathrm{Fe}} < 6.2$ indicates Fe(III), $N_{\mathrm{Fe}} > 6.3$ indicates Fe(II), while N_{Fe} in between

indicates mixed-valence character $Fe^{2.5+}$. This is also in line with previous data for [Fe_2S_2] and [Fe_4S_4] complexes[19].

To gain a deeper insight into the different spin states, for nonsinglet states ($S \neq 0$), the spin-density $\rho_S(\vec{r})$ of the high-spin component ($M_S = S$) was visualized in real space,

$$\rho_S(\vec{r}) = \sum_{pq} \gamma^S_{pq} \phi^*_p(\vec{r}) \phi_q(\vec{r}), \quad \gamma^S_{pq} = \langle \Psi | \frac{1}{2}(a^\dagger_{p\alpha} a_{q\alpha} - a^\dagger_{p\beta} a_{q\beta}) | \Psi \rangle, \quad \int d^3\vec{r}\, \rho_S(\vec{r}) = S, \quad (13)$$

and for general states, the following correlation density function was defined to visualize the spin-spin correlation in real space,

$$\sigma_A(\vec{r}) = \sum_{p \in A} \sigma_p(\vec{r}), \quad \sigma_p(\vec{r}) = \sum_q \langle \vec{s}_p \cdot \vec{s}_q(\vec{r}) \rangle, \quad (14)$$

where the operator $\vec{s}_q(r)$ is defined as

$$\hat{s}^\mu_q(\vec{r}) = \hat{s}^\mu_q |\phi_q(\vec{r})|^2, \quad \int d^3\vec{r}\, \hat{s}^\mu_q(\vec{r}) = \hat{s}^\mu_q, \quad (15)$$

such that

$$\int d^3\vec{r}\, \sigma_p(\vec{r}) = \sum_q \langle \vec{s}_p \cdot \vec{s}_q \rangle. \quad (16)$$

It should be mentioned that this is only one way to visualize the spin-spin correlation. The information contained in $\sigma_A(\vec{r})$ is similar to that contained in row A of the matrix $C_{AB} \equiv \langle \vec{S}_A \cdot \vec{S}_B \rangle$, but is expressed instead in real space. There are also other measures to interpret the correlations between two orbitals, such as the two-orbital mutual information [39, 40, 41]. The two-orbital mutual information sums all fluctuations between the two orbitals into a single number; the charge-charge fluctuations and spin-spin fluctuations contribute two fluctuation sectors that are added together in the mutual information. We have found it useful to break them out for separate analysis here.

3 Synthetic [Fe_8S_7] cluster

3.1 Cartesian coordinates

```
163
synthetic cluster
 Fe                  6.73964000    3.38505000   21.07858000
 Fe                  5.91210000    3.48752000   18.38996000
 Fe                  4.01843000    3.42724000   20.31636000
 Fe                  5.53394000    5.57387000   19.96809000
 Fe                  3.91050000    3.42724000   16.44690000
 Fe                  2.01684000    3.48752000   18.37330000
 Fe                  2.39499000    5.57387000   16.79517000
 Fe                  1.18929000    3.38505000   15.68468000
 S                   3.96447000    4.84109000   18.38163000
 S                   5.58747000    1.80265000   19.90240000
 S                   7.56149000    4.70353000   19.40414000
 S                   5.05525000    4.65182000   21.97070000
 S                   5.16472000    7.83523000   19.63575000
 Si                  9.63757000    3.32224000   22.16800000
 Si                  7.31830000    2.26104000   23.88877000
 Si                  6.74515000    4.41084000   15.44498000
 Si                  6.55847000    1.46820000   16.11775000
 N                   8.00434000    2.79682000   22.39618000
 N                   5.94495000    3.11087000   16.36700000
 N                   7.48105000    8.79757000   20.49919000
 N                   5.92487000    8.35346000   22.14864000
 C                   9.78352000    5.17914000   22.19766000
 C                  10.80177000    2.74924000   23.51868000
 C                  10.33145000    2.63610000   20.57272000
 C                   5.64422000    1.47296000   23.62897000
 C                   8.34161000    0.95483000   24.77108000
 C                   7.11282000    3.65754000   25.10195000
 C                   6.31523000    6.11283000   16.06064000
 C                   8.60547000    4.27718000   15.58762000
 C                   6.28263000    4.36600000   13.63427000
 C                   6.94223000    1.12084000   14.33032000
 C                   5.35910000    0.14909000   16.62925000
 C                   8.13844000    1.20438000   17.09737000
 C                   6.27537000    8.36086000   20.85702000
 C                   8.02182000    8.55436000   19.17326000
 C                   8.21285000    9.81267000   21.26877000
 C                   4.53036000    8.28261000   22.57264000
 C                   6.89836000    8.03518000   23.20252000
 H                  10.66946000    5.43292000   21.97953000
 H                   9.18061000    5.55346000   21.56288000
 H                   9.56295000    5.49954000   23.06527000
 H                  11.58785000    3.28851000   23.50888000
 H                  10.37723000    2.82431000   24.35933000
 H                  11.04616000    1.84199000   23.36182000
 H                  11.11433000    3.12250000   20.33498000
 H                  10.55400000    1.72145000   20.69036000
 H                   9.68529000    2.72175000   19.88402000
 H                   5.66599000    0.92945000   22.85694000
 H                   4.99037000    2.15921000   23.51868000
 H                   5.42165000    0.94954000   24.38875000
 H                   9.00580000    1.37991000   25.30047000
 H                   7.77666000    0.43353000   25.32498000
 H                   8.76051000    0.39547000   24.12650000
 H                   6.73475000    3.31389000   25.90829000
 H                   7.95849000    4.03821000   25.28822000
```

H	6.53541000	4.30890000	24.73432000
H	6.66757000	6.76101000	15.46263000
H	6.68710000	6.23866000	16.92335000
H	5.37047000	6.20165000	16.10231000
H	8.90961000	3.56344000	15.04107000
H	8.83758000	4.10588000	16.49200000
H	9.00126000	5.08927000	15.30332000
H	5.43273000	3.94939000	13.53378000
H	6.24275000	5.25105000	13.29359000
H	6.93506000	3.86903000	13.15144000
H	7.68068000	1.64954000	14.06072000
H	6.18613000	1.32809000	13.80093000
H	7.15779000	0.19879000	14.23228000
H	5.05526000	0.32251000	17.51402000
H	4.61940000	0.14381000	16.03613000
H	5.79168000	-0.69789000	16.60719000
H	8.40676000	0.29819000	17.02629000
H	8.82239000	1.76586000	16.74689000
H	7.98521000	1.42220000	18.00909000
H	8.84271000	9.02068000	19.07278000
H	8.17491000	7.62068000	19.06052000
H	7.40286000	8.85361000	18.52133000
H	9.10968000	9.52506000	21.40357000
H	8.21161000	10.63321000	20.79330000
H	7.79230000	9.93321000	22.11187000
H	3.97667000	8.64107000	21.88884000
H	4.41652000	8.78699000	23.36918000
H	4.29292000	7.37854000	22.73195000
H	6.92068000	8.73307000	23.84220000
H	6.64399000	7.22098000	23.63387000
H	7.76025000	7.92415000	22.82018000
N	1.98398000	3.11087000	20.39626000
S	2.34146000	1.80265000	16.86086000
S	2.87368000	4.65182000	14.79255000
S	0.36744000	4.70353000	17.35912000
Si	1.18378000	4.41084000	21.31828000
Si	1.37047000	1.46820000	20.64551000
S	2.76421000	7.83523000	17.12751000
C	1.61371000	6.11283000	20.70262000
C	-0.67654000	4.27718000	21.17564000
C	1.64631000	4.36600000	23.12899000
C	0.98670000	1.12084000	22.43294000
C	2.56984000	0.14909000	20.13401000
C	-0.20951000	1.20438000	19.66589000
N	-0.07541000	2.79682000	14.36708000
C	1.65356000	8.36086000	15.90624000
H	1.26136000	6.76101000	21.30063000
H	1.24183000	6.23866000	19.83990000
H	2.55846000	6.20165000	20.66095000
H	-0.98068000	3.56344000	21.72219000
H	-0.90865000	4.10588000	20.27126000
H	-1.07232000	5.08926000	21.45994000
H	2.49620000	3.94939000	23.22948000
H	1.68618000	5.25105000	23.46966000
H	0.99387000	3.86903000	23.61181000
H	0.24825000	1.64954000	22.70254000
H	1.74280000	1.32809000	22.96233000
H	0.77114000	0.19879000	22.53098000
H	2.87368000	0.32251000	19.24924000
H	3.30954000	0.14380000	20.72713000
H	2.13726000	-0.69789000	20.15607000
H	-0.47783000	0.29819000	19.73697000

```
H                -0.89345000    1.76586000   20.01637000
H                -0.05628000    1.42220000   18.75416000
Si               -1.70863000    3.32224000   14.59526000
Si                0.61063000    2.26104000   12.87449000
N                 0.44788000    8.79757000   16.26407000
N                 2.00407000    8.35346000   14.61462000
C                -1.85458000    5.17914000   14.56560000
C                -2.87284000    2.74924000   13.24458000
C                -2.40252000    2.63610000   16.19054000
C                 2.28471000    1.47296000   13.13429000
C                -0.41268000    0.95483000   11.99218000
C                 0.81611000    3.65755000   11.66131000
C                -0.09289000    8.55437000   17.58999000
C                -0.28392000    9.81267000   15.49449000
C                 3.39858000    8.28261000   14.19062000
C                 1.03058000    8.03518000   13.56074000
H                -2.74052000    5.43292000   14.78373000
H                -1.25168000    5.55346000   15.20038000
H                -1.63402000    5.49954000   13.69799000
H                -3.65892000    3.28851000   13.25438000
H                -2.44830000    2.82431000   12.40392000
H                -3.11722000    1.84199000   13.40143000
H                -3.18540000    3.12250000   16.42827000
H                -2.62506000    1.72145000   16.07290000
H                -1.75636000    2.72175000   16.87924000
H                 2.26294000    0.92945000   13.90631000
H                 2.93856000    2.15921000   13.24458000
H                 2.50729000    0.94954000   12.37451000
H                -1.07686000    1.37991000   11.46278000
H                 0.15228000    0.43353000   11.43827000
H                -0.83157000    0.39547000   12.63676000
H                 1.19419000    3.31389000   10.85496000
H                -0.02955000    4.03821000   11.47504000
H                 1.39352000    4.30890000   12.02894000
H                -0.91377000    9.02068000   17.69048000
H                -0.24598000    7.62068000   17.70273000
H                 0.52607000    8.85361000   18.24193000
H                -1.18075000    9.52506000   15.35969000
H                -0.28268000   10.63321000   15.96996000
H                 0.13663000    9.93322000   14.65138000
H                 3.95226000    8.64107000   14.87441000
H                 3.51241000    8.78699000   13.39408000
H                 3.63601000    7.37854000   14.03131000
H                 1.00825000    8.73307000   12.92106000
H                 1.28494000    7.22098000   13.12938000
H                 0.16869000    7.92416000   13.94308000
```

3.2 Active orbitals

The active orbitals for the synthetic [Fe_8S_7] complex were prepared with the initial orbitals obtained at the BP86[42, 43]/def2-SVP level for a high-spin state M_S=32/2 with charge deliberately set to -2 rather than in its neutral state, such that all Fe atoms become formally Fe(II) to converge the self-consistent-field (SCF) calculations. The final active orbitals ordered by the

genetic ordering method[37] for DMRG are shown in Supplementary Fig. 4. The orbitals in the CAS(108e,71o) active space can be classified as follows:

1. Five $3d$ orbitals of Fe(1): 65, 66, 67, 68, 69
2. Five $3d$ orbitals of Fe(2): 44, 45, 46, 47, 49
3. Five $3d$ orbitals of Fe(3): 40, 41, 42, 43, 48
4. Five $3d$ orbitals of Fe(4): 50, 51, 52, 53, 54
5. Five $3d$ orbitals of Fe(5): 24, 29, 30, 31, 32
6. Five $3d$ orbitals of Fe(6): 23, 25, 26, 27, 28
7. Five $3d$ orbitals of Fe(7): 18, 19, 20, 21, 22
8. Five $3d$ orbitals of Fe(8): 3, 4, 5, 6, 7
9. Twenty-one $3p$ orbitals of seven S atoms in the [Fe_8S_7] core: 8, 9, 10, 11, 12, 13, 14, 16, 17, 35, 36, 37, 55, 56, 58, 59, 60, 61, 62, 63, 64
10. Ten orbitals of peripheral atoms: 1, 2, 15, 33, 34, 38, 39, 57, 70, 71

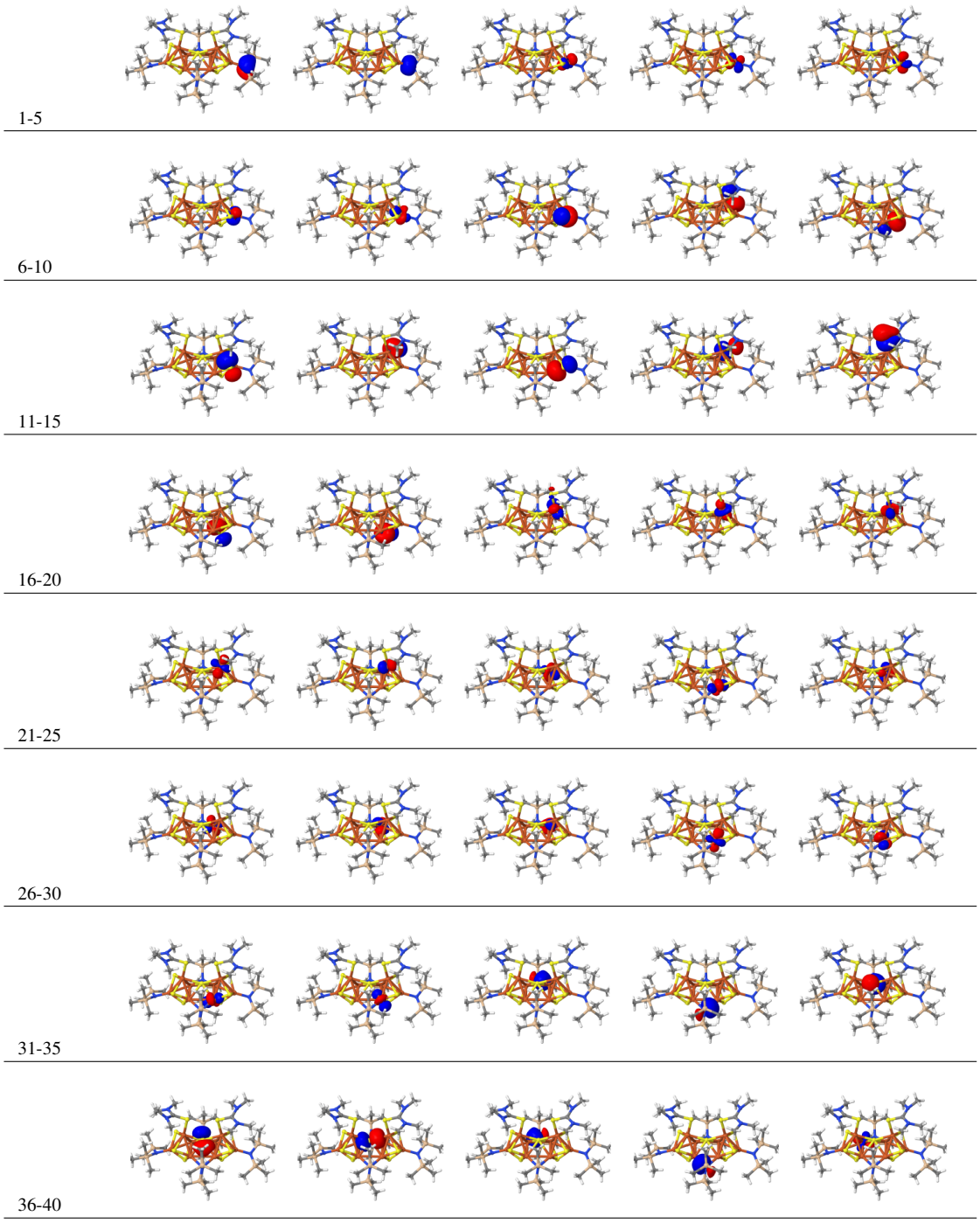

Supplementary Figure 4: Active orbitals of the synthetic [Fe_8S_7] complex.

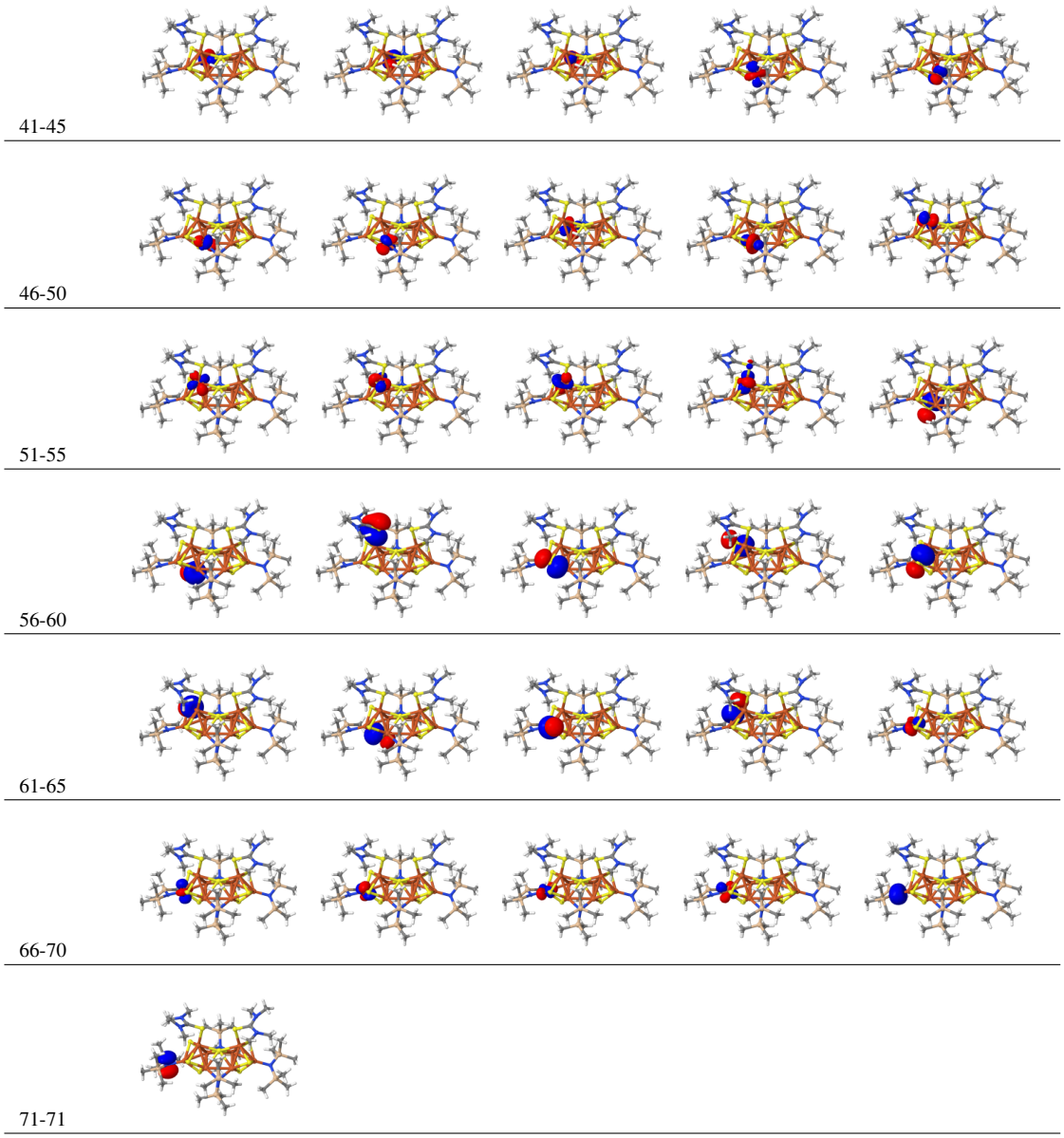

Supplementary Figure 5: Active orbitals of the synthetic [Fe_8S_7] complex.

3.3 DMRG results for $S = 0$ states

3.3.1 Initial guesses and DMRG energies

In Supplementary Table 2, we list the 20 initial product states for different spin alignments compatible with $S = 0$, as well as the relative energies (in kcal/mol) obtained using spin-adapted DMRG states with $D = 1000$ and $D = 2000$. Supplementary Fig. 6 displays the corresponding spin-spin correlation functions for each state starting from the correlated SP-MPS guesses with $D_{\rm SP} = 50$. In comparison, the computed results from a very crude initial guess with $D_{\rm SP} = 1$ are also listed, see Supplementary Fig. 6(a). It is clear that in such cases, the spin-adapted DMRG calculations from different initial guesses quickly converge to two local minima with high energies, see Supplementary Fig. 6(c). The SP-MPS optimization step ($D_{\rm SP} = 50$) is seen to be essential to stabilize the subsequent spin-adapted DMRG optimization.

The two low-lying states (no. 1 and no. 8) with distinct spin-spin correlation patterns were subsequently optimized with larger bond dimensions, see the last three columns in Supplementary Table 2. The energy convergence is shown in Supplementary Fig. 7. The $D = 4000$ states will be used in the energy extrapolation in the next section.

Supplementary Table 2: Relative energies (ΔE in kcal/mol) for the states computed from DMRG with different initial guesses for the synthetic [Fe_8S_7] cluster. The last three columns show the relative energies for the selected low-lying states obtained with larger bond dimensions in a forward sweep schedule, while the energies obtained in a reverse sweep schedule and extrapolated results are shown in Supplementary Table 3.

no.	Fe(III)↑,Fe(II)↑,Fe(III)↓,Fe(II)↓	$D = 1000$	$D = 2000$	$D = 3000$	$D = 3500$	$D = 4000$
1	{8}, {3, 2, 4}, {1}, {7, 6, 5}	0.00	0.00	0.00	0.00	0.00
2	{8}, {5, 2, 4}, {1}, {7, 6, 3}	13.06	15.74			
3	{8}, {5, 3, 4}, {1}, {7, 6, 2}	12.48	15.23			
4	{8}, {5, 3, 2}, {1}, {7, 6, 4}	21.90	24.46			
5	{8}, {6, 2, 4}, {1}, {7, 5, 3}	12.17	13.71			
6	{8}, {6, 3, 4}, {1}, {7, 5, 2}	12.48	14.82			
7	{8}, {6, 3, 2}, {1}, {7, 5, 4}	21.08	22.72			
8	{8}, {6, 5, 4}, {1}, {7, 3, 2}	8.75	7.15	7.00	6.90	6.90
9	{8}, {6, 5, 2}, {1}, {7, 3, 4}	22.27	21.22			
10	{8}, {6, 5, 3}, {1}, {7, 2, 4}	20.66	20.65			
11	{8}, {7, 2, 4}, {1}, {6, 5, 3}	19.15	22.12			
12	{8}, {7, 3, 4}, {1}, {6, 5, 2}	19.28	22.37			
13	{8}, {7, 3, 2}, {1}, {6, 5, 4}	27.44	30.42			
14	{8}, {7, 5, 4}, {1}, {6, 3, 2}	21.67	20.82			
15	{8}, {7, 5, 2}, {1}, {6, 3, 4}	34.01	35.56			
16	{8}, {7, 5, 3}, {1}, {6, 2, 4}	35.08	34.15			
17	{8}, {7, 6, 4}, {1}, {5, 3, 2}	18.56	20.21			
18	{8}, {7, 6, 2}, {1}, {5, 3, 4}	31.80	34.06			
19	{8}, {7, 6, 3}, {1}, {5, 2, 4}	30.59	34.34			
20	{8}, {7, 6, 5}, {1}, {3, 2, 4}	29.88	36.62			

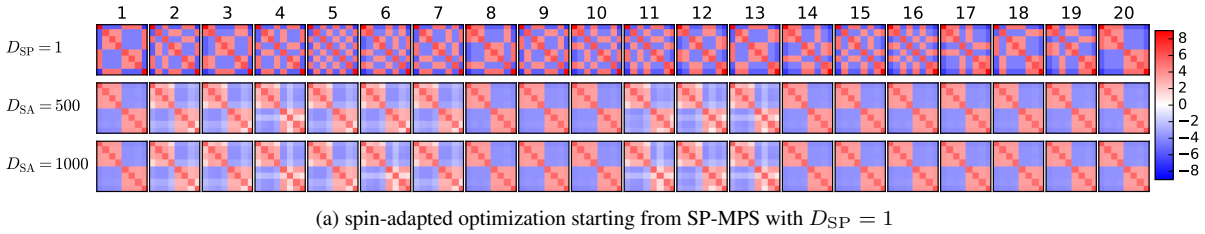

(a) spin-adapted optimization starting from SP-MPS with $D_{\mathrm{SP}} = 1$

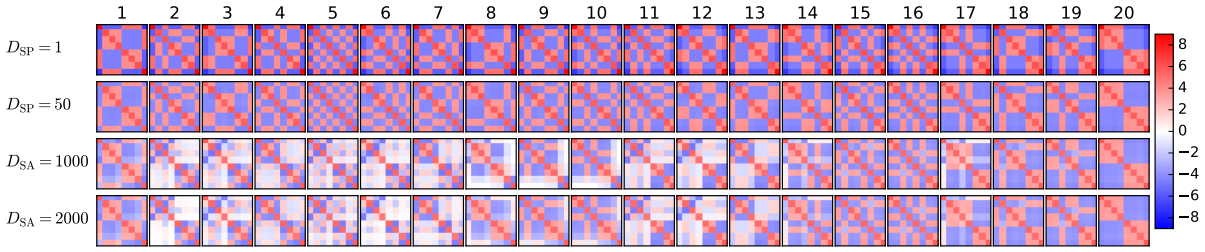

(b) spin-adapted optimization starting from SP-MPS with $D_{\mathrm{SP}} = 50$

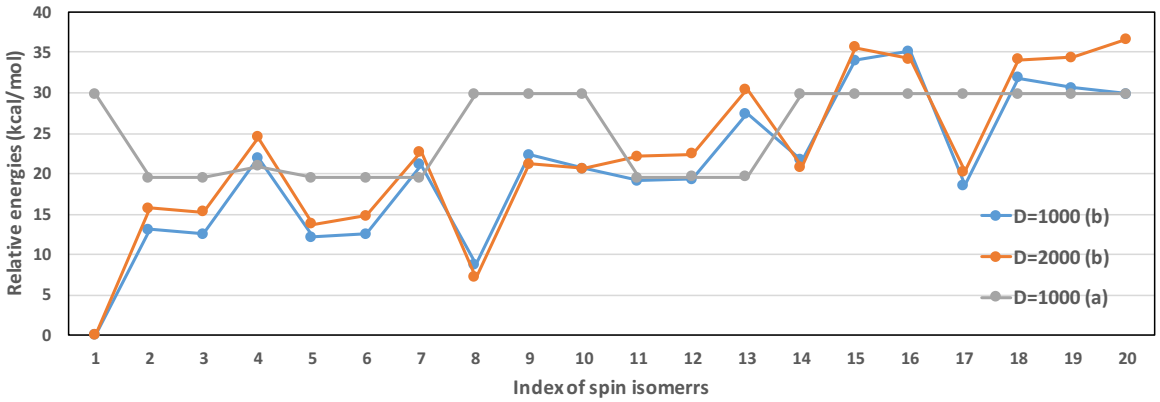

(c) relative energies

Supplementary Figure 6: Spin-spin correlation functions for the DMRG states with various D computed starting from different initial guesses for the synthetic [Fe_8S_7] cluster: (a) spin-adapted optimization starting from spin-projected MPS (SP-MPS) with $D_{\mathrm{SP}} = 1$, where the labels D_{SA} represent the DMRG results obtained with SA-MPS, (b) spin-adapted optimization starting from SP-MPS with $D_{\mathrm{SP}} = 50$, (c) relative energies (in kcal/mol) at $D = 1000$ and $D = 2000$ obtained in (b), whereas the relative energies at $D = 1000$ obtained in (a) are computed with respect to the lowest energy at $D = 1000$ obtained in (b). Comparing (a) and (b), it is clear that in the former case, the SA-MPS optimizations quickly get stuck in two local minima.

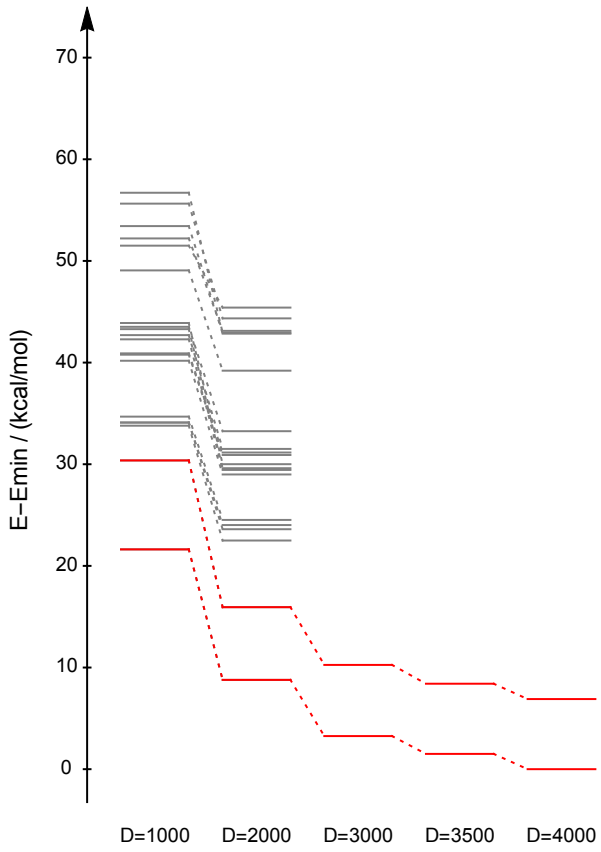

Supplementary Figure 7: Energy convergence for the DMRG states computed starting from different initial guesses for the synthetic [Fe_8S_7] cluster with progressively increasing bond dimensions D up to $D = 4000$. The lowest two states are highlighted in red.

3.3.2 Energy extrapolation

In Supplementary Table 3, the extrapolated energies obtained using the strategy described in Supplementary Sec. 2.5 are shown for the lowest two states (no. 1 and no. 8) obtained in the previous section. The extrapolation procedure is plotted in Supplementary Fig. 8. In addition, the results for the lowest $S = 1$ state are also shown.

Supplementary Table 3: Total energies (in Hartree) and relative energies ΔE (in kcal/mol) of the lowest two spin isomers of the synthetic [Fe_8S_7] cluster computed by DMRG with various bond dimensions D in a reverse sweep schedule.

no.	D	discarded weight	energy	ΔE
1	3000	3.2×10^{-4}	-17834.005619	0.00
	3500	3.0×10^{-4}	-17834.008462	0.00
	4000	2.6×10^{-4}	-17834.010666	0.00
	extrapolation		-17834.028543	0.00
	error bar		2.24	0.00
8	3000	3.8×10^{-4}	-17833.994499	6.98
	3500	3.5×10^{-4}	-17833.997442	6.92
	4000	3.2×10^{-4}	-17833.999730	6.86
	extrapolation		-17834.020315	5.16
	error bar		2.58	0.68
$S = 1$	3000	3.2×10^{-4}	-17834.003162	1.54
	3500	3.0×10^{-4}	-17834.006090	1.49
	4000	2.6×10^{-4}	-17834.008374	1.44
	extrapolation		-17834.026840	1.07
	error bar		2.32	0.15

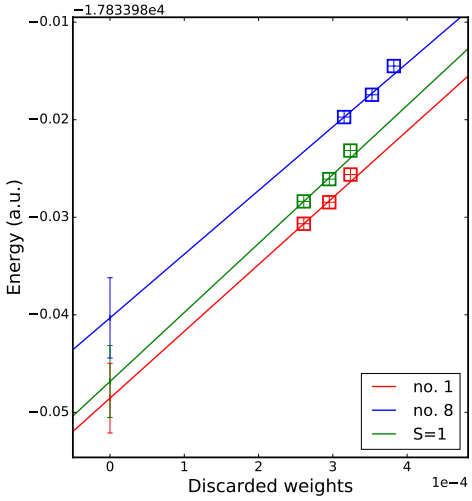

Supplementary Figure 8: Extrapolation of the DMRG energies (in Hartree) versus the discarded weight for the lowest two spin isomers of the synthetic [Fe_8S_7] complex. A linear fit of the computed data with D=3000, 3500, and 4000 is used to extrapolate to zero discarded weight, where the intercept is an estimate of the FCI energy ($D = \infty$). The error bars were estimated from an empirical rule $(E_{D=4000} - E_{D=\infty})/5$.

3.3.3 Population analysis

The analysis of the lowest two $S = 0$ states (no. 1 and no. 8) is summarized in Supplementary Fig. 9. It can be seen that the spin-spin correlation patterns are basically converged at $D = 2000$. The local populations and spin-spin correlation functions for the Fe atoms of these two states are shown in Supplementary Table 4.

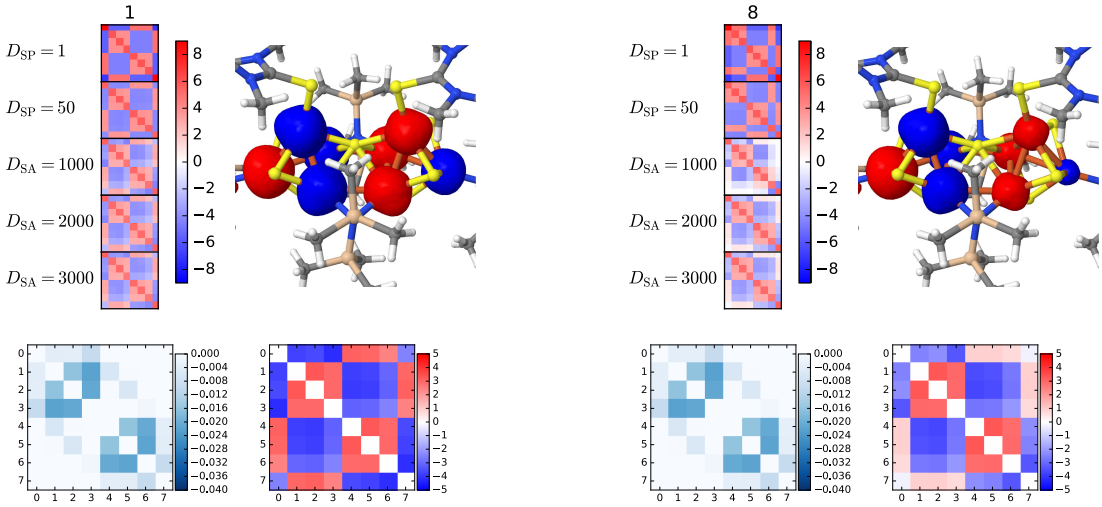

(1) no. 1: $(S_L, S_R) = (3.58, 3.57)$ (2) no. 8: $(S_L, S_R) = (4.34, 4.34)$

Supplementary Figure 9: Analysis of the lowest two $S = 0$ states of the synthetic [Fe_8S_7] cluster. First row: spin-spin correlation functions $\langle \vec{S}_A \cdot \vec{S}_B \rangle$ between the eight irons and spin-spin correlation density $\sigma_A(\vec{r}) = \langle \vec{S}_A \cdot \sum_B \vec{S}_B(\vec{r}) \rangle$ for the first iron atom. Second row: charge (left) and spin (right) fluctuations among different irons. The effective spins of the left cubane S_L and the right cubane S_R are computed from the expectation values of the local spin-square operators $\langle \hat{S}_L^2 \rangle$ and $\langle \hat{S}_R^2 \rangle$ for the irons on the left and right cubanes, respectively.

Supplementary Table 4: Local populations and spin-spin correlation functions for Fe atoms of the lowest two spin isomers of the synthetic [Fe_8S_7] cluster. The results were obtained from DMRG with $D = 3000$ in the localized active orbital basis. The effective spin of each iron S_{Fe} was computed from the expectation value of the local spin-square operator $\langle \hat{S}^2_{\mathrm{Fe}} \rangle$. The local S^z_{Fe} are all zero, as the computed states are singlets ($S = 0$).

				$\langle \vec{S}_A \cdot \vec{S}_B \rangle$							
no.	atom	N_{Fe}	S_{Fe}	Fe1	Fe2	Fe3	Fe4	Fe5	Fe6	Fe7	Fe8
1	Fe1	6.15	1.90	5.51	-3.70	-3.55	-4.10	3.07	2.98	2.45	-2.45
	Fe2	6.32	1.83	-3.70	5.18	3.28	2.96	-3.76	-3.64	-2.98	2.98
	Fe3	6.30	1.84	-3.55	3.28	5.24	2.93	-3.85	-3.77	-3.08	3.07
	Fe4	6.44	1.74	-4.10	2.96	2.93	4.78	-3.08	-2.99	-2.45	2.45
	Fe5	6.30	1.84	3.07	-3.76	-3.85	-3.08	5.24	3.28	2.92	-3.55
	Fe6	6.32	1.83	2.98	-3.64	-3.77	-2.99	3.28	5.18	2.95	-3.69
	Fe7	6.45	1.74	2.45	-2.98	-3.08	-2.45	2.92	2.95	4.76	-4.09
	Fe8	6.15	1.90	-2.45	2.98	3.07	2.45	-3.55	-3.69	-4.09	5.50
8	Fe1	6.14	1.90	5.53	-2.44	-2.20	-3.29	0.94	0.91	0.71	-0.27
	Fe2	6.32	1.84	-2.44	5.21	3.30	2.94	-3.49	-3.36	-2.63	0.91
	Fe3	6.30	1.85	-2.20	3.30	5.27	2.90	-3.60	-3.50	-2.72	0.94
	Fe4	6.44	1.74	-3.29	2.94	2.90	4.78	-2.72	-2.63	-2.05	0.71
	Fe5	6.30	1.85	0.94	-3.49	-3.60	-2.72	5.26	3.30	2.89	-2.20
	Fe6	6.32	1.84	0.91	-3.36	-3.50	-2.63	3.30	5.20	2.93	-2.43
	Fe7	6.45	1.74	0.71	-2.63	-2.72	-2.05	2.89	2.93	4.76	-3.28
	Fe8	6.14	1.90	-0.27	0.91	0.94	0.71	-2.20	-2.43	-3.28	5.53

3.3.4 Excited states

The lowest four excited states for each of the lowest two spin isomers (no. 1 and no. 8) were computed in a state-average manner (equal weights) with $D = 2000$, starting from the converged ground state solution. They are characterized in Supplementary Fig. 10 showing the density differences $\Delta\rho(\vec{r})$ with respect to the lowest state for each spin isomer, spin-spin correlation functions $\langle \vec{S}_A \cdot \vec{S}_B \rangle$, and relative energies ΔE (in kcal/mol).

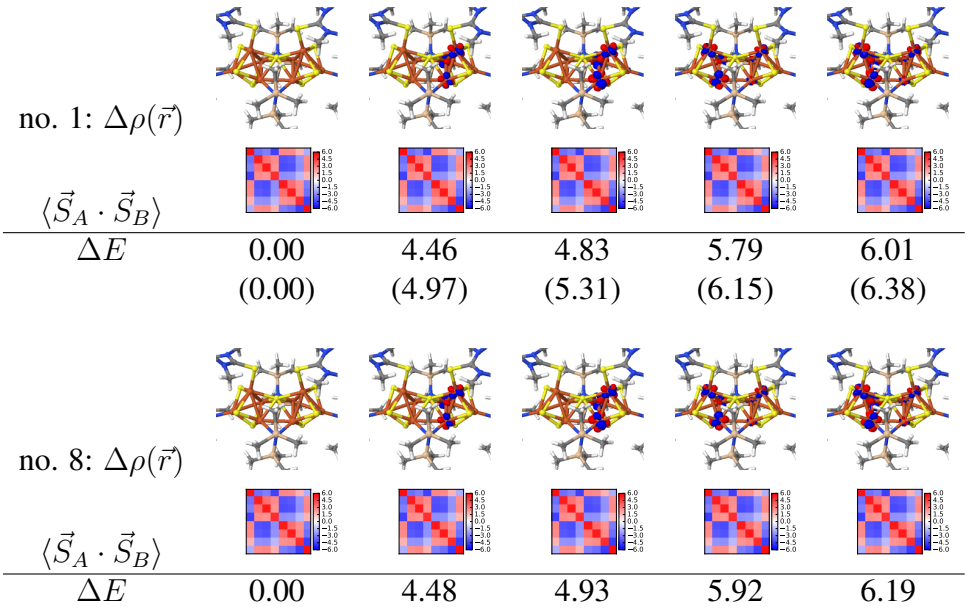

Supplementary Figure 10: Density differences $\Delta\rho(\vec{r})$ with respect to the lowest state in each spin isomer, spin-spin correlation functions $\langle \vec{S}_A \cdot \vec{S}_B \rangle$, and relative energies ΔE (in kcal/mol) for the lowest five states of the lowest two spin isomers of the synthetic [Fe_8S_7] complex. Numbers in parentheses are relative energies computed at $D = 3000$ for the lowest spin isomer (no. 1).

4 P^N cluster

4.1 Cartesian coordinates

```
107
pn model
  Fe  -7.97847232212347     -8.12261801211869      2.89412216713691
  Fe  -9.76818702837835     -6.93768251211466      1.75732837539646
  Fe  -8.88046717991214     -9.26733668361748      0.61795973008066
  Fe  -7.52271224828681     -7.12412388118416      0.58199539210509
  Fe  -5.42475526498280     -5.42778299430191      2.05523097897839
  Fe  -6.40580217384745     -3.62570791666318      3.60974581616456
  Fe  -4.03577725321331     -4.57222389448224      4.12119315403484
  Fe  -6.17468035460329     -6.05811066134073      4.28477810647058
  N   -9.97392121453924    -14.33979798837754      0.73661822419404
  C  -11.09923732068346    -13.48207091396702      0.36808881405788
  C  -11.44135454112770    -13.45921481402517     -1.12179688773704
  O  -10.69290534992907    -13.98671488647181     -1.95251494236076
  C  -10.80916033194580    -12.04367052313277      0.81585399882750
  S   -9.42840262522107    -11.25089201008572     -0.17207888974024
  N   -1.39381560260904     -3.31394606867299      0.86823683955000
  C   -1.25482511915665     -4.66981873577512      1.38089359968719
  C   -1.62533644842548     -5.79718607921077      0.43591041384286
  O   -0.78654398287886     -6.63173285011283      0.07837036242249
  N   -2.87690055395201     -5.77788290967292     -0.00787746665462
  C   -3.44595511571784     -6.86046707350379     -0.78625618363409
  C   -2.60278094173473     -7.33226386376567     -1.95338518163345
  O   -2.32731061472810     -8.53679918732190     -2.07643296389028
  C   -4.80874077458456     -6.45957004151864     -1.32026537106331
  S   -5.86929931485307     -5.87834999804134     -0.18857069662694
  N  -11.08874338830122     -4.12943013330996     -0.54460869866944
  C  -12.21663773043346     -3.77177244801509      0.33066287774038
  C  -12.69320485113729     -2.32095078435491      0.30500583219860
  O  -13.89744868830953     -2.15222224209414      0.06082463068422
  C  -11.94578878659110     -4.10780917860647      1.81528106818145
  S  -11.80601447236325     -5.74062586770615      2.36336938580421
  N    1.31572980027166     -3.20803416793569      4.33590388097819
  C    0.35729279569956     -2.39617711914755      5.07688812227310
  C    0.44773054496734     -2.52961164846664      6.58380093774919
  O    0.97588761983063     -3.52753895820938      7.10257660280615
  C   -1.05039372711048     -2.74925633650470      4.62921332873928
  S   -1.86251460372519     -4.27965270728148      4.98836877014934
  N   -7.18869057143926    -10.81482925157696      4.75667482006817
  C   -6.01058470608409    -10.13620749334254      5.26361867983890
  C   -5.18737498207877    -11.07788215617047      6.13130789460472
  O   -3.96220394419238    -11.24153239652615      5.89520391147588
  C   -6.46176209148925     -8.91902683829696      6.07124744763843
  S   -7.53310979076191     -7.77324407455341      5.01307876557903
  N   -8.53960536820179     -2.65398755984983      6.71448291049762
  C   -9.11458232542849     -1.47434831998502      6.08258041615830
  C  -10.62686609061949     -1.40102272414410      6.05459518408872
  O  -11.18106985340729     -0.30715536036222      6.17876191201441
  C   -8.61078659575122     -1.33137182371262      4.64963743863306
  S   -8.38262762832028     -2.47347169867370      3.59564580452628
  N   -4.44393986644507      0.42686424247857      6.71776225490365
  C   -3.56201363398119      0.13324320803136      5.60322297372025
  C   -3.28900587090958      1.29342762531626      4.65647227582145
  O   -2.30452156609520      1.24868607713876      3.87393831603705
  C   -4.15983008022572     -1.04140222156546      4.83008611348169
  O   -5.61141425794585     -1.04461259589221      4.36501185154567
  S   -7.77030039793698     -5.91982179713791      2.43696105164788
```

```
S   -9.91945944633573     -9.00177630848787      2.57708166653375
S   -4.53149258115732     -3.43816105361588      2.35608528508686
S   -6.67883076755094     -9.05907802148807      1.24116951403259
S   -5.72048707619940     -4.26094935478585      5.60843051694972
S   -9.44353845291276     -7.31523664902239     -0.38019616663052
S   -4.26849006882378     -6.77616467174444      3.24042996848847
H   -1.85094509782679     -4.75729308629084      2.30138769468216
H   -0.21095563319323     -4.85955548174360      1.66305716407441
H   -2.36143683745007     -3.00719519154197      0.98534317254060
H   -1.17088866036528     -3.26979678515803     -0.12424253935785
H   -5.60739680532300     -8.33172290653960      6.41871950144590
H   -7.07432453222253     -9.22249816496904      6.92928162449732
H   -5.33599954373810     -9.77574446939043      4.47165066995143
H   -7.93546776273766    -10.13719465126863      4.58637122908581
H   -6.98849652634901    -11.22863889363709      3.84828986315725
H   -2.56748241079719     -0.24644559883694      5.89241335998381
H   -3.92533835400692      0.69607301409425      7.54876788577732
H   -5.00343817105491     -0.38961760704462      6.94967426548126
H   -9.74904410988466    -14.17008584192431      1.71371617180820
H  -10.22966953837629    -15.32053764367158      0.64502378408542
H  -12.04692922763506    -13.76375578362304      0.88137886038315
H  -12.36679016329728    -12.91588344128307     -1.40459189741010
H  -10.54038905289132    -12.03046704024500      1.87960410515464
H  -11.71108054602039    -11.43112256229008      0.70314213783637
H   -3.57666506813873     -7.74183096305419     -0.14029828275067
H   -2.28849029293018     -6.57576478263639     -2.70284737186105
H   -4.65416437021306     -5.71541873798038     -2.12070603883355
H  -10.95497982240566     -5.14341219548276     -0.45357105820227
H  -10.23228241323000     -3.74397159424440     -0.13948720195403
H  -13.09230585258118     -4.33756754578185     -0.01064918166887
H  -12.00894329001392     -1.48558097999521      0.55657367530138
H  -12.76043742576221     -3.64553004474082      2.40222229408521
H  -11.04295421405512     -3.53916254069371      2.10084162411504
H    0.87541269323170     -4.11891885909124      4.18627829745002
H    2.11886988140854     -3.40575027334023      4.93322433084629
H    0.48149381020602     -1.32923755075860      4.82343508405518
H   -0.04271835008980     -1.74574439029225      7.19950458132516
H   -1.68743981425658     -1.93217252051261      4.99282932478823
H   -1.02993334679359     -2.61058709825455      3.53596489170429
H   -8.05942110182247     -3.22052192599939      6.00821218737181
H   -9.25584599383950     -3.24908850216121      7.12552499382824
H   -8.81609476584326     -0.55011566350358      6.60033939729172
H  -11.19966021752243     -2.33622929987362      5.86490488534863
H   -7.66248263546742     -0.79082467892056      4.81812067623998
H   -4.00224355018099      2.14240902032938      4.65433976469333
H   -5.55102523678760     -1.27713342644425      3.42278159468376
H   -3.54692870281032     -1.24734093730761      3.94748600321363
H   -4.09071224417416     -1.91957145739121      5.48755036275055
H   -5.71066467938978    -11.62505296079408      6.94214176750730
H   -5.22436919554626     -7.34967166733303     -1.81394233718102
H   -9.25230197043143     -0.52885665665011      4.23207622484111
H   -3.53272792846042     -5.10565652264769      0.39635793284802
```

4.2 Active orbitals

The active orbitals for the P^N cluster were prepared with the initial orbitals obtained at the BP86/def2-SVP level with the COSMO solvation model ($\epsilon = 4.0$) for a high-spin state M_S=32/2

with charge -4 using the PYSCF package[32]. The final active orbitals ordered by the genetic ordering method[37] for DMRG are shown in Supplementary Fig. 11. The orbitals in the active space CAS(114e,73o) can be classified as follows:

1. Five $3d$ orbitals of Fe(1): 65, 66, 67, 68, 69
2. Five $3d$ orbitals of Fe(2): 46, 47, 48, 49, 50
3. Five $3d$ orbitals of Fe(3): 41, 42, 43, 44, 45
4. Five $3d$ orbitals of Fe(4): 60, 61, 62, 63, 64
5. Five $3d$ orbitals of Fe(5): 24, 25, 26, 27, 28
6. Five $3d$ orbitals of Fe(6): 29, 30, 31, 32, 33
7. Five $3d$ orbitals of Fe(7): 16, 17, 18, 19, 20
8. Five $3d$ orbitals of Fe(8): 4, 5, 6, 7, 8
9. Twenty-one $3p$ orbitals of seven S atoms in the [Fe_8S_7] core: 10, 11, 12, 13, 14, 15, 21, 22, 23, 34, 35, 38, 51, 52, 53, 54, 55, 56, 57, 58, 59
10. Twelve orbitals of peripheral atoms: 1, 2, 3, 9, 36, 37, 39, 40, 70, 71, 72, 73

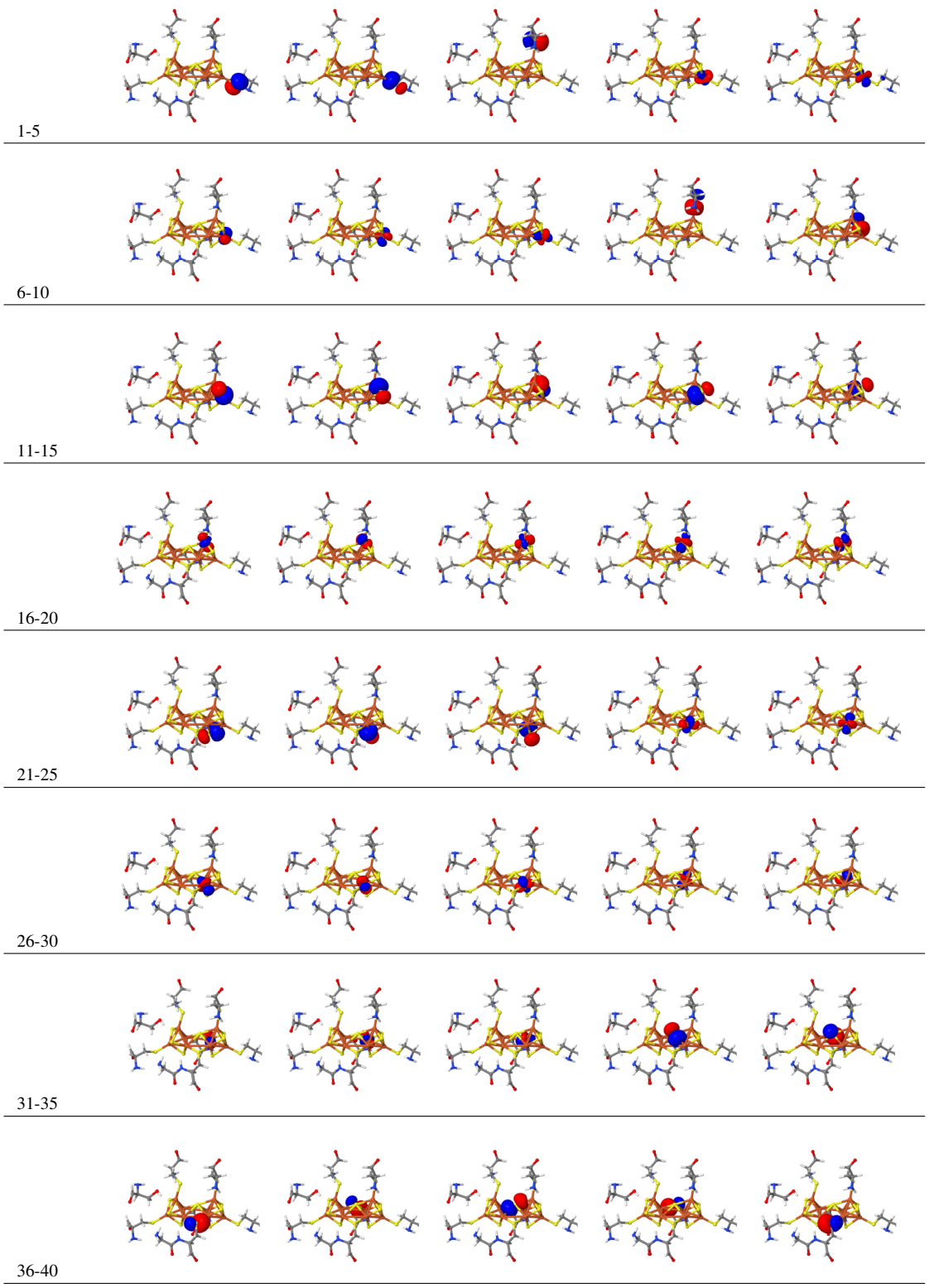

Supplementary Figure 11: Active orbitals of the P^N cluster.

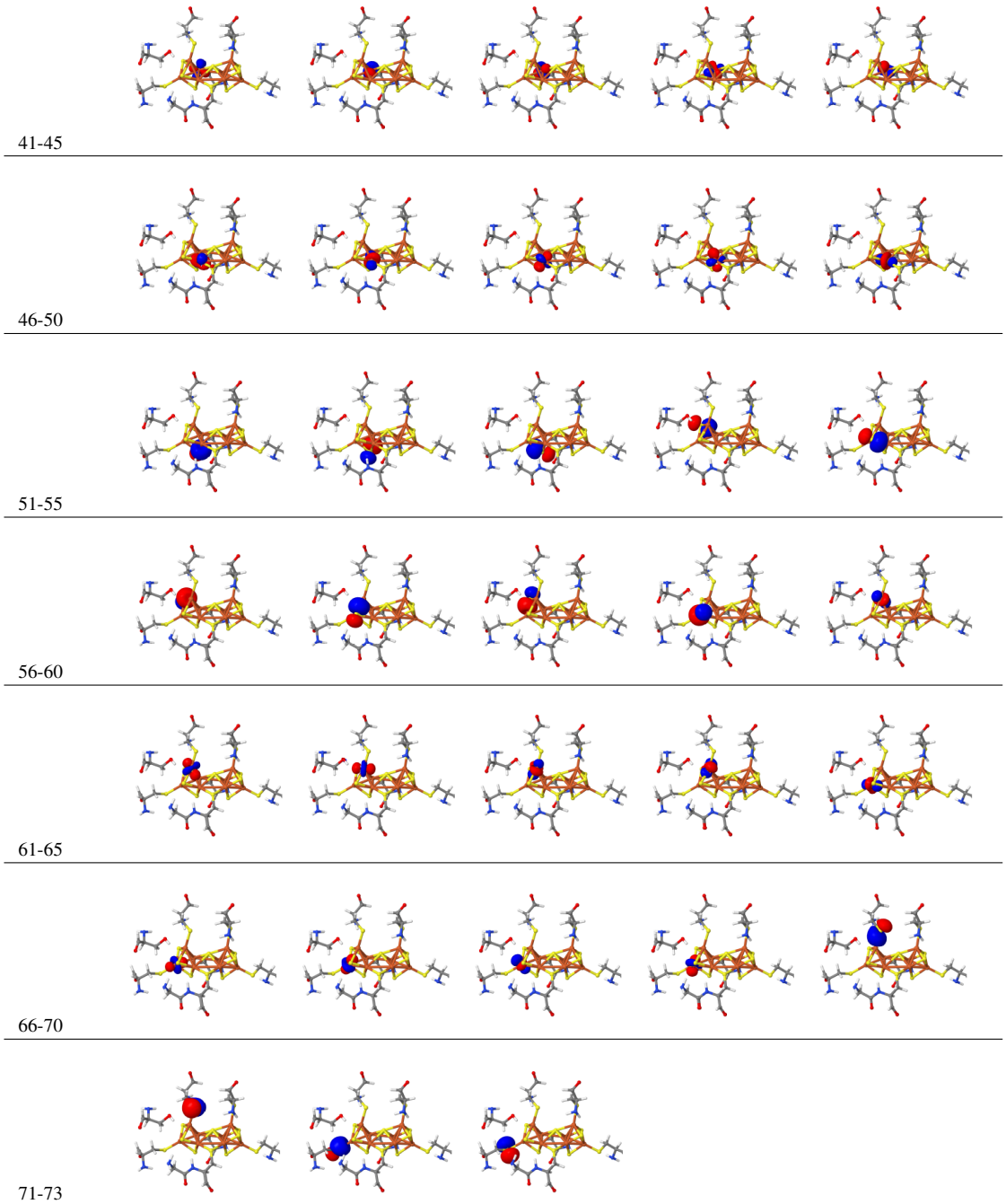

Supplementary Figure 12: Active orbitals of the P^N cluster.

4.3 DMRG results for $S = 0$ states

4.3.1 Initial guesses and DMRG energies

Supplementary Table 5 lists the DMRG results obtained from 35 initial product states for different spin alignments compatible with $S = 0$. The column labeled $E(D = 2000)$ contains the relative DMRG energies $\langle\Psi_{\mathrm{DMRG}}|\hat{H}_{\mathrm{act}}|\Psi_{\mathrm{DMRG}}\rangle$, while the column labeled Eq. (6) contains the relative energies computed using the energy defined by Eq. (6) with $E_{\mathrm{diel}}^{\mathrm{COSMO}}$ updated by the DMRG wavefunction $|\Psi_{\mathrm{DMRG}}\rangle$ at $D = 2000$. It can be seen that the difference between the energies in these two columns is in general less than 0.1kcal/mol. The corresponding spin-spin correlation functions for each state can be found in Supplementary Fig. 13. The energy convergence is shown in Supplementary Fig. 14.

Supplementary Table 5: Relative energies (ΔE in kcal/mol) for states computed from DMRG with different initial guesses for the P^N cluster. The last three columns show the relative energies for the selected low-lying states obtained with larger bond dimensions in a forward schedule, while the energies obtained in a reverse schedule and extrapolated results are shown in Supplementary Table 6.

no.	Fe(III)↑,Fe(II)↑,Fe(III)↓,Fe(II)↓	$D = 1000$	$D = 2000$	Eq. (6)	$D = 3000$	$D = 3500$	$D = 4000$
1	{}, {8, 2, 4, 1}, {}, {7, 5, 6, 3}	10.36	11.72	11.70			
2	{}, {8, 3, 4, 1}, {}, {7, 5, 6, 2}	9.33	10.37	10.32			
3	{}, {8, 3, 2, 1}, {}, {7, 5, 6, 4}	0.00	0.01	0.00	0.00	0.00	0.00
4	{}, {8, 3, 2, 4}, {}, {7, 5, 6, 1}	0.92	0.95	0.90			
5	{}, {8, 6, 4, 1}, {}, {7, 5, 3, 2}	8.17	10.81	10.85			
6	{}, {8, 6, 2, 1}, {}, {7, 5, 3, 4}	7.43	9.33	9.24			
7	{}, {8, 6, 2, 4}, {}, {7, 5, 3, 1}	7.70	9.42	9.33			
8	{}, {8, 6, 3, 1}, {}, {7, 5, 2, 4}	7.70	9.41	9.32			
9	{}, {8, 6, 3, 4}, {}, {7, 5, 2, 1}	7.48	9.34	9.25			
10	{}, {8, 6, 3, 2}, {}, {7, 5, 4, 1}	8.15	10.80	10.85			
11	{}, {8, 5, 4, 1}, {}, {7, 6, 3, 2}	11.27	14.38	14.48			
12	{}, {8, 5, 2, 1}, {}, {7, 6, 3, 4}	10.76	12.99	12.97			
13	{}, {8, 5, 2, 4}, {}, {7, 6, 3, 1}	10.98	13.05	13.04			
14	{}, {8, 5, 3, 1}, {}, {7, 6, 2, 4}	12.06	13.68	13.64			
15	{}, {8, 5, 3, 4}, {}, {7, 6, 2, 1}	12.67	0.49	0.53			
16	{}, {8, 5, 3, 2}, {}, {7, 6, 4, 1}	11.27	14.39	14.49			
17	{}, {8, 5, 6, 1}, {}, {7, 3, 2, 4}	1.49	0.00	0.00			
18	{}, {8, 5, 6, 4}, {}, {7, 3, 2, 1}	1.64	0.94	0.88			
19	{}, {8, 5, 6, 2}, {}, {7, 3, 4, 1}	11.26	10.36	10.32			
20	{}, {8, 5, 6, 3}, {}, {7, 2, 4, 1}	13.55	11.73	11.72			
21	{}, {8, 7, 4, 1}, {}, {5, 6, 3, 2}	6.02	9.43	9.42			
22	{}, {8, 7, 2, 1}, {}, {5, 6, 3, 4}	5.41	7.99	7.86			
23	{}, {8, 7, 2, 4}, {}, {5, 6, 3, 1}	5.72	8.08	7.95			
24	{}, {8, 7, 3, 1}, {}, {5, 6, 2, 4}	5.66	8.07	7.94			
25	{}, {8, 7, 3, 4}, {}, {5, 6, 2, 1}	5.40	7.99	7.86			
26	{}, {8, 7, 3, 2}, {}, {5, 6, 4, 1}	6.04	9.43	9.42			
27	{}, {8, 7, 6, 1}, {}, {5, 3, 2, 4}	3.68	6.09	5.95	6.11	6.41	6.63
28	{}, {8, 7, 6, 4}, {}, {5, 3, 2, 1}	3.78	6.09	5.96			
29	{}, {8, 7, 6, 2}, {}, {5, 3, 4, 1}	12.96	16.42	16.25			
30	{}, {8, 7, 6, 3}, {}, {5, 2, 4, 1}	13.05	17.09	16.97			
31	{}, {8, 7, 5, 1}, {}, {6, 3, 2, 4}	10.52	12.13	12.09			
32	{}, {8, 7, 5, 4}, {}, {6, 3, 2, 1}	10.57	12.13	12.09			
33	{}, {8, 7, 5, 2}, {}, {6, 3, 4, 1}	19.03	21.88	21.83			
34	{}, {8, 7, 5, 3}, {}, {6, 2, 4, 1}	20.42	23.53	23.50			
35	{}, {8, 7, 5, 6}, {}, {3, 2, 4, 1}	13.82	19.38	19.47			

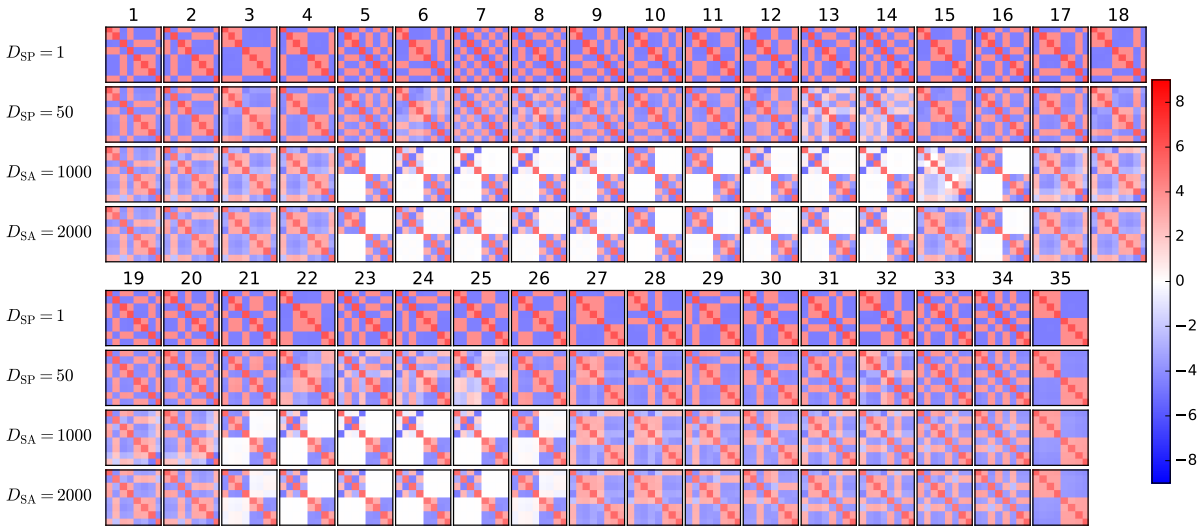

Supplementary Figure 13: Spin-spin correlation functions between the eight Fe atoms for the P^N cluster.

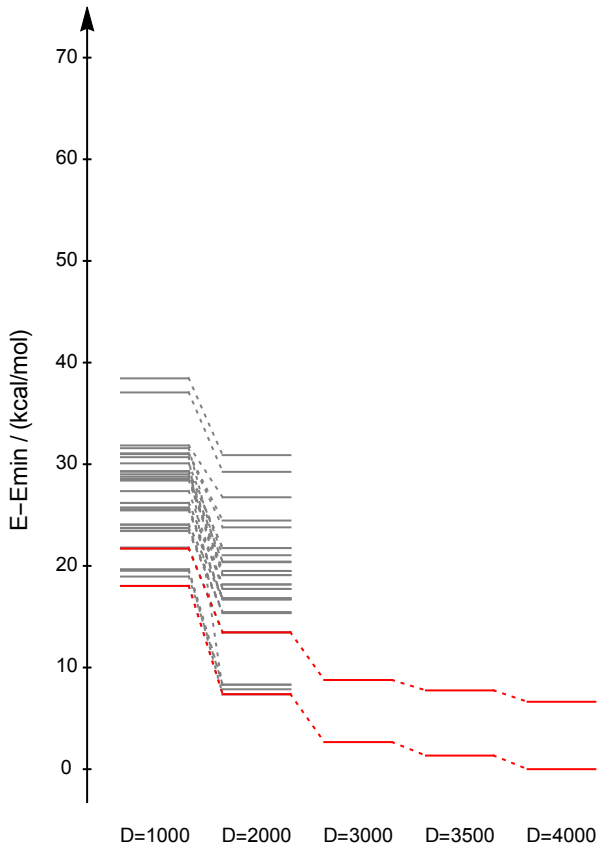

Supplementary Figure 14: Energy convergence for the DMRG states computed starting from different initial guesses of the P^N cluster with progressively increasing bond dimensions D up to $D = 4000$. The lowest two states are highlighted in red. The two states slightly above the ground state obtained at $D = 2000$ are essentially the same as the ground state as shown by the spin-spin correlation function in Supplementary Fig. 13, and they will collapse to the ground state with further optimization steps.

4.3.2 Energy extrapolation

In Supplementary Table 6, the extrapolated energies are shown for the lowest two states (no. 3 and no. 27) obtained in the previous section. The obtained results are shown in Supplementary Fig. 15. In addition, the results for the lowest $S = 1$ state are also shown.

Supplementary Table 6: Total energies (in Hartree) and relative energies ΔE (in kcal/mol) of the lowest two spin isomers of the P^N cluster computed from DMRG with various bond dimensions D in a reverse schedule similar to that for the synthetic $[Fe_8S_7]$ cluster.

no.	D	discarded weight	energy	ΔE
3	3000	2.3×10^{-4}	-17492.213966	0.00
	3500	2.0×10^{-4}	-17492.216321	0.00
	4000	1.6×10^{-4}	-17492.218127	0.00
	extrapolation		-17492.225988	0.00
	error bar		0.99	0.00
27	3000	1.4×10^{-4}	-17492.204232	6.11
	3500	1.2×10^{-4}	-17492.206065	6.44
	4000	1.0×10^{-4}	-17492.207484	6.68
	extrapolation		-17492.216132	6.18
	error bar		1.09	0.20
$S = 1$	3000	2.3×10^{-4}	-17492.211624	1.47
	3500	2.0×10^{-4}	-17492.214105	1.39
	4000	1.7×10^{-4}	-17492.216017	1.32
	extrapolation		-17492.225089	0.56
	error bar		1.14	0.30

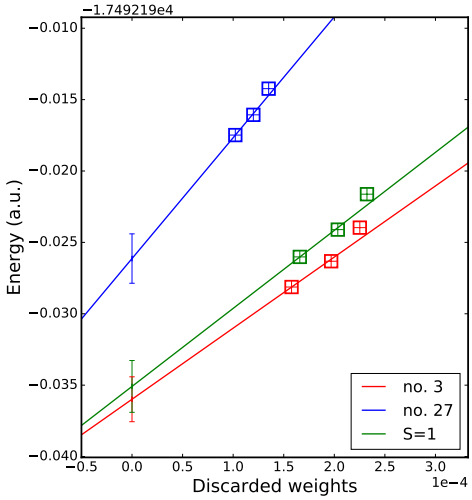

Supplementary Figure 15: Extrapolation of the DMRG energies (in Hartree) versus the discarded weight for the lowest two spin isomers of the P^N cluster. A linear fit of the computed data with D=3000, 3500, and 4000 is used to extrapolate to zero discarded weight, where the intercept is an estimate of the FCI energy ($D = \infty$). The error bars are estimated from an empirical rule $(E_{D=4000} - E_{D=\infty})/5$.

4.3.3 Population analysis

Analysis of the lowest two $S = 0$ states (no. 3 and no. 27) of the P^N cluster is summarized in Supplementary Fig. 16. The local populations and spin-spin correlation functions for Fe atoms of these two states are shown in Supplementary Table 7.

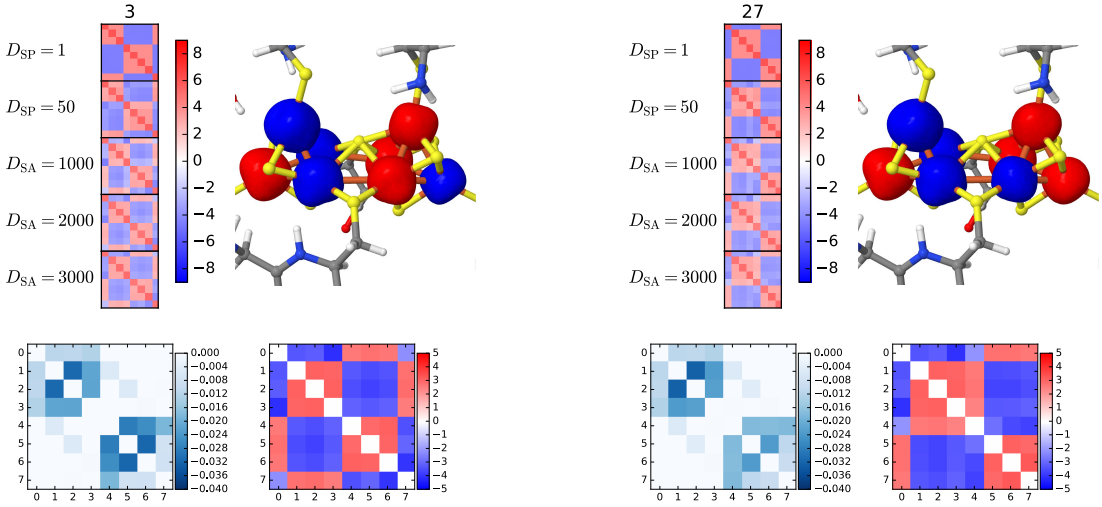

(1) no. 3: $(S_L, S_R) = (3.69, 3.64)$ (2) no. 27: $(S_L, S_R) = (3.70, 3.80)$

Supplementary Figure 16: Analysis of the lowest two $S = 0$ states of the P^N cluster. First row: spin-spin correlation functions $\langle \vec{S}_A \cdot \vec{S}_B \rangle$ between the eight irons and spin-spin correlation density $\sigma_A(\vec{r}) = \langle \vec{S}_A \cdot \sum_B \vec{S}_B(\vec{r}) \rangle$ for the first iron atom. Second row: charge (left) and spin (right) fluctuations among different irons. The effective spins of the left cubane S_L and the right cubane S_R are computed from the expectation values of the local spin-square operators $\langle \hat{S}_L^2 \rangle$ and $\langle \hat{S}_R^2 \rangle$ for the irons on the left and right cubanes, respectively.

Supplementary Table 7: Local populations and spin-spin correlation functions for Fe atoms of the lowest two spin isomers of the P^N cluster. The results were obtained from DMRG with $D = 3000$ in the localized active orbital basis. The effective spin of each iron S_{Fe} was computed from the expectation value of the local spin-square operator $\langle \hat{S}^2_{\mathrm{Fe}} \rangle$. The local S^z_{Fe} are all zero, as the computed states are singlets ($S = 0$).

				$\langle \vec{S}_A \cdot \vec{S}_B \rangle$							
no.	atom	N_{Fe}	S_{Fe}	Fe1	Fe2	Fe3	Fe4	Fe5	Fe6	Fe7	Fe8
3	Fe1	6.33	1.78	4.94	-3.32	-3.18	-4.06	2.61	2.80	2.66	-2.19
	Fe2	6.46	1.77	-3.32	4.89	3.09	3.03	-3.28	-3.51	-3.33	2.74
	Fe3	6.38	1.81	-3.18	3.09	5.09	3.05	-3.44	-3.68	-3.49	2.87
	Fe4	6.35	1.82	-4.06	3.03	3.05	5.14	-3.05	-3.27	-3.10	2.55
	Fe5	6.51	1.73	2.61	-3.28	-3.44	-3.05	4.73	2.91	3.05	-3.41
	Fe6	6.48	1.76	2.80	-3.51	-3.68	-3.27	2.91	4.88	3.04	-3.04
	Fe7	6.33	1.84	2.66	-3.33	-3.49	-3.10	3.05	3.04	5.22	-3.96
	Fe8	6.32	1.77	-2.19	2.74	2.87	2.55	-3.41	-3.04	-3.96	4.91
27	Fe1	6.33	1.78	4.94	-3.34	-3.19	-4.05	-2.08	2.79	2.77	2.64
	Fe2	6.46	1.77	-3.34	4.91	3.11	3.04	2.60	-3.50	-3.48	-3.31
	Fe3	6.38	1.81	-3.19	3.11	5.10	3.06	2.72	-3.67	-3.64	-3.46
	Fe4	6.35	1.82	-4.05	3.04	3.06	5.14	2.43	-3.26	-3.24	-3.09
	Fe5	6.54	1.68	-2.08	2.60	2.72	2.43	4.50	-2.81	-3.55	-3.70
	Fe6	6.48	1.76	2.79	-3.50	-3.67	-3.26	-2.81	4.84	3.06	2.97
	Fe7	6.31	1.84	2.77	-3.48	-3.64	-3.24	-3.55	3.06	5.23	3.25
	Fe8	6.28	1.83	2.64	-3.31	-3.46	-3.09	-3.70	2.97	3.25	5.19

4.3.4 Excited states

The lowest four excited states for the lowest two spin isomers (no. 3 and no. 27) were computed in a state-averaged manner with $D = 2000$ starting from the converged ground state solutions. They are characterized in Supplementary Fig. 17.

no. 3: $\Delta\rho(\vec{r})$	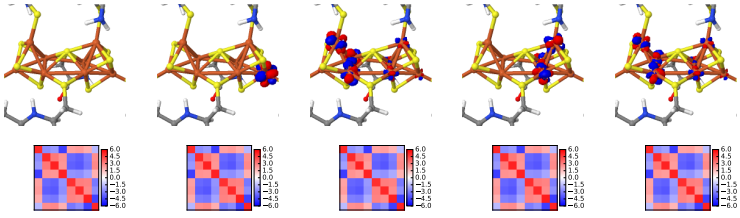				
$\langle \vec{S}_A \cdot \vec{S}_B \rangle$					
ΔE	0.00 (0.00)	2.01 (2.43)	4.69 (4.89)	4.86 (5.16)	5.37 (5.27)
no. 27: $\Delta\rho(\vec{r})$	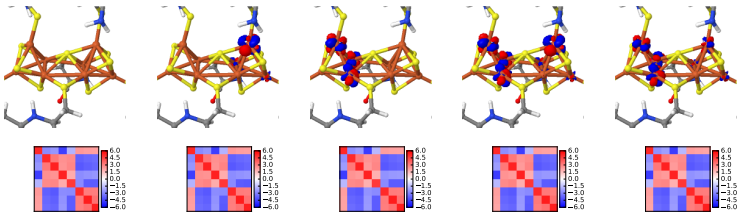				
$\langle \vec{S}_A \cdot \vec{S}_B \rangle$					
ΔE	0.00	1.88	2.53	4.40	4.95

Supplementary Figure 17: Density differences $\Delta\rho(\vec{r})$ with respect to the lowest spin isomer in each case, spin-spin correlation functions $\langle \vec{S}_A \cdot \vec{S}_B \rangle$, and relative energies ΔE (in kcal/mol) for the lowest five states of the lowest two spin isomers of the P^N cluster. Numbers in parentheses are relative energies computed at $D = 3000$ for the lowest spin isomer (no. 3).

5 P^{1+} cluster

5.1 Cartesian coordinates

```
106
p+ model
  Fe  61.86748392689687    -26.30704852154170      2.41281023164788
  Fe  63.46146059474952    -27.25516711637824      1.52807777703291
  Fe  62.75864332158999    -24.96836763849698      0.52849034851247
  Fe  61.42770378324470    -27.27746764705458      0.56203278901969
  Fe  59.17684365303630    -28.78524130385825      1.71874938303604
  Fe  59.85396819185830    -31.49430516178965      3.57861506581195
  Fe  57.82064770709519    -29.63147720439655      3.95525521776204
  Fe  60.11155866169985    -28.14942484425368      4.09373912793806
  N   63.89117419416158    -19.89473795698304      0.51377885298417
  C   65.00229004621055    -20.76065019862769      0.12155882210152
  C   65.30922492161980    -20.71587032905424     -1.36274126439929
  O   64.58704469260674    -20.07841158984895     -2.15475898654885
  C   64.70251744773074    -22.20387353932526      0.50190574018228
  S   63.27085224189918    -22.93593815436681     -0.36488381850127
  N   55.29661879083708    -30.84979733428059      0.76983531794255
  C   55.15674932062765    -29.49683210205508      1.28399736955245
  C   55.46665133181764    -28.38271279373300      0.27923077289715
  O   54.55394102212607    -27.62227054965375     -0.09763722083288
  N   56.72804303261188    -28.33018294757099     -0.18088072037332
  C   57.19426299875759    -27.24990323104883     -1.04484754424686
  C   56.31765401739169    -26.85327490604902     -2.21104635232498
  O   55.98690703687993    -25.65977376985943     -2.39215258520212
  C   58.55221481140390    -27.56997045831200     -1.63596500349772
  S   59.66560836273175    -28.28004117615249     -0.48192844225008
  N   64.98813705819711    -30.10954418325014     -0.71573160478123
  C   66.05283962175653    -30.48144555216838      0.23851617346821
  C   66.58870211920403    -31.92908198555224      0.13636851974045
  O   67.79714161516135    -32.10105272930838     -0.05334190380565
  C   65.61622645488222    -30.12746022572133      1.67967727858258
  S   65.56234854409735    -28.36205610252888      2.02188400951367
  S   61.64399461762319    -28.36935709072162      2.26268728561991
  S   63.49056890123635    -25.32899901428902      2.17496505362937
  S   58.49629708833827    -30.74158000546522      2.27231532429014
  S   61.04270465599647    -25.23120157013476      1.17684967866186
  S   59.62638816475066    -29.97691971794211      5.07855031248339
  S   63.17278020351991    -26.52624176350338     -0.31748296623231
  S   58.18268591030908    -27.73651631624729      3.15087622437703
  N   52.51748260431361    -31.04194776914304      4.19358808643030
  C   53.48017128504343    -31.81780791848224      4.95071062455732
  C   53.42258558500433    -31.62204392002886      6.45469910166023
  O   52.92471370000110    -30.64886335239490      6.94338834261197
  C   54.91737679307832    -31.56180412561193      4.43983647978131
  S   55.73588294732853    -30.01143641981001      4.80445771944486
  N   61.10176752721607    -23.57575871889663      4.53355901121577
  C   59.87766315719867    -24.21721988678024      5.00404074702945
  C   59.03001766297135    -23.25930578122426      5.82582215811554
  O   57.84104555287851    -23.10866519715843      5.56860097706307
  C   60.24524432697250    -25.48650075370530      5.80224884040289
  S   61.37196493131998    -26.52554771979271      4.81685953209285
  N   62.44171777442543    -31.67044595447086      6.47940603132759
  C   62.98969114179835    -32.87936705930444      5.88665317928042
  C   64.53719527680988    -32.89971541732836      5.80699201087931
  O   65.13994595193537    -33.94250511802691      5.92478106044078
  C   62.37279211015338    -33.19086501713861      4.51885582299938
  S   62.18721128866304    -31.86261620123751      3.32670908541684
```

```
N   58.41059886307610   -34.80372917818858     6.51518237528166
C   57.50368794864223   -34.44527081794732     5.42076691699540
C   57.20545116939657   -35.63264826522276     4.48546288715410
O   56.12904794525260   -35.69721389637667     3.84454060349020
C   58.00498009865606   -33.16303119827119     4.64327625147290
O   59.22892949187861   -33.28028467885630     3.96671915194895
H   55.79610095322890   -29.39054025704814     2.16988514909024
H   54.12406423066990   -29.31376880181362     1.60523696359325
H   56.26551380434027   -31.15910900494962     0.85809663802512
H   55.02873016362717   -30.91067524375900    -0.20972840994382
H   63.76410385592104   -19.96647374456891     1.52071389202298
H   64.11202060402364   -18.92451561710491     0.29846143662248
H   65.96089376630827   -20.50845598878440     0.63056494596520
H   66.18582856057462   -21.30512155154693    -1.70126052850092
H   64.53923510704961   -22.26136284618527     1.58829712673325
H   65.59281116585271   -22.81363738680147     0.29448280543987
H   57.28852614793919   -26.34192423114970    -0.43174991791762
H   56.03374536561479   -27.65913365488904    -2.92040372361016
H   58.97786492283364   -26.64469627546383    -2.03856085253077
H   58.44002819489065   -28.27747795465064    -2.46987095807118
H   64.83488260277154   -29.10543966982254    -0.56783960806075
H   64.11563040165157   -30.53935541741487    -0.40037449958423
H   66.93526310198754   -29.87539737267935    -0.00385774571686
H   65.88903520447177   -32.77982923184911     0.27817519147080
H   66.32521675730698   -30.56982909998297     2.39820997750561
H   64.64049703153064   -30.59091505042736     1.88640171982668
H   52.94383788390883   -30.13282399970509     4.00076291295489
H   51.71612180887733   -30.82944805064431     4.78836867999911
H   53.31808774894941   -32.89492427090361     4.76304119795607
H   53.92451614140153   -32.40685409946268     7.06944510058499
H   55.53109805883612   -32.38045762910180     4.82733676299868
H   54.87622360655917   -31.70067557391543     3.34969674497949
H   61.75695743641460   -24.29768059723450     4.22053078889202
H   60.89431749255880   -23.02900778223647     3.69968004016295
H   59.22505554032372   -24.55419957237894     4.18075277067290
H   59.54534615090810   -22.70235855551285     6.64074445923526
H   60.76168844731163   -25.22056569226276     6.73423367051205
H   59.33675537798172   -26.04654835050110     6.04782116325691
H   62.11149417984951   -31.05554852454161     5.72908267545082
H   63.14450961521705   -31.15703989533779     7.00720415504627
H   62.76647117564837   -33.75796157323268     6.51596384544334
H   65.05103326000818   -31.92328767495847     5.64279782437698
H   61.36833117969618   -33.59596884586406     4.70302870128349
H   62.95969255412702   -34.00600531031873     4.07332674301937
H   59.36051211204326   -34.76150330844367     6.13765358740593
H   58.37702138424601   -34.04783140053665     7.19889974084839
H   56.52980032120377   -34.16416426310510     5.84583027411139
H   57.98393011829694   -36.41736525042803     4.38729315947468
H   58.02479582563021   -32.36501767760031     5.41087308255301
H   57.20775142577418   -32.89185654694577     3.92959743374589
H   57.37428646296175   -29.07959287701428     0.05447207179171
```

5.2 Active orbitals

The active orbitals for the P^{1+} cluster were prepared with the initial orbitals obtained at the B3LYP[44, 45, 46]/def2-SVP level with the COSMO solvation model ($\epsilon = 4.0$) for a high-spin

state M_S=33/2 with charge -4. (Unlike for P^N and P^{OX}, no converged BP86 solution could be found even when starting from the converged B3LYP solution). The final active orbitals ordered by the genetic ordering method[37] for DMRG were shown in Supplementary Fig. 30. The orbitals in the active space CAS(117e,75o) can be classified as follows:

1. Five $3d$ orbitals of Fe(1): 60, 61, 62, 63, 64
2. Five $3d$ orbitals of Fe(2): 46, 47, 48, 49, 50
3. Five $3d$ orbitals of Fe(3): 41, 42, 43, 44, 45
4. Five $3d$ orbitals of Fe(4): 67, 68, 69, 70, 71
5. Five $3d$ orbitals of Fe(5): 29, 30, 31, 32, 33
6. Five $3d$ orbitals of Fe(6): 24, 25, 26, 27, 28
7. Five $3d$ orbitals of Fe(7): 17, 18, 19, 20, 21
8. Five $3d$ orbitals of Fe(8): 5, 6, 7, 8, 9
9. Twenty-one $3p$ orbitals of seven S atoms in the [Fe_8S_7] core: 10, 11, 12, 13, 14, 15, 16, 22, 23, 34, 35, 36, 51, 52, 53, 54, 55, 56, 57, 58, 59
10. Fourteen orbitals of peripheral atoms: 1, 2, 3, 4, 37, 38, 39, 40, 65, 66, 72, 73, 74, 75

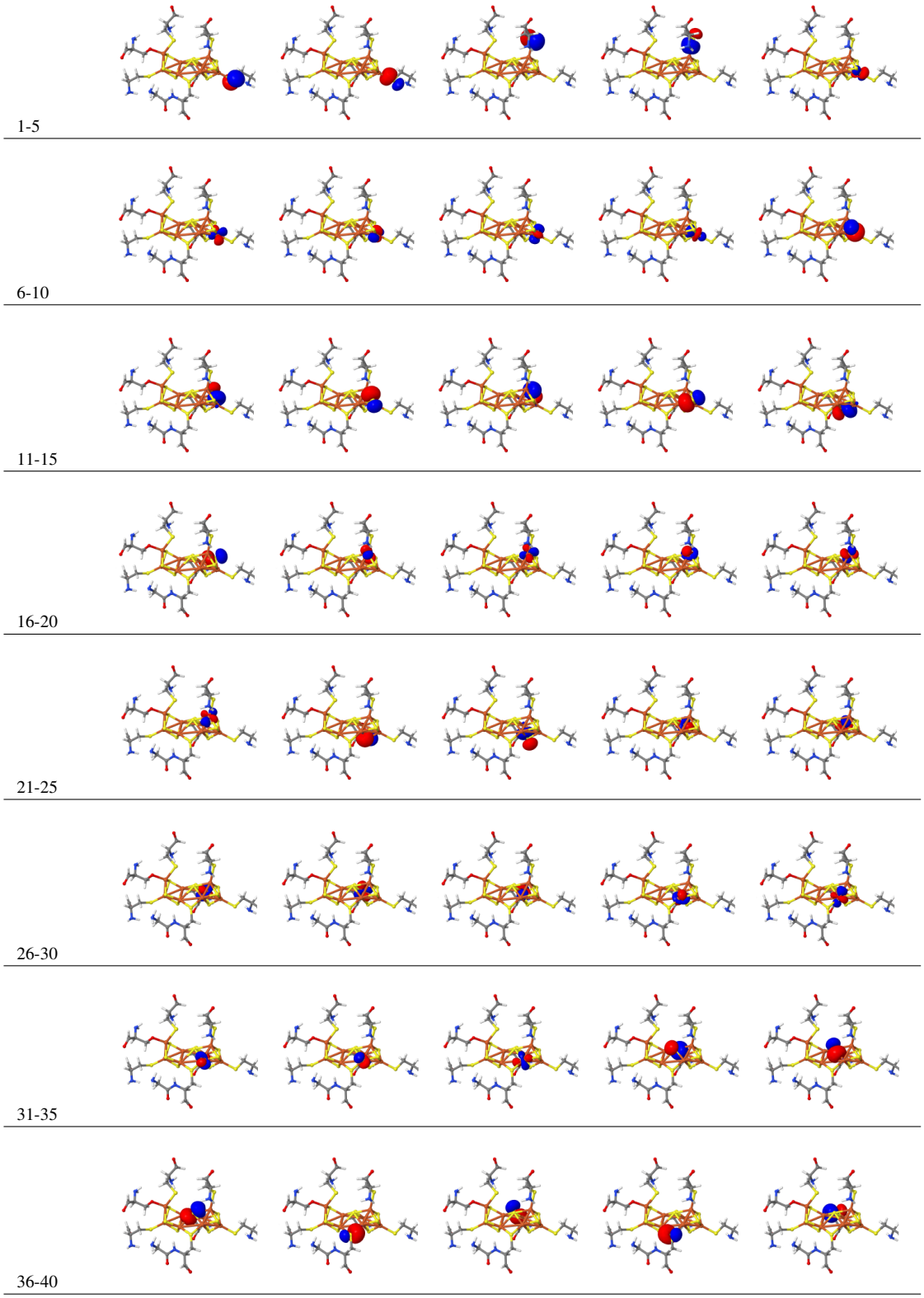

Supplementary Figure 18: Active orbitals of the P^{1+} cluster.

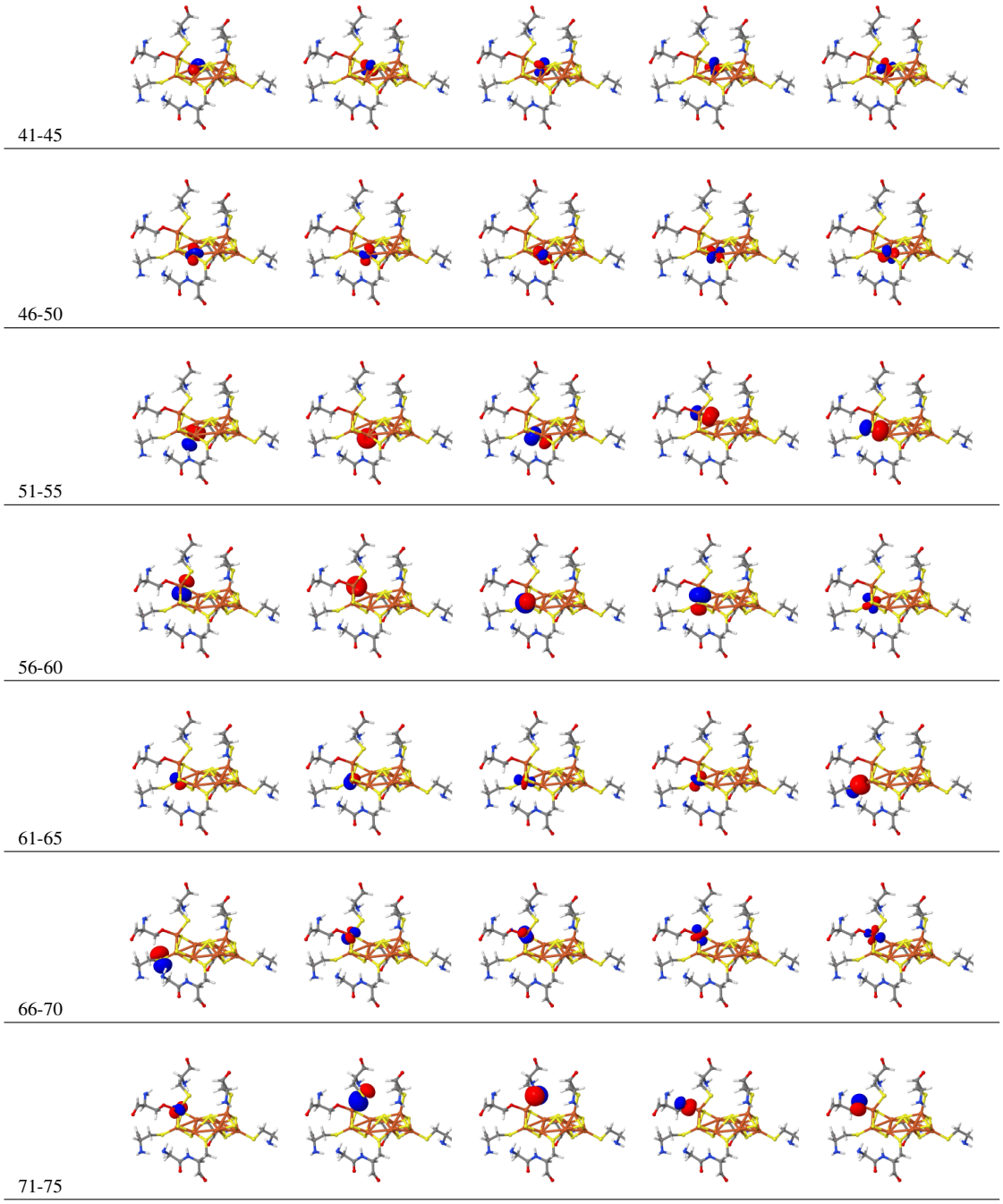

Supplementary Figure 19: Active orbitals of the P^{1+} cluster.

5.3 DMRG results for $S = 1/2$ states

5.3.1 Initial guesses and DMRG energies

Supplementary Table 8 lists the DMRG results obtained from 35 initial product states for different spin alignments compatible with $S = 1/2$. The corresponding spin-spin correlation functions for each state can be found in Supplementary Fig. 20. The energy convergence is shown in Supplementary Fig. 21.

Supplementary Table 8: Relative energies (ΔE in kcal/mol) for the states computed from DMRG with different initial guesses for the $S = 1/2$ states of the P^{1+} cluster. The last three columns show the relative energies for the selected low-lying states obtained with larger bond dimensions in a forward sweep schedule, while the energies obtained in a reverse sweep schedule and extrapolated results are shown in Supplementary Table 9.

no.	Fe(III)↑,Fe(II)↑,Fe(III)↓,Fe(II)↓	$D = 1000$	$D = 2000$	Eq. (6)	$D = 3000$	$E = 3500$	$D = 4000$
1	{4}, {3, 2, 1}, {}, {8, 7, 6, 5}	25.79	44.36	44.52			
2	{4}, {5, 2, 1}, {}, {8, 7, 6, 3}	27.84	28.80	28.76			
3	{4}, {5, 3, 1}, {}, {8, 7, 6, 2}	27.38	28.36	28.30			
4	{4}, {5, 3, 2}, {}, {8, 7, 6, 1}	27.68	29.51	29.38			
5	{4}, {6, 2, 1}, {}, {8, 7, 5, 3}	32.13	25.15	25.11			
6	{4}, {6, 3, 1}, {}, {8, 7, 5, 2}	30.90	24.48	24.42			
7	{4}, {6, 3, 2}, {}, {8, 7, 5, 1}	31.95	26.08	25.95			
8	{4}, {6, 5, 1}, {}, {8, 7, 3, 2}	23.97	23.12	23.05			
9	{4}, {6, 5, 2}, {}, {8, 7, 3, 1}	35.83	34.54	34.41			
10	{4}, {6, 5, 3}, {}, {8, 7, 2, 1}	36.78	35.61	35.42			
11	{4}, {7, 2, 1}, {}, {8, 6, 5, 3}	29.83	12.70	12.68			
12	{4}, {7, 3, 1}, {}, {8, 6, 5, 2}	26.06	12.28	12.25			
13	{4}, {7, 3, 2}, {}, {8, 6, 5, 1}	23.08	15.37	15.33			
14	{4}, {7, 5, 1}, {}, {8, 6, 3, 2}	26.37	23.49	23.53			
15	{4}, {7, 5, 2}, {}, {8, 6, 3, 1}	37.95	35.34	35.31			
16	{4}, {7, 5, 3}, {}, {8, 6, 2, 1}	38.50	36.06	35.99			
17	{4}, {7, 6, 1}, {}, {8, 5, 3, 2}	21.57	19.29	19.22			
18	{4}, {7, 6, 2}, {}, {8, 5, 3, 1}	33.54	27.52	27.42			
19	{4}, {7, 6, 3}, {}, {8, 5, 2, 1}	33.57	31.54	31.39			
20	{4}, {7, 6, 5}, {}, {8, 3, 2, 1}	9.26	8.07	8.02			
21	{4}, {8, 2, 1}, {}, {7, 6, 5, 3}	1.90	0.56	0.57	0.01		
22	{4}, {8, 3, 1}, {}, {7, 6, 5, 2}	0.00	0.00	0.00	0.00	0.00	0.00
23	{4}, {8, 3, 2}, {}, {7, 6, 5, 1}	0.96	1.31	1.24	1.17	1.06	0.88
24	{4}, {8, 5, 1}, {}, {7, 6, 3, 2}	25.92	21.03	21.00			
25	{4}, {8, 5, 2}, {}, {7, 6, 3, 1}	36.99	29.90	29.80			
26	{4}, {8, 5, 3}, {}, {7, 6, 2, 1}	38.84	33.69	33.53			
27	{4}, {8, 6, 1}, {}, {7, 5, 3, 2}	30.29	25.40	25.29			
28	{4}, {8, 6, 2}, {}, {7, 5, 3, 1}	42.37	38.62	38.55			
29	{4}, {8, 6, 3}, {}, {7, 5, 2, 1}	41.51	39.49	39.40			
30	{4}, {8, 6, 5}, {}, {7, 3, 2, 1}	33.28	18.54	18.43			
31	{4}, {8, 7, 1}, {}, {6, 5, 3, 2}	25.05	23.56	23.53			
32	{4}, {8, 7, 2}, {}, {6, 5, 3, 1}	41.79	35.07	34.98			
33	{4}, {8, 7, 3}, {}, {6, 5, 2, 1}	34.01	35.12	35.01			
34	{4}, {8, 7, 5}, {}, {6, 3, 2, 1}	30.42	20.80	20.72			
35	{4}, {8, 7, 6}, {}, {5, 3, 2, 1}	27.32	29.51	29.39			

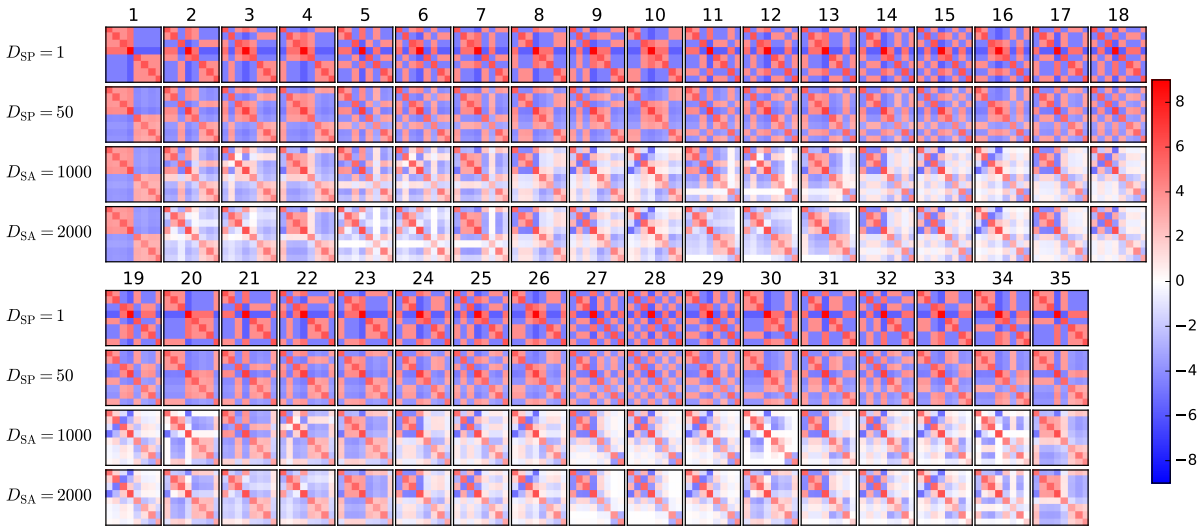

Supplementary Figure 20: Spin-spin correlation functions between the eight Fe atoms for the $S = 1/2$ states of the P^{1+} cluster.

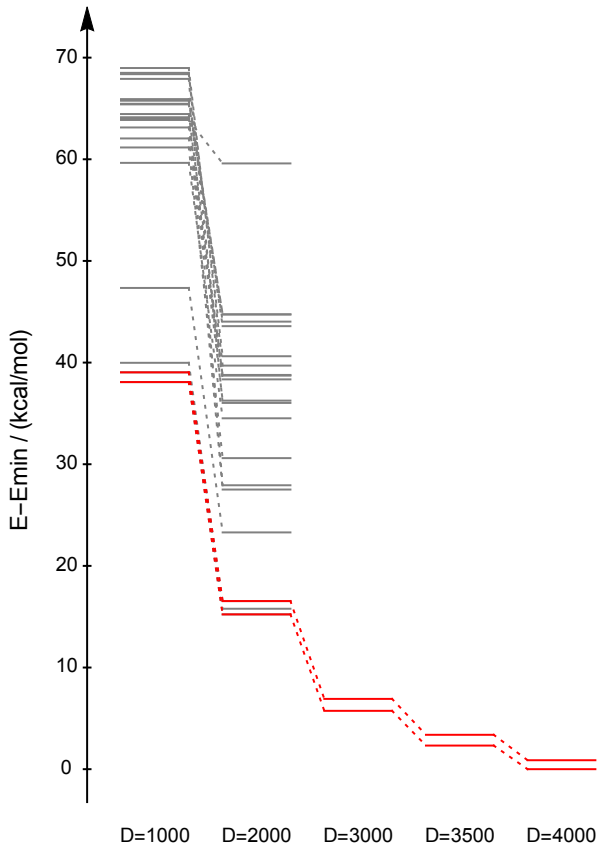

Supplementary Figure 21: Energy convergence for the $S = 1/2$ DMRG states computed starting from different initial guesses of the P^{1+} cluster with progressively increasing bond dimensions D up to $D = 4000$. The lowest two states are highlighted in red.

5.3.2 Energy extrapolation

In Supplementary Table 9 and Supplementary Fig. 22, the extrapolated energies are shown for the lowest two states (no. 22 and no. 23) obtained in the previous section.

Supplementary Table 9: Total energies (in Hartree) and relative energies ΔE (in kcal/mol) of the lowest two spin isomers of the P^{1+} cluster with $S = 1/2$ computed from DMRG with various bond dimensions D in a reverse sweep schedule.

no.	D	discarded weight	energy	ΔE
22	3000	6.1×10^{-4}	-17491.257991	0.00
	3500	5.2×10^{-4}	-17491.262678	0.00
	4000	4.3×10^{-4}	-17491.266319	0.00
	extrapolation		-17491.285228	0.00
	error bar		2.37	0.00
23	3000	6.1×10^{-4}	-17491.256626	0.86
	3500	5.2×10^{-4}	-17491.261335	0.84
	4000	4.3×10^{-4}	-17491.265031	0.81
	extrapolation		-17491.284152	0.68
	error bar		2.40	0.05

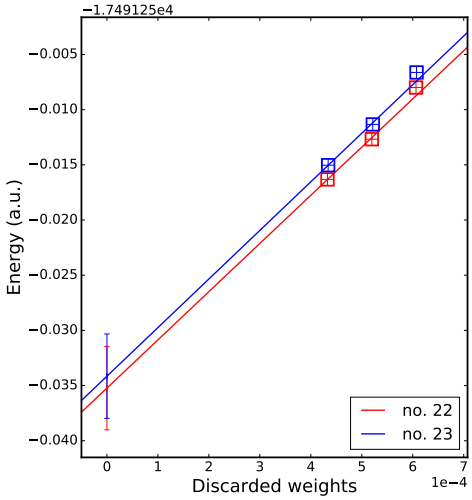

Supplementary Figure 22: Extrapolation of the DMRG energies (in Hartree) versus the discarded weight for the lowest two spin isomers of the P^{1+} cluster with $S = 1/2$. A linear fit of the computed data with D=3000, 3500, and 4000 is used to extrapolate to zero discarded weight, where the intercept is an estimate of the FCI energy ($D = \infty$). The error bars were estimated from an empirical rule $(E_{D=4000} - E_{D=\infty})/5$.

5.3.3 Population analysis

Analysis of the lowest two $S = 1/2$ states (no. 22 and no. 23) of the P^{1+} cluster is summarized in Supplementary Fig. 23. The local populations and spin-spin correlation functions for Fe atoms of these two states are shown in Supplementary Table 10. We observe that the values of N_{Fe} for irons on the right cubane are much larger than those for the corresponding irons in P^{N} and P^{OX} . This can be attributed to the more compressed structure of the right cubane.

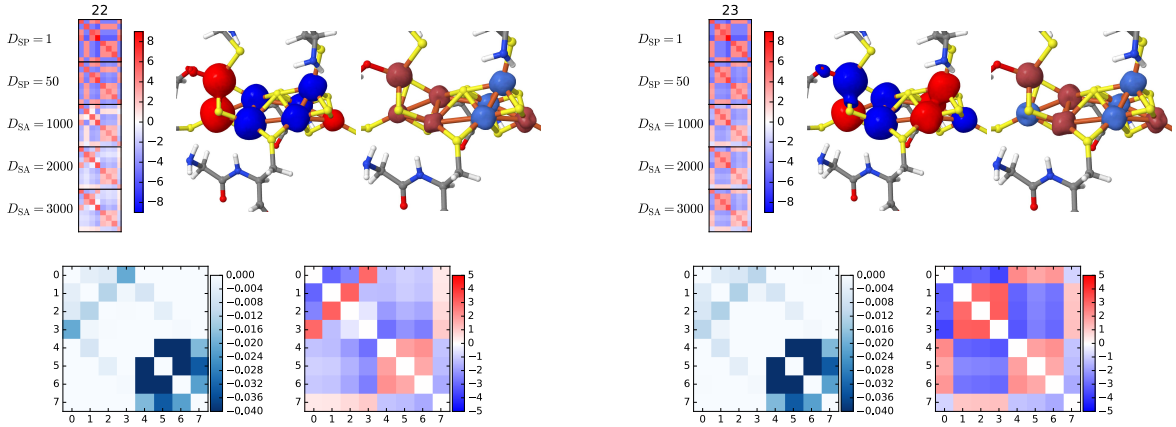

(1) no. 22: $(S_L, S_R) = (4.14, 3.84)$ (2) no. 23: $(S_L, S_R) = (4.12, 3.84)$

Supplementary Figure 23: Analysis of the lowest two $S = 1/2$ states of the P^{1+} cluster. First row: spin-spin correlation functions $\langle \vec{S}_A \cdot \vec{S}_B \rangle$ between the eight irons and spin-spin correlation density $\sigma_A(\vec{r}) = \langle \vec{S}_A \cdot \sum_B \vec{S}_B(\vec{r}) \rangle$ for the first iron atom. Second row: charge (left) and spin (right) fluctuations among different irons. The effective spins of the left cubane S_L and the right cubane S_R are computed from the expectation values of local spin-square operators $\langle \hat{S}_L^2 \rangle$ and $\langle \hat{S}_R^2 \rangle$ for the irons on the left and right cubanes, respectively.

Supplementary Table 10: Local populations and spin-spin correlation functions for Fe atoms of the lowest two spin isomers of the $S = 1/2$ states of the P^{1+} cluster. The results were obtained from DMRG with $D = 3000$ in the localized active orbital basis. The effective spin of each iron S_{Fe} was computed from the expectation value of the local spin-square operator $\langle \hat{S}^2_{\mathrm{Fe}} \rangle$. The local S^z_{Fe} values were computed for the high-spin states ($M_S = S$).

					$\langle \vec{S}_A \cdot \vec{S}_B \rangle$							
no.	atom	N_{Fe}	S_{Fe}	S^z_{Fe}	Fe1	Fe2	Fe3	Fe4	Fe5	Fe6	Fe7	Fe8
22	Fe1	6.24	1.87	0.25	5.38	-2.98	-2.29	3.09	-1.32	-1.02	-1.21	0.54
	Fe2	6.33	1.82	0.27	-2.98	5.14	3.22	-1.11	-1.46	-1.12	-1.31	0.59
	Fe3	6.25	1.86	0.41	-2.29	3.22	5.34	-0.27	-2.17	-1.66	-1.95	0.87
	Fe4	6.00	2.01	0.59	3.09	-1.11	-0.27	6.05	-3.10	-2.39	-2.82	1.26
	Fe5	6.63	1.68	-0.52	-1.32	-1.46	-2.17	-3.10	4.48	2.08	2.45	-1.36
	Fe6	6.91	1.43	-0.42	-1.02	-1.12	-1.66	-2.39	2.08	3.46	1.93	-1.46
	Fe7	6.57	1.66	-0.53	-1.21	-1.31	-1.95	-2.82	2.45	1.93	4.40	-1.85
	Fe8	6.67	1.21	0.38	0.54	0.59	0.87	1.26	-1.36	-1.46	-1.85	2.66
23	Fe1	6.29	1.77	-0.48	4.91	-3.46	-3.36	-3.98	2.52	1.94	2.28	-1.02
	Fe2	6.33	1.83	0.63	-3.46	5.18	3.32	3.58	-3.36	-2.58	-3.04	1.36
	Fe3	6.26	1.87	0.66	-3.36	3.32	5.35	3.65	-3.50	-2.69	-3.16	1.41
	Fe4	5.96	2.03	0.69	-3.98	3.58	3.65	6.14	-3.66	-2.82	-3.32	1.48
	Fe5	6.63	1.67	-0.51	2.52	-3.36	-3.50	-3.66	4.48	2.07	2.44	-1.34
	Fe6	6.91	1.42	-0.42	1.94	-2.58	-2.69	-2.82	2.07	3.45	1.93	-1.45
	Fe7	6.57	1.66	-0.52	2.28	-3.04	-3.16	-3.32	2.44	1.93	4.40	-1.85
	Fe8	6.67	1.20	0.39	-1.02	1.36	1.41	1.48	-1.34	-1.45	-1.85	2.65

5.3.4 Excited states

The lowest four excited states of the lowest two spin isomers (no. 22 and no. 23) were computed in a state-averaged manner with $D = 2000$, starting from the converged ground state solutions. They are characterized in Supplementary Fig. 24.

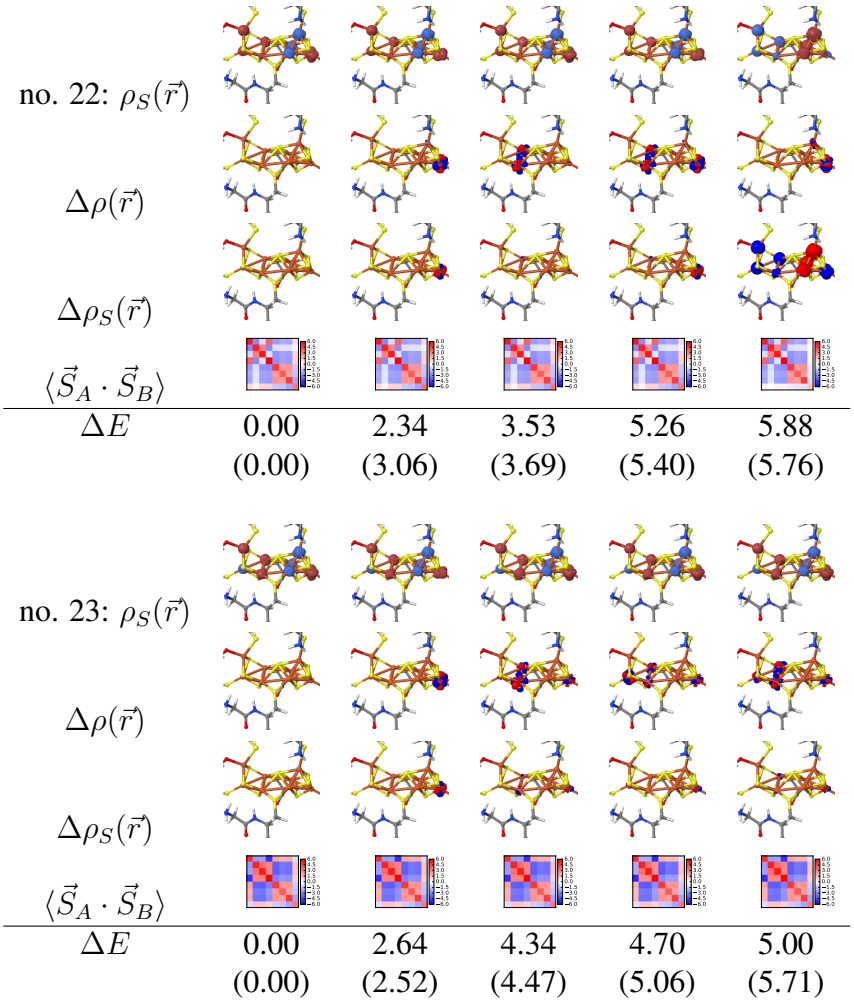

Supplementary Figure 24: Spin densities $\rho_S(\vec{r})$, density differences $\Delta\rho(\vec{r})$, spin density differences $\Delta\rho_S(\vec{r})$, spin-spin correlation functions $\langle \vec{S}_A \cdot \vec{S}_B \rangle$, and relative energies ΔE (in kcal/mol) for the lowest five states of the lowest two spin isomers with $S = 1/2$ of the P^{1+} cluster. Numbers in parentheses are relative energies computed at $D = 3000$ for the lowest two spin isomers (no. 22 and no. 23).

5.4 DMRG results for $S = 5/2$ states

5.4.1 Initial guesses and DMRG energies

Supplementary Table 11 lists the DMRG results obtained from 35 initial product states for different spin alignments compatible with $S = 5/2$. The corresponding spin-spin correlation functions for each state are shown in Supplementary Fig. 25. The energy convergence is shown in Supplementary Fig. 26.

Supplementary Table 11: Relative energies (ΔE in kcal/mol) for the states computed from DMRG with different initial guesses for $S = 5/2$ states of the P^{1+} cluster. The last three columns show the relative energies for the selected low-lying states obtained with larger bond dimensions in a forward sweep schedule, while the energies obtained in a reverse sweep schedule and extrapolated results are shown in Supplementary Table 12.

no.	Fe(III)↑,Fe(II)↑,Fe(III)↓,Fe(II)↓	$D = 1000$	$D = 2000$	Eq. (6)	$D = 3000$	$D = 3500$	$D = 4000$
1	{4}, {3, 2, 1}, {}, {8, 7, 6, 5}	0.00	2.26	2.22	12.44	14.50	-
2	{4}, {5, 2, 1}, {}, {8, 7, 6, 3}	22.13	13.98	14.00			
3	{4}, {5, 3, 1}, {}, {8, 7, 6, 2}	20.75	13.51	13.52			
4	{4}, {5, 3, 2}, {}, {8, 7, 6, 1}	21.00	14.68	14.61			
5	{4}, {6, 2, 1}, {}, {8, 7, 5, 3}	9.87	4.67	4.64			
6	{4}, {6, 3, 1}, {}, {8, 7, 5, 2}	24.01	10.01	10.01			
7	{4}, {6, 3, 2}, {}, {8, 7, 5, 1}	25.99	12.91	12.81			
8	{4}, {6, 5, 1}, {}, {8, 7, 3, 2}	11.38	6.70	6.70			
9	{4}, {6, 5, 2}, {}, {8, 7, 3, 1}	29.39	21.27	21.24			
10	{4}, {6, 5, 3}, {}, {8, 7, 2, 1}	25.44	19.43	19.32			
11	{4}, {7, 2, 1}, {}, {8, 6, 5, 3}	9.37	4.63	4.60	10.53	-	-
12	{4}, {7, 3, 1}, {}, {8, 6, 5, 2}	7.40	3.97	3.93	10.52	11.10	-
13	{4}, {7, 3, 2}, {}, {8, 6, 5, 1}	11.02	5.34	5.24	11.72	12.21	-
14	{4}, {7, 5, 1}, {}, {8, 6, 3, 2}	17.19	0.00	0.00	0.00	0.00	0.00
15	{4}, {7, 5, 2}, {}, {8, 6, 3, 1}	19.64	11.10	11.00			
16	{4}, {7, 5, 3}, {}, {8, 6, 2, 1}	31.85	19.33	19.15			
17	{4}, {7, 6, 1}, {}, {8, 5, 3, 2}	23.64	4.71	4.71			
18	{4}, {7, 6, 2}, {}, {8, 5, 3, 1}	27.27	14.33	14.29			
19	{4}, {7, 6, 3}, {}, {8, 5, 2, 1}	27.65	15.88	15.82			
20	{4}, {7, 6, 5}, {}, {8, 3, 2, 1}	18.94	8.44	8.46			
21	{4}, {8, 2, 1}, {}, {7, 6, 5, 3}	19.04	7.81	7.90			
22	{4}, {8, 3, 1}, {}, {7, 6, 5, 2}	11.65	4.04	4.01			
23	{4}, {8, 3, 2}, {}, {7, 6, 5, 1}	17.12	6.97	6.91			
24	{4}, {8, 5, 1}, {}, {7, 6, 3, 2}	34.02	24.30	24.29			
25	{4}, {8, 5, 2}, {}, {7, 6, 3, 1}	52.61	17.20	17.13			
26	{4}, {8, 5, 3}, {}, {7, 6, 2, 1}	31.92	10.78	10.74			
27	{4}, {8, 6, 1}, {}, {7, 5, 3, 2}	23.98	11.84	11.82			
28	{4}, {8, 6, 2}, {}, {7, 5, 3, 1}	31.04	22.61	22.52			
29	{4}, {8, 6, 3}, {}, {7, 5, 2, 1}	21.57	3.93	3.85	7.68	7.31	6.76
30	{4}, {8, 6, 5}, {}, {7, 3, 2, 1}	27.01	12.17	12.10			
31	{4}, {8, 7, 1}, {}, {6, 5, 3, 2}	15.57	10.94	10.87			
32	{4}, {8, 7, 2}, {}, {6, 5, 3, 1}	30.74	18.07	18.08			
33	{4}, {8, 7, 3}, {}, {6, 5, 2, 1}	26.44	19.46	19.34			
34	{4}, {8, 7, 5}, {}, {6, 3, 2, 1}	25.98	9.56	9.52			
35	{4}, {8, 7, 6}, {}, {5, 3, 2, 1}	20.76	14.67	14.61			

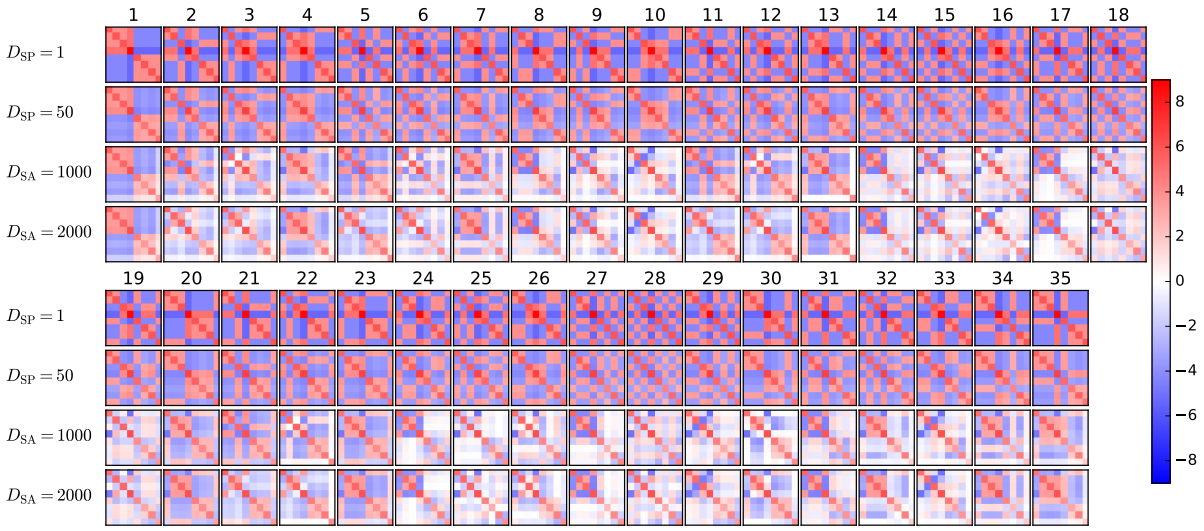

Supplementary Figure 25: Spin-spin correlation functions between the eight Fe atoms for the $S = 5/2$ states of the P^{1+} cluster.

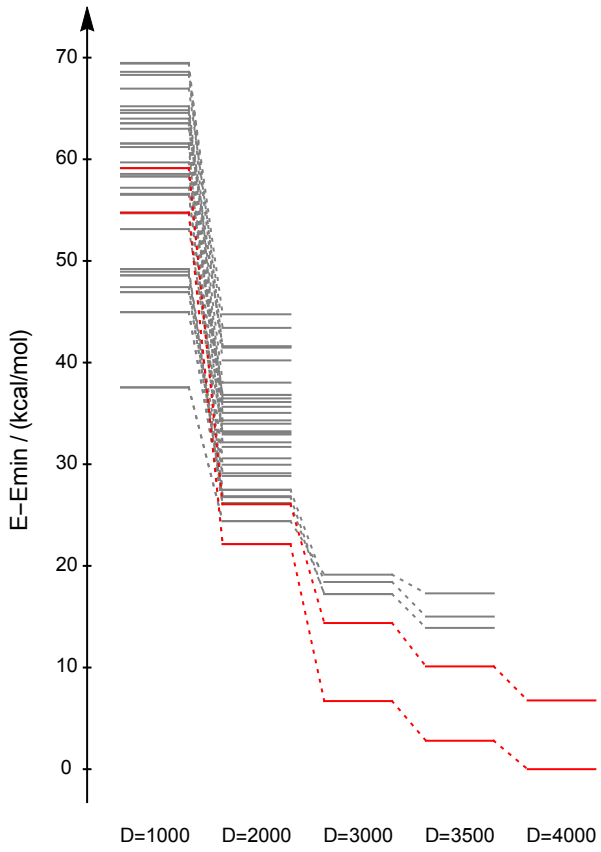

Supplementary Figure 26: Energy convergence for the $S = 5/2$ DMRG states computed starting from different initial guesses of the P^{1+} cluster with progressively increasing bond dimensions D up to $D = 4000$. The lowest two states are highlighted in red.

5.4.2 Energy extrapolation

In Supplementary Table 12 and Supplementary Fig. 27, the extrapolated energies are shown for the lowest two states (no. 14 and no. 29) obtained in the previous section.

Supplementary Table 12: Total energies (in Hartree) and relative energies ΔE (in kcal/mol) of the lowest two spin isomers of the P^{1+} cluster with $S = 5/2$ computed from DMRG with various bond dimensions D in a reverse sweep schedule.

no.	D	discarded weight	energy	ΔE
14	3000	7.1×10^{-4}	-17491.250047	0.00 (4.99[a])
	3500	6.4×10^{-4}	-17491.255270	0.00 (4.65[a])
	4000	5.6×10^{-4}	-17491.259446	0.00 (4.31[a])
	extrapolation		-17491.289540	0.00 (-2.71[a])
	error bar		3.78	0.00 (2.81)
29	3000	4.5×10^{-4}	-17491.240775	5.82
	3500	4.1×10^{-4}	-17491.245219	6.31
	4000	3.7×10^{-4}	-17491.248738	6.72
	extrapolation		-17491.278751	6.77
	error bar		3.77	0.02

[a] Relative to the $S = 1/2$ ground state in Supplementary Table 9.

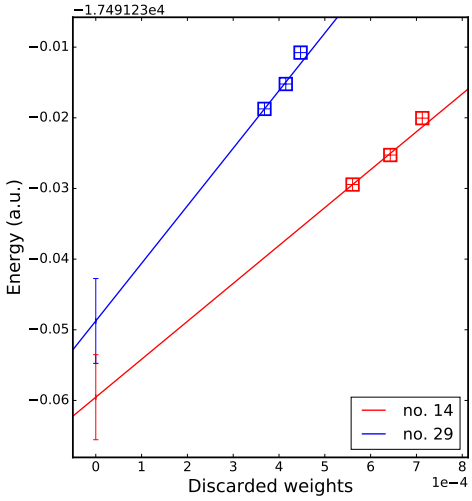

Supplementary Figure 27: Extrapolation of the DMRG energies (in Hartree) versus the discarded weight for the lowest two spin isomers of the P^{1+} cluster with $S = 5/2$. A linear fit of the computed data with D=3000, 3500, and 4000 is used to extrapolate to zero discarded weight, where the intercept is an estimate of the FCI energy ($D = \infty$). The error bars were estimated from an empirical rule $(E_{D=4000} - E_{D=\infty})/5$.

5.4.3 Population analysis

Analysis of the lowest two $S = 5/2$ states (no. 14 and no. 29) of the P^{1+} cluster is summarized in Supplementary Fig. 28. The local populations and spin-spin correlation functions for Fe atoms of these two states are shown in Supplementary Table 13.

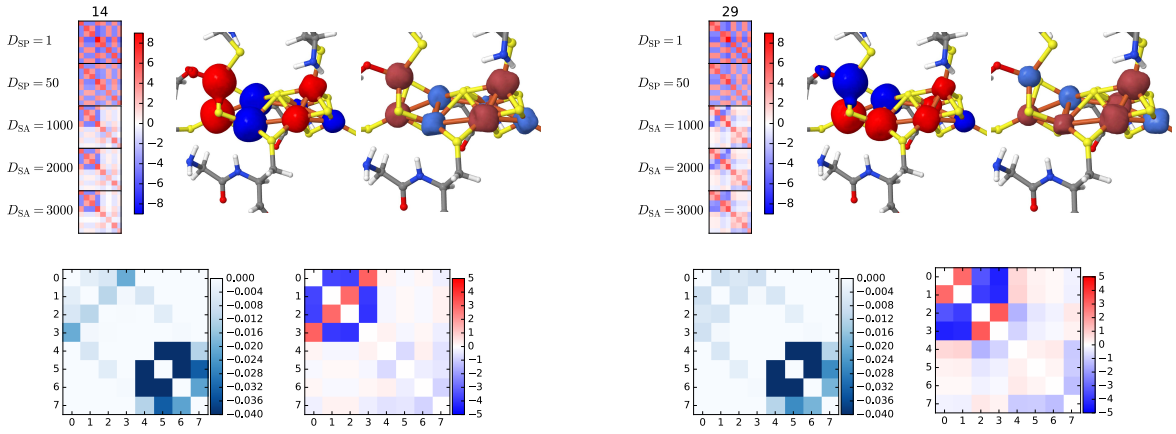

(1) no. 14: $(S_L, S_R) = (0.85, 2.27)$ (2) no. 29: $(S_L, S_R) = (0.90, 3.04)$

Supplementary Figure 28: Analysis of the lowest two $S = 5/2$ states of the P^{1+} cluster. First row: spin-spin correlation functions $\langle \vec{S}_A \cdot \vec{S}_B \rangle$ between the eight irons and spin-spin correlation density $\sigma_A(\vec{r}) = \langle \vec{S}_A \cdot \sum_B \vec{S}_B(\vec{r}) \rangle$ for the first iron atom. Second row: charge (left) and spin (right) fluctuations among different irons. The effective spins of the left cubane S_L and the right cubane S_R are computed from the expectation values of local spin-square operators $\langle \hat{S}_L^2 \rangle$ and $\langle \hat{S}_R^2 \rangle$ for the irons on the left and right cubanes, respectively.

Supplementary Table 13: Local populations and spin-spin correlation functions for Fe atoms of the lowest two spin isomers of the $S = 5/2$ states of the P^{1+} cluster. The results were obtained from DMRG with $D = 3000$ in the localized active orbital basis. The effective spin of each iron S_{Fe} was computed from the expectation value of the local spin-square operator $\langle \hat{S}^2_{\mathrm{Fe}} \rangle$. The local S^z_{Fe} values were computed for the high-spin states ($M_S = S$).

					$\langle \vec{S}_A \cdot \vec{S}_B \rangle$							
no.	atom	N_{Fe}	S_{Fe}	S^z_{Fe}	Fe1	Fe2	Fe3	Fe4	Fe5	Fe6	Fe7	Fe8
14	Fe1	6.25	1.86	0.69	5.34	-4.03	-4.12	3.62	1.06	-0.16	1.06	-0.69
	Fe2	6.33	1.81	-0.56	-4.03	5.08	3.23	-4.32	-0.86	0.13	-0.86	0.56
	Fe3	6.26	1.85	-0.57	-4.12	3.23	5.27	-4.43	-0.89	0.13	-0.88	0.57
	Fe4	6.02	2.00	0.78	3.62	-4.32	-4.43	6.00	1.19	-0.18	1.19	-0.78
	Fe5	6.66	1.53	1.22	1.06	-0.86	-0.89	1.19	3.86	-0.76	1.89	-1.26
	Fe6	6.98	1.04	-0.02	-0.16	0.13	0.13	-0.18	-0.76	2.12	-0.37	-0.49
	Fe7	6.58	1.58	1.31	1.06	-0.86	-0.88	1.19	1.89	-0.37	4.06	-1.59
	Fe8	6.67	1.17	-0.57	-0.69	0.56	0.57	-0.78	-1.26	-0.49	-1.59	2.53
29	Fe1	6.27	1.79	0.30	4.98	3.01	-3.52	-4.45	1.14	0.55	0.54	-0.52
	Fe2	6.32	1.83	0.34	3.01	5.17	-3.98	-4.37	1.28	0.61	0.61	-0.59
	Fe3	6.26	1.86	-0.56	-3.52	-3.98	5.31	3.39	-2.16	-1.03	-1.01	0.97
	Fe4	5.97	2.02	-0.33	-4.45	-4.37	3.39	6.08	-1.25	-0.60	-0.59	0.57
	Fe5	6.66	1.62	1.27	1.14	1.28	-2.16	-1.25	4.24	1.54	2.12	-2.21
	Fe6	6.91	1.32	0.97	0.55	0.61	-1.03	-0.60	1.54	3.06	1.54	-1.90
	Fe7	6.57	1.62	1.35	0.54	0.61	-1.01	-0.59	2.12	1.54	4.26	-2.51
	Fe8	6.63	1.45	-0.91	-0.52	-0.59	0.97	0.57	-2.21	-1.90	-2.51	3.55

5.4.4 Excited states

The lowest four excited states of the lowest two spin isomers (no. 14 and no. 29) were computed in a state-averaged manner with $D = 2000$ starting from the converged ground state solutions. They are characterized in Supplementary Fig. 29.

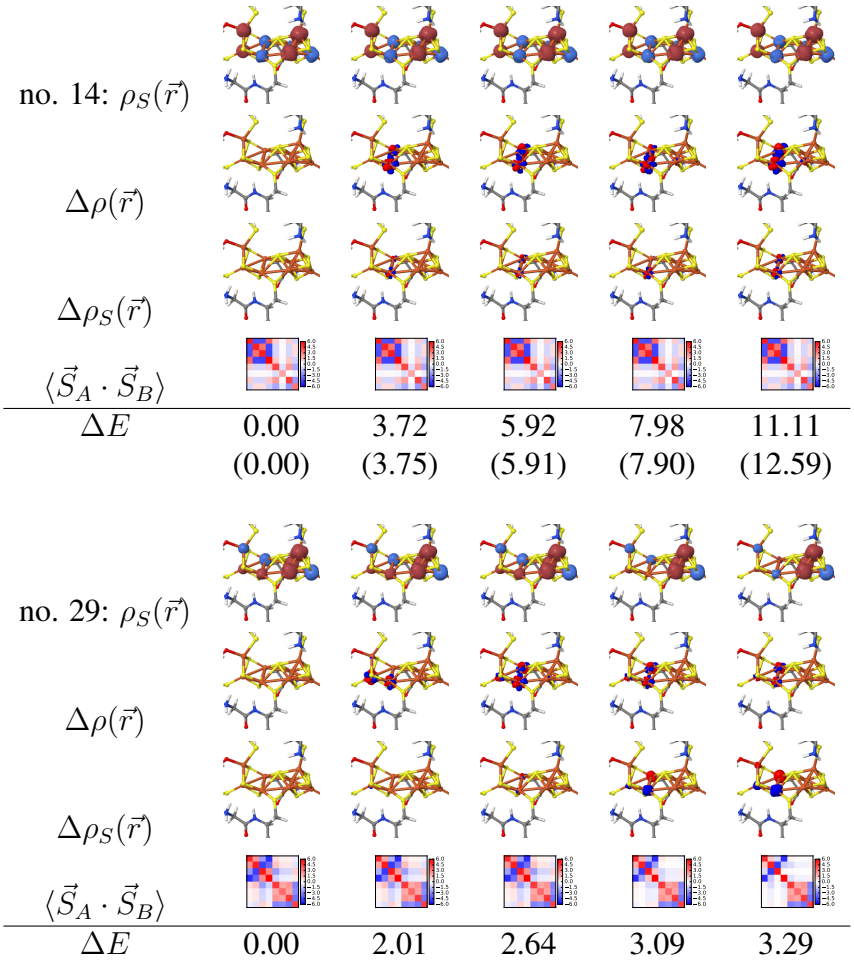

Supplementary Figure 29: Spin densities $\rho_S(\vec{r})$, density differences $\Delta\rho(\vec{r})$, spin density differences $\Delta\rho_S(\vec{r})$, spin-spin correlation functions $\langle\vec{S}_A \cdot \vec{S}_B\rangle$, and relative energies ΔE (in kcal/mol) for the lowest five states of the lowest two spin isomers with $S = 5/2$ of the P^{1+} cluster. Numbers in parentheses are relative energies computed at $D = 3000$ for the lowest spin isomer (no. 14).

6 P^{OX} cluster

6.1 Cartesian coordinates

```
105
pox model
  Fe  -8.01047749054629     -7.94695332233664      2.58075279534974
  Fe  -9.84307851899345     -6.92323662889709      1.43847541627426
  Fe  -8.96968352057896     -9.36673351452133      0.42728396507313
  Fe  -7.50364619783215     -7.13770310544009      0.29510603197579
  Fe  -4.28872728472759     -5.21013269170239      1.09333448739954
  Fe  -5.96253592013313     -2.75087830468647      3.51653681246718
  Fe  -3.94695223327159     -4.54585831949205      3.77056465481288
  Fe  -6.31868414065402     -5.85558268787079      3.82740516405962
  N  -10.05065002068183    -14.32657543589042      0.41135374012592
  C  -11.15400699854884    -13.44039777961122      0.05661504254301
  C  -11.51182118897331    -13.42824944083507     -1.42451642605726
  O  -10.80489615769469    -14.04443793397617     -2.23755193477883
  C  -10.82528228197557    -12.01667959489511      0.46367105712194
  S   -9.49463143658132    -11.39713782896006     -0.45252397010113
  N   -1.29198177048441     -3.34760729465444      0.61129871455921
  C   -1.21148569652411     -4.70804364816012      1.11102094720957
  C   -1.54323437492112     -5.81345846620431      0.11605014644788
  O   -0.64911718374369     -6.55122408874286     -0.30911021849016
  N   -2.80612852888405     -5.90869924658447     -0.29145022440657
  C   -3.29540761005311     -7.00983493059299     -1.10002933979191
  C   -2.47812548471503     -7.30910905024289     -2.35326432335645
  O   -2.14877073309613     -8.46917991810716     -2.56276139664809
  C   -4.73191957784627     -6.76643148937220     -1.53306297647833
  S   -5.87488608917100     -5.93660824688709     -0.59952832825174
  N  -11.00047146485734     -4.14470867196241     -0.85059816453292
  C  -12.09293931251528     -3.69794611667069      0.03391199658262
  C  -12.56247998748218     -2.24489943812175     -0.03307981131467
  O  -13.74952951510439     -2.07470349441599     -0.33253892692070
  C  -11.76367915477872     -3.99516319250796      1.50793871200972
  S  -11.77180268661218     -5.69594168959122      1.93986869780322
  S   -8.02052219791651     -5.77164646263840      1.99449929001968
  S   -9.97550344794258     -8.89981406737732      2.35852230071407
  S   -4.22373011986103     -3.17641713838694      1.99530865876830
  S   -6.86571141468004     -9.13077452492581      0.95322952600439
  S   -5.65689485392691     -4.13845964661916      5.22677087614574
  S   -9.51174790407870     -7.53006379158588     -0.77163743634619
  S   -4.19873472943421     -6.63073109435635      2.92021584981980
  N    1.40470980109474     -3.18212775722595      4.10595463944089
  C    0.45310882063592     -2.33567549076847      4.80195042639234
  C    0.49627436465357     -2.51524946846992      6.31436932655210
  O    1.00022429943801     -3.51895382803881      6.82698030953169
  C   -0.95373416943759     -2.62945840572489      4.28838990849440
  S   -1.81094076396874     -4.18144185817796      4.78406139921977
  N   -7.22914798011055    -10.79341579293762      4.41198015829782
  C   -6.06820450225801    -10.04821617817221      4.86186656431801
  C   -5.19754851494529    -10.92830098895857      5.72818629432135
  O   -4.00388938472582    -11.08602726639291      5.49258854945115
  C   -6.50913181134816     -8.81358461077598      5.67643823469876
  S   -7.42054837150031     -7.52967966526377      4.77005755512294
  N   -8.53277562713802     -2.46594302985609      6.34230544335590
  C   -9.09222598649386     -1.25350836057478      5.76723374200957
  C  -10.59752936002136     -1.24629197788913      5.65605967040765
  O  -11.16115555679763     -0.15804044527917      5.71436154031004
  C   -8.55523981120178     -0.97964394566444      4.37306082202467
  S   -8.13329772053419     -2.15831185921364      3.20937365266704
```

```
N   -4.67226331287050      0.51278063061608      6.47784663986723
C   -3.75637910582675      0.14121173517575      5.41356957437420
C   -3.55769162058072      1.28979575755424      4.45974148304333
O   -2.65062070791082      1.17188868753277      3.62975697604365
C   -4.33130929376247     -1.09792481860136      4.65360781662335
O   -5.54541322948811     -1.05406634978254      4.25258154961421
H   -1.84976357880175     -4.78717615325622      2.00445259221814
H   -0.18834501983326     -4.92386665832021      1.45253204610764
H   -2.24640352344778     -3.00095590909653      0.72258715375572
H   -1.06046139383514     -3.31292629838726     -0.37959770671062
H  -10.00003336311035    -14.39052354285267      1.42508901426106
H  -10.22070196780334    -15.26174824201547      0.04678354639980
H  -12.10441624222324    -13.70082631612894      0.57689500474620
H  -12.38991657963832    -12.82136694586264     -1.72281200016992
H  -10.61827585195426    -11.99873034375234      1.54485639999017
H  -11.72846643712018    -11.40158192420825      0.33094266167566
H   -3.24698986622796     -7.94377231519705     -0.51693306572868
H   -2.23380093603881     -6.46915376265754     -3.03902732316997
H   -5.13443486377081     -7.75176216287674     -1.80978341130218
H   -4.67471574301930     -6.21956838119025     -2.49175768866658
H  -10.92752385208304     -5.15927409129132     -0.72383465671834
H  -10.11568988762873     -3.78479756786432     -0.48625626243047
H  -12.98958129491473     -4.26279094549176     -0.24624939432618
H  -11.88778111897147     -1.41016946861633      0.24518179054741
H  -12.50346306848344     -3.49783124890152      2.15672457004033
H  -10.79207375799003     -3.53656142391254      1.75320858513562
H    0.92816012115112     -4.06636694519351      3.91476092791479
H    2.15815001452952     -3.43298159520427      4.74693879794809
H    0.64294323376840     -1.27049454201423      4.58139472632510
H   -0.00373177246724     -1.73873627464266      6.93338040490776
H   -1.60095530480348     -1.79076073488893      4.56892079805260
H   -0.89477790243321     -2.60427101287372      3.19066690165447
H   -7.00839176997428    -11.46936954229337      3.68770910472423
H   -7.73156593783611    -11.24633155903320      5.17118678946714
H   -5.48170804782486     -9.71822321850162      3.99724047039528
H   -5.70973749560662    -11.45950311510647      6.56548015890420
H   -7.14848142255057     -9.14041176204511      6.50789615378112
H   -5.62378108183286     -8.32959810272113      6.10560532351760
H   -7.53632189834348     -2.30925925159686      6.50292994822828
H   -8.51801958786424     -3.17093596602973      5.59692324564823
H   -8.84635597735984     -0.38998737724194      6.39543626045808
H  -11.14267690725086     -2.19495146336263      5.46478452639671
H   -7.63328961902137     -0.40140194935207      4.55209245554028
H   -9.23526976072677     -0.25430116441184      3.89617046667046
H   -4.57791668182963     -0.16752820245776      7.23232878964892
H   -5.61126104874783      0.33900250333337      6.10589995816396
H   -2.77244975510165     -0.13885665759654      5.80549954223757
H   -4.23312734779937      2.17127703910465      4.50127284122449
H   -3.59052421947107     -1.27374952857751      3.83786639335372
H   -4.12679889878747     -1.92346040070023      5.38268099718778
```

6.2 Active orbitals

The active orbitals for the P^{OX} cluster were prepared with initial orbitals obtained at the BP86/def2-SVP level with the COSMO solvation model ($\epsilon = 4.0$) for a high-spin state M_S=34/2 with charge -4. The final active orbitals ordered by the genetic ordering method[37] for DMRG

are shown in Supplementary Fig. 30. The orbitals in the active space CAS(120e,77o) can be classified as follows:

1. Five $3d$ orbitals of Fe(1): 60, 61, 62, 63, 64
2. Five $3d$ orbitals of Fe(2): 48, 49, 50, 51, 52
3. Five $3d$ orbitals of Fe(3): 43, 44, 45, 46, 47
4. Five $3d$ orbitals of Fe(4): 68, 69, 70, 71, 72
5. Five $3d$ orbitals of Fe(5): 29, 30, 31, 32, 33
6. Five $3d$ orbitals of Fe(6): 24, 25, 26, 27, 28
7. Five $3d$ orbitals of Fe(7): 16, 17, 18, 19, 20
8. Five $3d$ orbitals of Fe(8): 4, 5, 6, 7, 8
9. Twenty-one $3p$ orbitals of seven S atoms in the [Fe_8S_7] core: 10, 11, 12, 13, 14, 15, 21, 22, 23, 34, 35, 36, 53, 54, 55, 56, 57, 58, 59, 65, 66
10. Sixteen orbitals of peripheral atoms: 1, 2, 3, 9, 37, 38, 39, 40, 41, 42, 67, 73, 74, 75, 76, 77

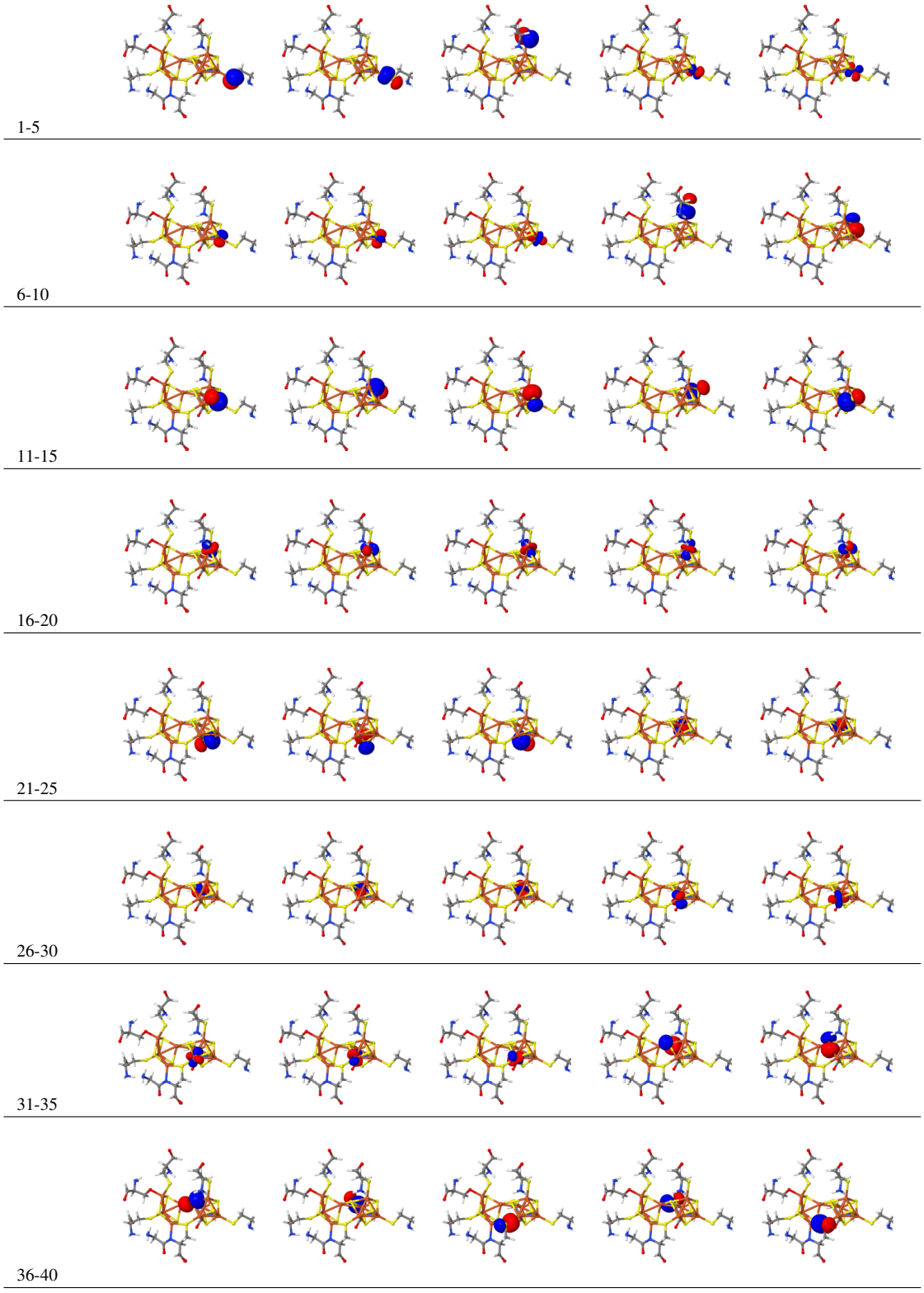

Supplementary Figure 30: Active orbitals of the P^{OX} cluster.

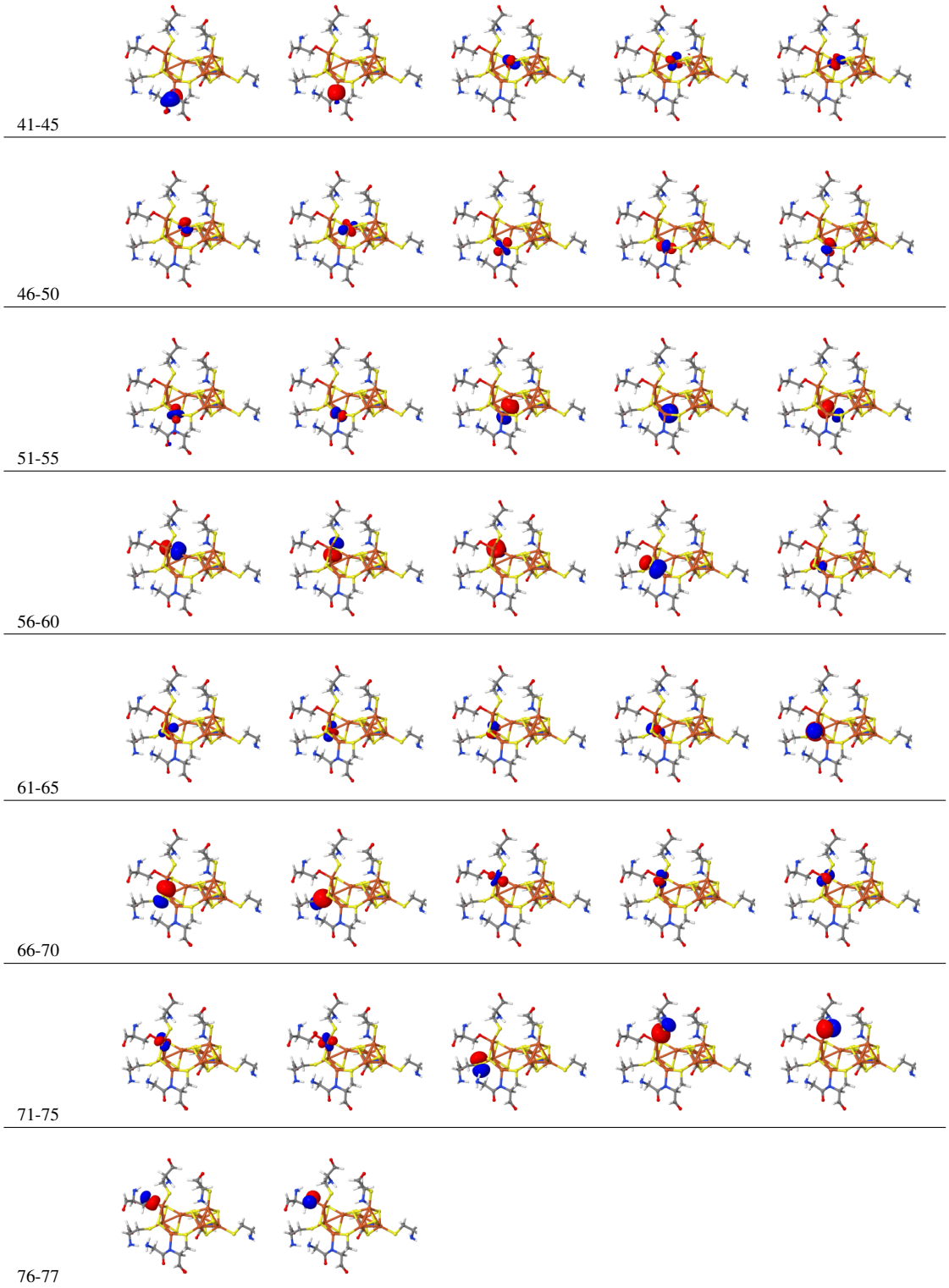

Supplementary Figure 31: Active orbitals of the P^{OX} cluster.

6.3 DMRG results for $S = 3$ states

6.3.1 Initial guesses and DMRG energies

Supplementary Tables 14 and 15 list the DMRG results obtained from the following three classes of initial guesses for $S = 3$: (a) {2Fe(III)↓, 5Fe(II)↑, Fe(II)↓}, (b) {2Fe(III)↓, 4Fe(II)↑, 2Fe(II)↓}, and (c) {Fe(III)↑, Fe(III)↓, 3Fe(II)↑, 3Fe(II)↓}. The corresponding spin-spin correlation functions for each state can be found in Supplementary Fig. 32. The energy convergence is shown in Supplementary Fig. 33.

Supplementary Table 14: Relative energies (ΔE in kcal/mol) for the states computed from DMRG with different initial guesses for the $S = 3$ states of the P^{OX} cluster. The last three columns show the relative energies for the selected low-lying states obtained with larger bond dimensions in a forward sweep schedule, while the energies obtained in a reverse sweep schedule and extrapolated results are shown in Supplementary Table 16.

no.	Fe(III)↑,Fe(II)↑,Fe(III)↓,Fe(II)↓	$D = 1000$	$D = 2000$	Eq. (6)	$D = 3000$	$D = 3500$	$D = 4000$
a1	{}, {7, 6, 5, 3, 1}, {2, 4}, {8}	7.60	6.85	6.46			
a2	{}, {8, 6, 5, 3, 1}, {2, 4}, {7}	16.97	13.53	13.26			
a3	{}, {8, 7, 5, 3, 1}, {2, 4}, {6}	23.01	16.30	15.93			
a4	{}, {8, 7, 6, 3, 1}, {2, 4}, {5}	20.05	14.79	14.42			
a5	{}, {8, 7, 6, 5, 1}, {2, 4}, {3}	17.80	14.10	14.06			
a6	{}, {8, 7, 6, 5, 3}, {2, 4}, {1}	13.72	11.85	11.85			
b1	{}, {6, 5, 3, 1}, {2, 4}, {8, 7}	12.63	7.41	7.07			
b2	{}, {7, 5, 3, 1}, {2, 4}, {8, 6}	21.72	13.52	13.14			
b3	{}, {7, 6, 3, 1}, {2, 4}, {8, 5}	18.99	14.73	14.36			
b4	{}, {7, 6, 5, 1}, {2, 4}, {8, 3}	29.13	16.68	16.59			
b5	{}, {7, 6, 5, 3}, {2, 4}, {8, 1}	20.43	13.43	13.40			
b6	{}, {8, 5, 3, 1}, {2, 4}, {7, 6}	20.84	14.40	14.07			
b7	{}, {8, 6, 3, 1}, {2, 4}, {7, 5}	18.10	15.15	14.75			
b8	{}, {8, 6, 5, 1}, {2, 4}, {7, 3}	22.20	15.83	15.76			
b9	{}, {8, 6, 5, 3}, {2, 4}, {7, 1}	12.88	11.84	11.84			
b10	{}, {8, 7, 3, 1}, {2, 4}, {6, 5}	16.87	14.01	13.70			
b11	{}, {8, 7, 5, 1}, {2, 4}, {6, 3}	24.53	16.66	16.55			
b12	{}, {8, 7, 5, 3}, {2, 4}, {6, 1}	21.11	14.57	14.49			
b13	{}, {8, 7, 6, 1}, {2, 4}, {5, 3}	18.16	12.42	12.37			
b14	{}, {8, 7, 6, 3}, {2, 4}, {5, 1}	14.15	6.38	6.40			
b15	{}, {8, 7, 6, 5}, {2, 4}, {3, 1}	15.17	15.43	15.33			

Supplementary Table 15: (Continued).

no.	Fe(III)↑,Fe(II)↑,Fe(III)↓,Fe(II)↓	$D = 1000$	$D = 2000$	Eq. (6)	$D = 3000$	$D = 3500$	$D = 4000$
c1	{4}, {5, 3, 1}, {2}, {8, 7, 6}	12.23	4.42	4.40			
c2	{2}, {5, 3, 1}, {4}, {8, 7, 6}	17.02	12.06	11.97			
c3	{4}, {6, 3, 1}, {2}, {8, 7, 5}	12.90	9.16	9.18			
c4	{2}, {6, 3, 1}, {4}, {8, 7, 5}	26.63	14.75	14.65			
c5	{4}, {6, 5, 1}, {2}, {8, 7, 3}	22.94	8.95	8.90			
c6	{2}, {6, 5, 1}, {4}, {8, 7, 3}	27.91	19.11	18.89			
c7	{4}, {6, 5, 3}, {2}, {8, 7, 1}	27.63	19.53	19.29			
c8	{2}, {6, 5, 3}, {4}, {8, 7, 1}	29.70	11.24	11.17			
c9	{4}, {7, 3, 1}, {2}, {8, 6, 5}	15.53	9.58	9.54			
c10	{2}, {7, 3, 1}, {4}, {8, 6, 5}	46.68	19.89	19.69			
c11	{4}, {7, 5, 1}, {2}, {8, 6, 3}	4.75	3.46	3.47	3.03	2.90	2.73
c12	{2}, {7, 5, 1}, {4}, {8, 6, 3}	19.81	12.66	12.36			
c13	{4}, {7, 5, 3}, {2}, {8, 6, 1}	30.73	15.85	15.63			
c14	{2}, {7, 5, 3}, {4}, {8, 6, 1}	5.84	3.07	3.07	2.27	1.96	1.76
c15	{4}, {7, 6, 1}, {2}, {8, 5, 3}	8.01	5.78	5.77			
c16	{2}, {7, 6, 1}, {4}, {8, 5, 3}	49.79	15.36	15.14			
c17	{4}, {7, 6, 3}, {2}, {8, 5, 1}	48.69	15.28	15.04			
c18	{2}, {7, 6, 3}, {4}, {8, 5, 1}	0.01	0.00	0.00	0.00	0.00	0.00
c19	{4}, {7, 6, 5}, {2}, {8, 3, 1}	48.42	16.33	15.96			
c20	{2}, {7, 6, 5}, {4}, {8, 3, 1}	4.30	1.47	1.45			
c21	{4}, {8, 3, 1}, {2}, {7, 6, 5}	4.09	1.44	1.42	1.06	1.01	0.92
c22	{2}, {8, 3, 1}, {4}, {7, 6, 5}	44.60	12.02	11.85			
c23	{4}, {8, 5, 1}, {2}, {7, 6, 3}	0.00	0.00	0.00			
c24	{2}, {8, 5, 1}, {4}, {7, 6, 3}	49.63	15.30	15.06			
c25	{4}, {8, 5, 3}, {2}, {7, 6, 1}	45.20	15.25	15.01			
c26	{2}, {8, 5, 3}, {4}, {7, 6, 1}	0.00	0.00	0.00			
c27	{4}, {8, 6, 1}, {2}, {7, 5, 3}	4.83	3.47	3.48			
c28	{2}, {8, 6, 1}, {4}, {7, 5, 3}	30.68	15.85	15.63			
c29	{4}, {8, 6, 3}, {2}, {7, 5, 1}	19.30	12.66	12.35			
c30	{2}, {8, 6, 3}, {4}, {7, 5, 1}	8.10	6.06	6.07			
c31	{4}, {8, 6, 5}, {2}, {7, 3, 1}	45.81	17.06	16.80			
c32	{2}, {8, 6, 5}, {4}, {7, 3, 1}	6.97	3.94	3.92			
c33	{4}, {8, 7, 1}, {2}, {6, 5, 3}	29.23	11.14	11.07			
c34	{2}, {8, 7, 1}, {4}, {6, 5, 3}	27.74	19.92	19.68			
c35	{4}, {8, 7, 3}, {2}, {6, 5, 1}	27.85	19.14	18.91			
c36	{2}, {8, 7, 3}, {4}, {6, 5, 1}	23.15	5.68	5.65			
c37	{4}, {8, 7, 5}, {2}, {6, 3, 1}	32.87	15.96	15.85			
c38	{2}, {8, 7, 5}, {4}, {6, 3, 1}	13.09	9.34	9.35			
c39	{4}, {8, 7, 6}, {2}, {5, 3, 1}	16.89	12.07	11.98			
c40	{2}, {8, 7, 6}, {4}, {5, 3, 1}	16.10	5.24	5.23			

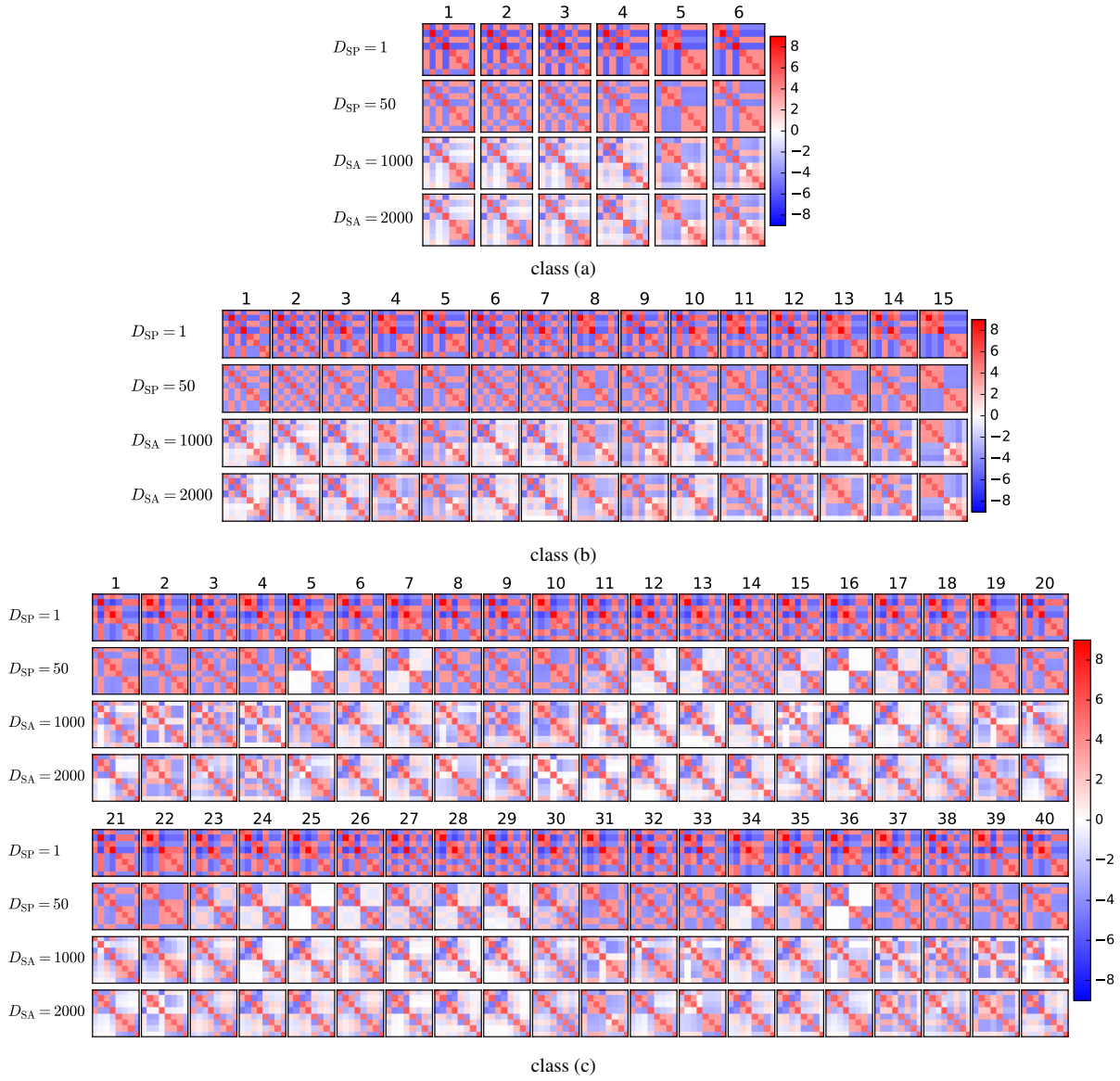

Supplementary Figure 32: Spin-spin correlation functions between the eight Fe atoms for the $S = 3$ states of the P^{OX} cluster.

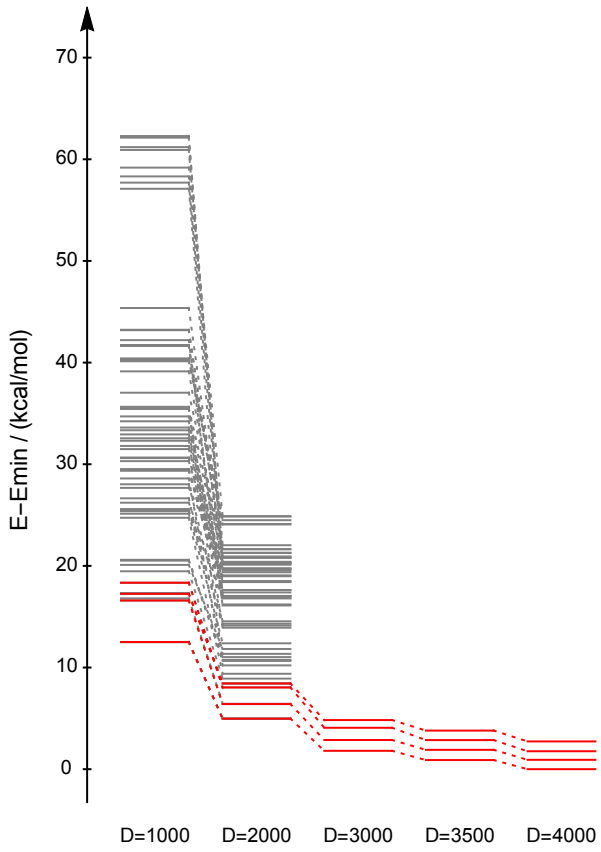

Supplementary Figure 33: Energy convergence for the $S = 3$ DMRG states computed starting from different initial guesses of the P^{OX} cluster with progressively increasing bond dimensions D up to $D = 4000$. The lowest four states are highlighted in red.

6.3.2 Energy extrapolation

In Supplementary Table 16 and Supplementary Fig. 34, the extrapolated energies are shown for the lowest four states (c18, c21, c14, and c11) with $S = 3$ obtained in the previous section.

Supplementary Table 16: Total energies (in Hartree) and relative energies ΔE (in kcal/mol) of the lowest four spin isomers of the $S = 3$ states of the P^{OX} cluster computed from DMRG with various bond dimensions D in a reverse sweep schedule.

no.	D	discarded weight	energy	ΔE
c18	3000	2.1×10^{-4}	-17489.901438	0.00 (3.94[a])
	3500	1.9×10^{-4}	-17489.903005	0.00 (3.62[a])
	4000	1.6×10^{-4}	-17489.904223	0.00 (3.37[a])
	extrapolation		-17489.912241	0.00 (1.40[a])
	error bar		1.01	0.00 (0.79)
c21	3000	1.7×10^{-4}	-17489.899693	1.10
	3500	1.5×10^{-4}	-17489.901405	1.00
	4000	1.3×10^{-4}	-17489.902717	0.94
	extrapolation		-17489.911176	0.67
	error bar		1.06	0.11
c14	3000	2.6×10^{-4}	-17489.897860	2.25
	3500	2.3×10^{-4}	-17489.899883	1.96
	4000	1.9×10^{-4}	-17489.901456	1.74
	extrapolation		-17489.909969	1.43
	error bar		1.07	0.12
c11	3000	1.8×10^{-4}	-17489.896566	3.06
	3500	1.6×10^{-4}	-17489.898402	2.89
	4000	1.4×10^{-4}	-17489.899846	2.75
	extrapolation		-17489.909322	1.83
	error bar		1.19	0.37

[a] Relative to the $S = 4$ ground state in Supplementary Table 21.

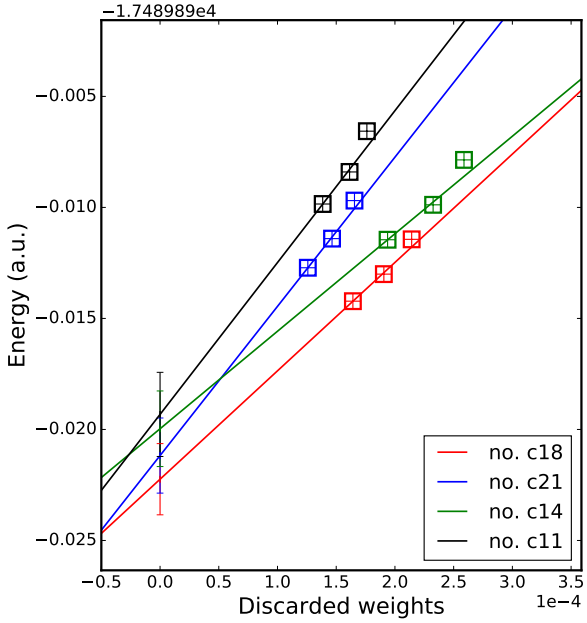

Supplementary Figure 34: Extrapolation of the DMRG energies (in Hartree) versus the discarded weight for the lowest four spin isomers of the $S = 3$ states of the P^{OX} cluster. A linear fit of the computed data with D=3000, 3500, and 4000 is used to extrapolate to zero discarded weight, where the intercept is an estimate of the FCI energy ($D = \infty$). The error bars were estimated from an empirical rule $(E_{D=4000} - E_{D=\infty})/5$.

6.3.3 Population analysis

Analysis of the four $S = 3$ states (c18, c21, c14, and c11) of the P^{OX} cluster is summarized in Supplementary Fig. 35. The local populations and spin-spin correlation functions for Fe atoms of these four states are shown in Supplementary Table 17.

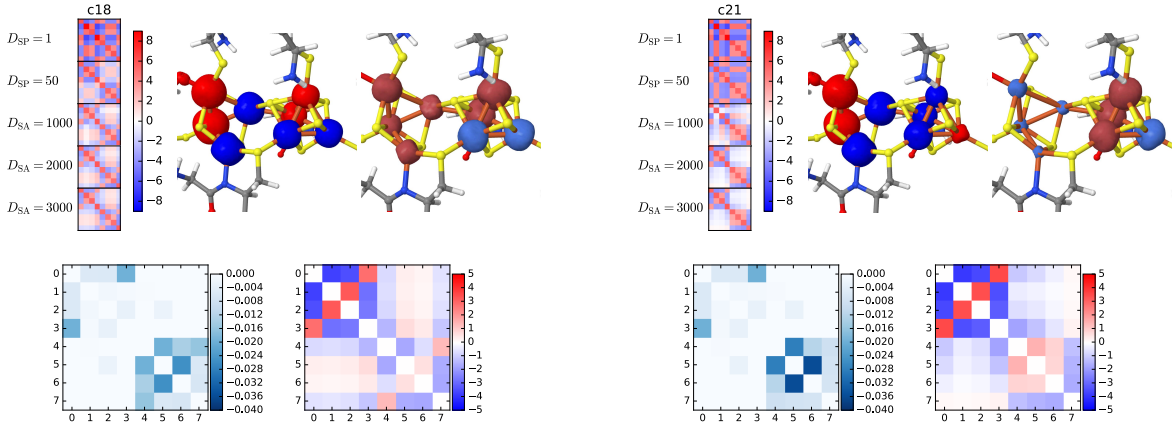

(1) no. c18: $(S_L, S_R) = (3.28, 1.83)$ (2) no. c21: $(S_L, S_R) = (2.39, 3.93)$

(1) no. c14: $(S_L, S_R) = (0.80, 2.65)$ (2) no. c11: $(S_L, S_R) = (1.54, 2.28)$

Supplementary Figure 35: Analysis of the lowest four $S = 3$ states of the P^{OX} cluster. First row: spin-spin correlation functions $\langle \vec{S}_A \cdot \vec{S}_B \rangle$ between the eight irons, spin-spin correlation density $\sigma_A(\vec{r}) = \langle \vec{S}_A \cdot \sum_B \vec{S}_B(\vec{r}) \rangle$ for the first iron atom, and spin-density $\rho_S(\vec{r})$. Second row: charge (left) and spin (right) fluctuations among different irons. The effective spins of the left cubane S_L and the right cubane S_R are computed from the expectation values of local spin-square operators $\langle \hat{S}_L^2 \rangle$ and $\langle \hat{S}_R^2 \rangle$ for the irons on the left and right cubanes, respectively.

Supplementary Table 17: Local populations and spin-spin correlation functions for Fe atoms of the lowest four spin isomers of the $S = 3$ state of the P^{OX} cluster. The results were obtained from DMRG with $D = 3000$ in the localized active orbital basis. The effective spin of each iron S_{Fe} was computed from the expectation value of the local spin-square operator $\langle \hat{S}^2_{Fe} \rangle$. The local S^z_{Fe} values were computed for the high-spin states ($M_S = S$).

					$\langle \vec{S}_A \cdot \vec{S}_B \rangle$							
no.	atom	N_{Fe}	S_{Fe}	S^z_{Fe}	Fe1	Fe2	Fe3	Fe4	Fe5	Fe6	Fe7	Fe8
c18	Fe1	6.24	1.89	0.52	5.44	-3.47	-3.19	3.37	-1.34	1.07	1.00	-1.28
	Fe2	6.15	1.91	0.47	-3.47	5.55	3.51	-2.29	-1.23	0.98	0.91	-1.16
	Fe3	6.22	1.88	0.55	-3.19	3.51	5.42	-2.05	-1.45	1.15	1.07	-1.37
	Fe4	6.07	1.98	1.04	3.37	-2.29	-2.05	5.88	-2.73	2.17	2.03	-2.59
	Fe5	6.34	1.81	-1.24	-1.34	-1.23	-1.45	-2.73	5.08	-3.47	-2.58	3.09
	Fe6	6.41	1.76	1.42	1.07	0.98	1.15	2.17	-3.47	4.84	2.79	-3.60
	Fe7	6.33	1.79	1.55	1.00	0.91	1.07	2.03	-2.58	2.79	5.02	-3.87
	Fe8	6.18	1.90	-1.40	-1.28	-1.16	-1.37	-2.59	3.09	-3.60	-3.87	5.52
c21	Fe1	6.24	1.88	-0.10	5.43	-3.90	-3.57	3.54	-1.21	-0.86	-0.46	0.27
	Fe2	6.15	1.91	-0.07	-3.90	5.54	3.48	-3.44	-0.46	-0.36	-0.22	0.17
	Fe3	6.22	1.88	-0.10	-3.57	3.48	5.40	-3.17	-0.76	-0.58	-0.35	0.24
	Fe4	6.08	1.97	-0.18	3.54	-3.44	-3.17	5.87	-2.00	-1.45	-0.78	0.47
	Fe5	6.31	1.85	1.15	-1.21	-0.46	-0.76	-2.00	5.28	3.14	2.76	-2.71
	Fe6	6.39	1.82	1.41	-0.86	-0.36	-0.58	-1.45	3.14	5.11	3.12	-3.24
	Fe7	6.28	1.87	1.65	-0.46	-0.22	-0.35	-0.78	2.76	3.12	5.36	-3.73
	Fe8	6.25	1.77	-1.27	0.27	0.17	0.24	0.47	-2.71	-3.24	-3.73	4.90
c14	Fe1	6.24	1.88	0.31	5.42	-4.32	-4.22	3.62	1.29	-1.36	0.59	-0.48
	Fe2	6.15	1.90	-0.26	-4.32	5.52	3.48	-4.48	-1.08	1.15	-0.50	0.40
	Fe3	6.23	1.87	-0.25	-4.22	3.48	5.38	-4.45	-1.07	1.13	-0.49	0.39
	Fe4	6.08	1.97	0.34	3.62	-4.48	-4.45	5.86	1.41	-1.50	0.65	-0.52
	Fe5	6.34	1.79	0.78	1.29	-1.08	-1.07	1.41	4.97	-3.00	1.54	-1.28
	Fe6	6.40	1.77	0.28	-1.36	1.15	1.13	-1.50	-3.00	4.90	0.83	-0.69
	Fe7	6.28	1.86	1.51	0.59	-0.50	-0.49	0.65	1.54	0.83	5.34	-2.73
	Fe8	6.24	1.82	-0.17	-0.48	0.40	0.39	-0.52	-1.28	-0.69	-2.73	5.11
c11	Fe1	6.24	1.88	0.42	5.43	-4.15	-3.91	3.62	1.13	-1.40	0.92	-0.71
	Fe2	6.15	1.90	-0.10	-4.15	5.53	3.47	-4.16	-0.26	0.33	-0.22	0.17
	Fe3	6.23	1.87	-0.02	-3.91	3.47	5.39	-3.99	-0.03	0.04	-0.03	0.03
	Fe4	6.08	1.97	0.53	3.62	-4.16	-3.99	5.86	1.43	-1.77	1.16	-0.90
	Fe5	6.35	1.80	1.16	1.13	-0.26	-0.03	1.43	5.03	-3.71	2.57	-2.10
	Fe6	6.40	1.75	-0.79	-1.40	0.33	0.04	-1.77	-3.71	4.81	-1.77	1.32
	Fe7	6.29	1.86	1.50	0.92	-0.22	-0.03	1.16	2.57	-1.77	5.32	-2.73
	Fe8	6.24	1.82	-0.17	-0.71	0.17	0.03	-0.90	-2.10	1.32	-2.73	5.13

6.3.4 Excited states

The lowest four excited states of the lowest four spin isomers (c18, c21, c14, and c11) were computed in a state-averaged manner with $D = 2000$ starting from the converged ground state solutions. They are characterized in Supplementary Figs. 36 and 37.

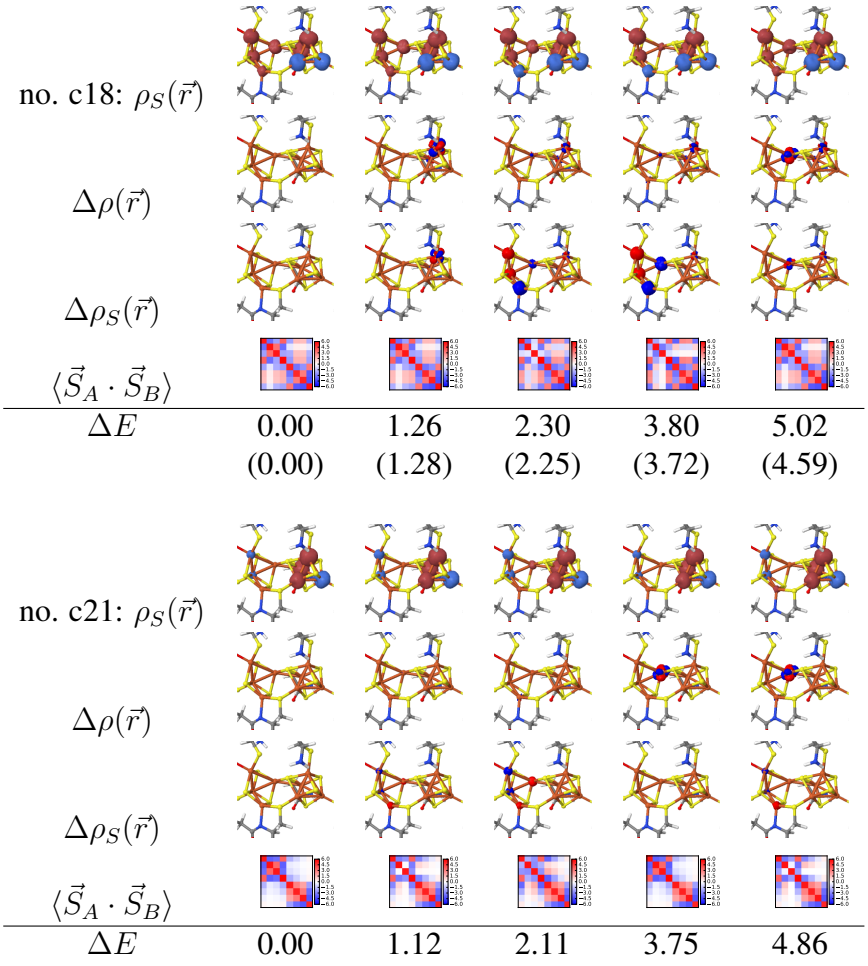

Supplementary Figure 36: Spin densities $\rho_S(\vec{r})$, density differences $\Delta\rho(\vec{r})$, spin density differences $\Delta\rho_S(\vec{r})$, spin-spin correlation functions $\langle\vec{S}_A \cdot \vec{S}_B\rangle$, and relative energies ΔE (in kcal/mol) for the lowest five states of the lowest four spin isomers with $S = 3$ of the P^{OX} cluster. Numbers in parentheses are relative energies computed at $D = 3000$ for the lowest spin isomer (no. c18).

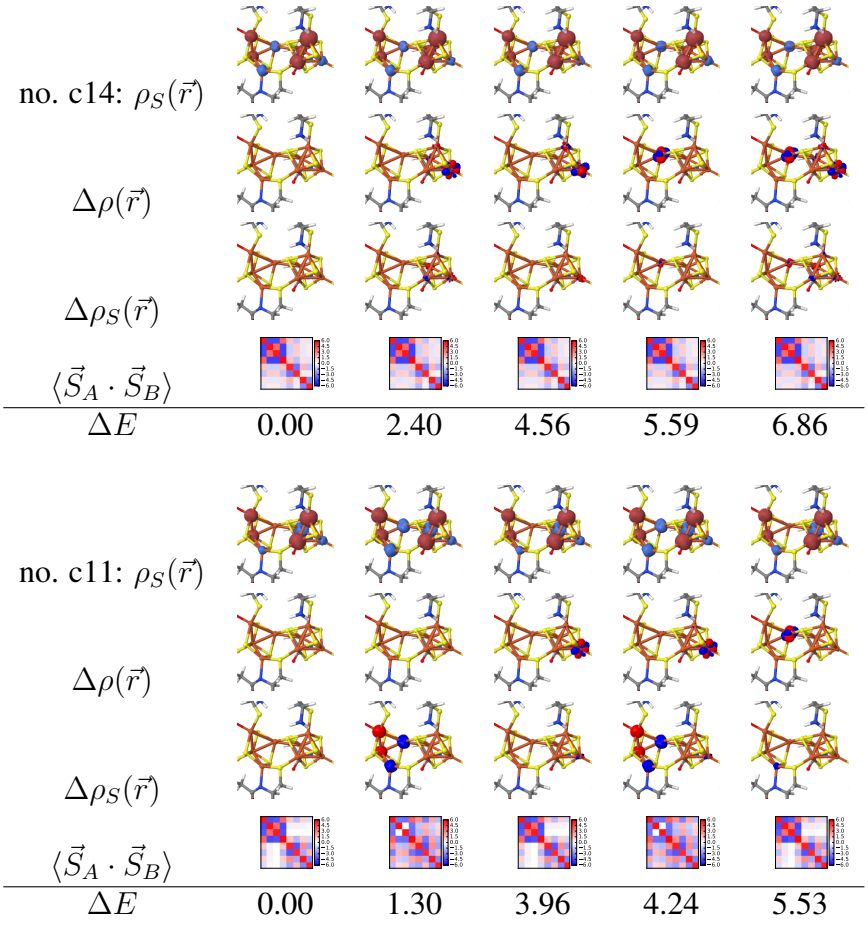

Supplementary Figure 37: (Continued.) Spin densities $\rho_S(\vec{r})$, density differences $\Delta\rho(\vec{r})$, spin density differences $\Delta\rho_S(\vec{r})$, spin-spin correlation functions $\langle\vec{S}_A\cdot\vec{S}_B\rangle$, and relative energies ΔE (in kcal/mol) for the lowest five states of the lowest four spin isomers with $S = 3$ of the P^{OX} cluster.

6.4 DMRG results for $S = 4$ states

6.4.1 Initial guesses and DMRG energies

Supplementary Tables 18, 19, and 20 list the DMRG results obtained from the following four classes of initial guesses for $S = 4$: (a) {2Fe(III)↓, 5Fe(II)↑, Fe(II)↓}, (b) {2Fe(III)↓, 4Fe(II)↑, 2Fe(II)↓}, (c) {Fe(III)↑, Fe(III)↓, 3Fe(II)↑, 3Fe(II)↓}, (d) {Fe(III)↑, Fe(III)↓, 4Fe(II)↑, 2Fe(II)↓}. The corresponding spin-spin correlation functions for each state can be found in Supplementary Fig. 38. The energy convergence is shown in Supplementary Fig. 39.

Supplementary Table 18: Relative energies (ΔE in kcal/mol) for the states computed from DMRG with different initial guesses for $S = 4$ states of the P^{OX} cluster. The last three columns show the relative energies for the selected low-lying states obtained with larger bond dimensions in a forward sweep schedule, while the energies obtained in a reverse sweep schedule and extrapolated results are shown in Supplementary Table 21.

no.	Fe(III)↑,Fe(II)↑,Fe(III)↓,Fe(II)↓	$D = 1000$	$D = 2000$	Eq. (6)	$D = 3000$	$D = 3500$	$D = 4000$
a1	{}, {7, 6, 5, 3, 1}, {2, 4}, {8}	10.51	9.53	9.16			
a2	{}, {8, 6, 5, 3, 1}, {2, 4}, {7}	19.20	15.64	15.39			
a3	{}, {8, 7, 5, 3, 1}, {2, 4}, {6}	63.12	21.42	21.08			
a4	{}, {8, 7, 6, 3, 1}, {2, 4}, {5}	26.31	19.21	18.87			
a5	{}, {8, 7, 6, 5, 1}, {2, 4}, {3}	29.36	20.64	20.60			
a6	{}, {8, 7, 6, 5, 3}, {2, 4}, {1}	26.09	18.41	18.39			
b1	{}, {6, 5, 3, 1}, {2, 4}, {8, 7}	23.81	17.86	17.82			
b2	{}, {7, 5, 3, 1}, {2, 4}, {8, 6}	55.04	17.26	17.00			
b3	{}, {7, 6, 3, 1}, {2, 4}, {8, 5}	27.92	20.33	19.97			
b4	{}, {7, 6, 5, 1}, {2, 4}, {8, 3}	27.36	16.28	16.18			
b5	{}, {7, 6, 5, 3}, {2, 4}, {8, 1}	37.45	15.01	14.95			
b6	{}, {8, 5, 3, 1}, {2, 4}, {7, 6}	19.39	13.20	12.82			
b7	{}, {8, 6, 3, 1}, {2, 4}, {7, 5}	22.73	18.09	17.67			
b8	{}, {8, 6, 5, 1}, {2, 4}, {7, 3}	25.56	17.61	17.53			
b9	{}, {8, 6, 5, 3}, {2, 4}, {7, 1}	23.23	15.17	15.12			
b10	{}, {8, 7, 3, 1}, {2, 4}, {6, 5}	30.31	22.45	22.14			
b11	{}, {8, 7, 5, 1}, {2, 4}, {6, 3}	35.72	17.98	17.88			
b12	{}, {8, 7, 5, 3}, {2, 4}, {6, 1}	34.41	15.53	15.47			
b13	{}, {8, 7, 6, 1}, {2, 4}, {5, 3}	20.01	15.58	15.50			
b14	{}, {8, 7, 6, 3}, {2, 4}, {5, 1}	16.02	13.33	13.29			
b15	{}, {8, 7, 6, 5}, {2, 4}, {3, 1}	22.33	20.31	20.22			

Supplementary Table 19: (Continued.)

no.	Fe(III)↑,Fe(II)↑,Fe(III)↓,Fe(II)↓	$D = 1000$	$D = 2000$	Eq. (6)	$D = 3000$	$D = 3500$	$D = 4000$
c1	{4}, {5, 3, 1}, {2}, {8, 7, 6}	10.58	6.27	6.26			
c2	{2}, {5, 3, 1}, {4}, {8, 7, 6}	18.91	11.77	11.70			
c3	{4}, {6, 3, 1}, {2}, {8, 7, 5}	22.07	5.86	5.87	4.95	4.62	4.40
c4	{2}, {6, 3, 1}, {4}, {8, 7, 5}	37.12	18.96	18.80			
c5	{4}, {6, 5, 1}, {2}, {8, 7, 3}	14.10	10.31	10.39			
c6	{2}, {6, 5, 1}, {4}, {8, 7, 3}	24.03	19.61	19.39			
c7	{4}, {6, 5, 3}, {2}, {8, 7, 1}	24.34	19.62	19.41			
c8	{2}, {6, 5, 3}, {4}, {8, 7, 1}	32.33	22.31	22.34			
c9	{4}, {7, 3, 1}, {2}, {8, 6, 5}	22.35	13.50	13.45			
c10	{2}, {7, 3, 1}, {4}, {8, 6, 5}	52.92	17.89	17.69			
c11	{4}, {7, 5, 1}, {2}, {8, 6, 3}	7.75	4.32	4.35			
c12	{2}, {7, 5, 1}, {4}, {8, 6, 3}	19.67	13.67	13.38			
c13	{4}, {7, 5, 3}, {2}, {8, 6, 1}	32.84	18.39	18.06			
c14	{2}, {7, 5, 3}, {4}, {8, 6, 1}	21.81	10.76	10.71			
c15	{4}, {7, 6, 1}, {2}, {8, 5, 3}	29.11	6.82	6.84			
c16	{2}, {7, 6, 1}, {4}, {8, 5, 3}	40.18	13.69	13.40			
c17	{4}, {7, 6, 3}, {2}, {8, 5, 1}	53.29	13.70	13.41			
c18	{2}, {7, 6, 3}, {4}, {8, 5, 1}	12.80	4.31	4.34	2.88	2.34	1.98
c19	{4}, {7, 6, 5}, {2}, {8, 3, 1}	50.04	15.83	15.70			
c20	{2}, {7, 6, 5}, {4}, {8, 3, 1}	18.51	12.49	12.44			
c21	{4}, {8, 3, 1}, {2}, {7, 6, 5}	18.57	12.51	12.46			
c22	{2}, {8, 3, 1}, {4}, {7, 6, 5}	50.04	15.83	15.70			
c23	{4}, {8, 5, 1}, {2}, {7, 6, 3}	14.35	4.31	4.34			
c24	{2}, {8, 5, 1}, {4}, {7, 6, 3}	58.19	16.46	16.13			
c25	{4}, {8, 5, 3}, {2}, {7, 6, 1}	43.41	13.69	13.40			
c26	{2}, {8, 5, 3}, {4}, {7, 6, 1}	22.96	6.79	6.80			
c27	{4}, {8, 6, 1}, {2}, {7, 5, 3}	21.79	6.24	6.25			
c28	{2}, {8, 6, 1}, {4}, {7, 5, 3}	31.77	18.39	18.06			
c29	{4}, {8, 6, 3}, {2}, {7, 5, 1}	19.27	13.67	13.38			
c30	{2}, {8, 6, 3}, {4}, {7, 5, 1}	7.82	4.33	4.36			
c31	{4}, {8, 6, 5}, {2}, {7, 3, 1}	53.28	18.28	18.07			
c32	{2}, {8, 6, 5}, {4}, {7, 3, 1}	22.44	13.48	13.43			
c33	{4}, {8, 7, 1}, {2}, {6, 5, 3}	30.39	22.22	22.25			
c34	{2}, {8, 7, 1}, {4}, {6, 5, 3}	24.36	19.59	19.38			
c35	{4}, {8, 7, 3}, {2}, {6, 5, 1}	24.58	19.64	19.42			
c36	{2}, {8, 7, 3}, {4}, {6, 5, 1}	14.07	10.30	10.38			
c37	{4}, {8, 7, 5}, {2}, {6, 3, 1}	39.90	18.28	18.15			
c38	{2}, {8, 7, 5}, {4}, {6, 3, 1}	22.33	5.90	5.91			
c39	{4}, {8, 7, 6}, {2}, {5, 3, 1}	20.93	11.81	11.74			
c40	{2}, {8, 7, 6}, {4}, {5, 3, 1}	10.15	6.26	6.26			

Supplementary Table 20: (Continued.)

no.	Fe(III)↑,Fe(II)↑,Fe(III)↓,Fe(II)↓	$D = 1000$	$D = 2000$	Eq. (6)	$D = 3000$	$D = 3500$	$D = 4000$
d1	{4}, {6, 5, 3, 1}, {2}, {8, 7}	18.81	9.88	9.95			
d2	{2}, {6, 5, 3, 1}, {4}, {8, 7}	17.96	12.77	12.79			
d3	{4}, {7, 5, 3, 1}, {2}, {8, 6}	17.79	13.82	13.80			
d4	{2}, {7, 5, 3, 1}, {4}, {8, 6}	17.15	12.28	12.26			
d5	{4}, {7, 6, 3, 1}, {2}, {8, 5}	7.85	5.88	5.88			
d6	{2}, {7, 6, 3, 1}, {4}, {8, 5}	13.89	10.08	9.96			
d7	{4}, {7, 6, 5, 1}, {2}, {8, 3}	0.01	0.00	0.00	0.00	0.00	0.00
d8	{2}, {7, 6, 5, 1}, {4}, {8, 3}	21.22	9.79	9.53			
d9	{4}, {7, 6, 5, 3}, {2}, {8, 1}	11.03	9.75	9.51			
d10	{2}, {7, 6, 5, 3}, {4}, {8, 1}	0.00	0.00	0.00			
d11	{4}, {8, 5, 3, 1}, {2}, {7, 6}	13.79	10.42	10.40			
d12	{2}, {8, 5, 3, 1}, {4}, {7, 6}	15.84	11.57	11.50			
d13	{4}, {8, 6, 3, 1}, {2}, {7, 5}	15.15	11.40	11.41			
d14	{2}, {8, 6, 3, 1}, {4}, {7, 5}	18.30	13.71	13.64			
d15	{4}, {8, 6, 5, 1}, {2}, {7, 3}	8.44	6.14	6.25	5.16	4.77	4.69
d16	{2}, {8, 6, 5, 1}, {4}, {7, 3}	19.43	15.94	15.80			
d17	{4}, {8, 6, 5, 3}, {2}, {7, 1}	19.50	16.08	15.94			
d18	{2}, {8, 6, 5, 3}, {4}, {7, 1}	8.41	6.22	6.32			
d19	{4}, {8, 7, 3, 1}, {2}, {6, 5}	20.23	15.43	15.47			
d20	{2}, {8, 7, 3, 1}, {4}, {6, 5}	54.00	20.27	20.03			
d21	{4}, {8, 7, 5, 1}, {2}, {6, 3}	13.62	9.91	9.93			
d22	{2}, {8, 7, 5, 1}, {4}, {6, 3}	30.25	19.80	19.57			
d23	{4}, {8, 7, 5, 3}, {2}, {6, 1}	33.08	19.81	19.58			
d24	{2}, {8, 7, 5, 3}, {4}, {6, 1}	13.54	9.83	9.85			
d25	{4}, {8, 7, 6, 1}, {2}, {5, 3}	19.88	12.29	12.29			
d26	{2}, {8, 7, 6, 1}, {4}, {5, 3}	39.05	20.12	19.91			
d27	{4}, {8, 7, 6, 3}, {2}, {5, 1}	39.27	19.74	19.54			
d28	{2}, {8, 7, 6, 3}, {4}, {5, 1}	20.38	12.29	12.28			
d29	{4}, {8, 7, 6, 5}, {2}, {3, 1}	53.98	21.53	21.46			
d30	{2}, {8, 7, 6, 5}, {4}, {3, 1}	17.37	14.64	14.61			

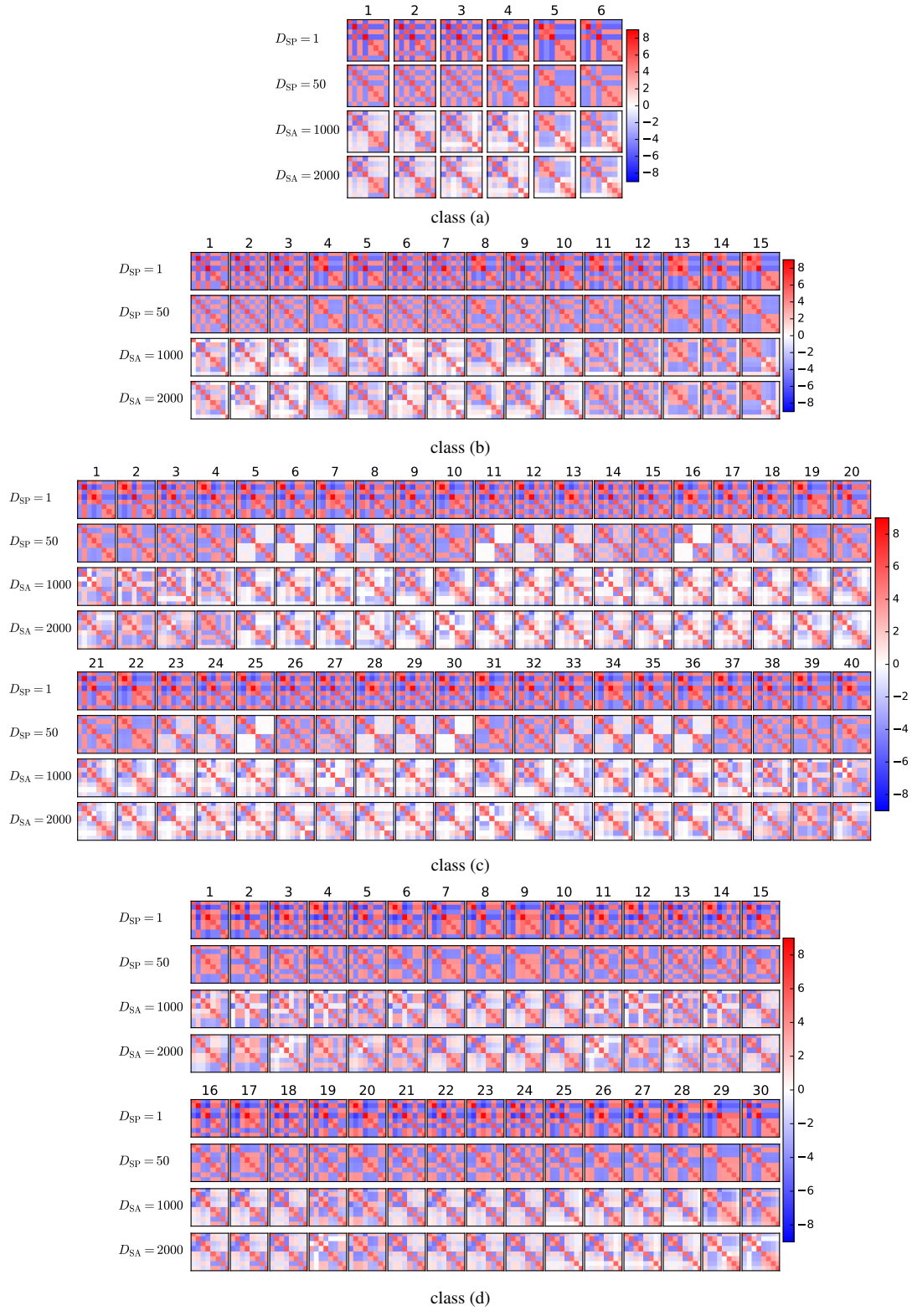

Supplementary Figure 38: Spin-spin correlation functions between the eight Fe atoms for the $S = 4$ states of the P^{OX} cluster.

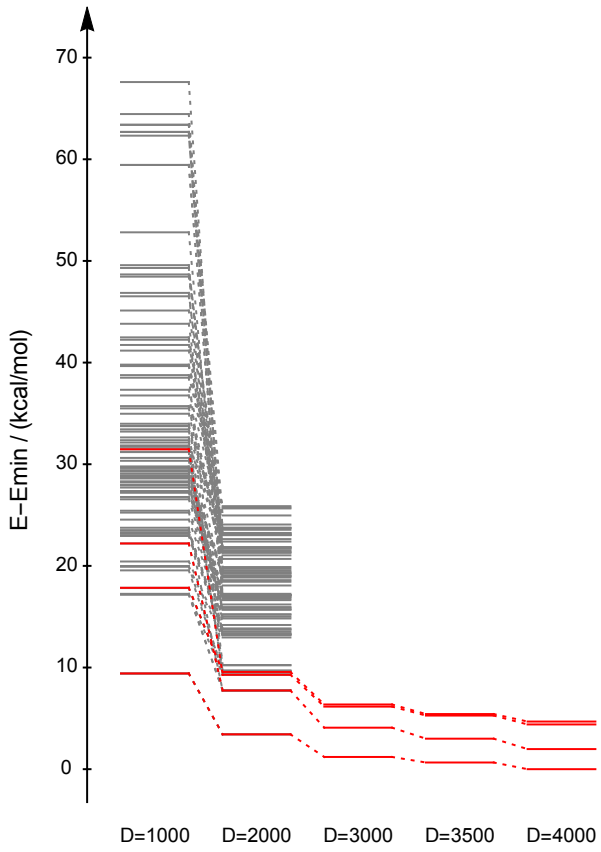

Supplementary Figure 39: Energy convergence for the $S = 4$ DMRG states computed starting from different initial guesses of the P^{OX} cluster with progressively increasing bond dimensions D up to $D = 4000$. The lowest four states are highlighted in red.

6.4.2 Energy extrapolation

In Supplementary Table 21 and Supplementary Fig. 40, the extrapolated energies are shown for the lowest four states (d7, c18, c3, and d15) with $S = 4$ obtained in the previous section.

Supplementary Table 21: Total energies (in Hartree) and relative energies ΔE (in kcal/mol) of the lowest four spin isomers of the $S = 4$ states of the P^{OX} cluster computed from DMRG with various bond dimensions D in a reverse sweep schedule.

no.	D	discarded weight	energy	ΔE
d7	3000	1.2×10^{-4}	-17489.907713	0.00
	3500	1.0×10^{-4}	-17489.908779	0.00
	4000	8.8×10^{-5}	-17489.909595	0.00
	extrapolation		-17489.914468	0.00
	error bar		0.61	0.00
c18	3000	2.4×10^{-4}	-17489.903295	2.77
	3500	2.1×10^{-4}	-17489.905130	2.29
	4000	1.8×10^{-4}	-17489.906554	1.91
	extrapolation		-17489.914449	0.01
	error bar		0.99	0.76
c3	3000	2.1×10^{-4}	-17489.899950	4.87
	3500	1.9×10^{-4}	-17489.901473	4.58
	4000	1.6×10^{-4}	-17489.902654	4.36
	extrapolation		-17489.910557	2.45
	error bar		0.99	0.76
d15	3000	3.9×10^{-4}	-17489.899918	4.89
	3500	3.4×10^{-4}	-17489.901320	4.68
	4000	2.8×10^{-4}	-17489.902363	4.54
	extrapolation		-17489.908162	3.95
	error bar		0.73	0.24

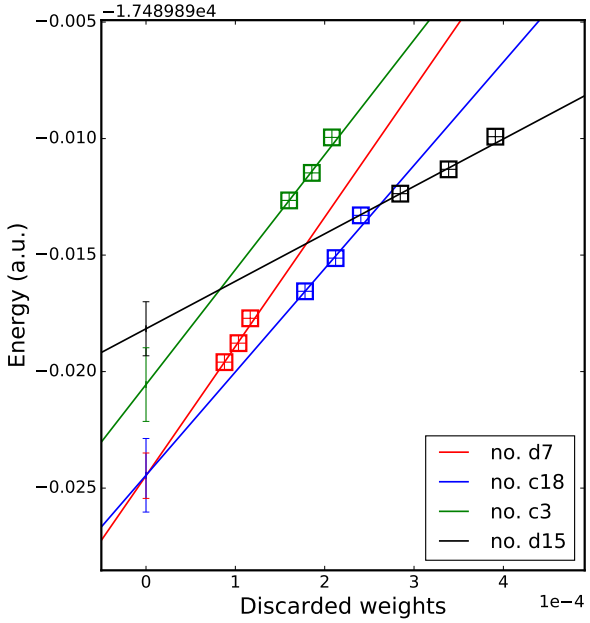

Supplementary Figure 40: Extrapolation of the DMRG energies (in Hartree) versus the discarded weight for the lowest four spin isomers of the $S = 4$ states of the P^{OX} cluster. A linear fit of the computed data with D=3000, 3500, and 4000 is used to extrapolate to zero discarded weight, where the intercept is an estimate of the FCI energy ($D = \infty$). The error bars were estimated from an empirical rule $(E_{D=4000} - E_{D=\infty})/5$.

6.4.3 Population analysis

Analysis of the lowest four $S = 4$ states (d7, c18, c3, and d15) of the P^{OX} cluster is summarized in Supplementary Fig. 41. The local populations and spin-spin correlation functions for Fe atoms of these four states is shown in Supplementary Table 22.

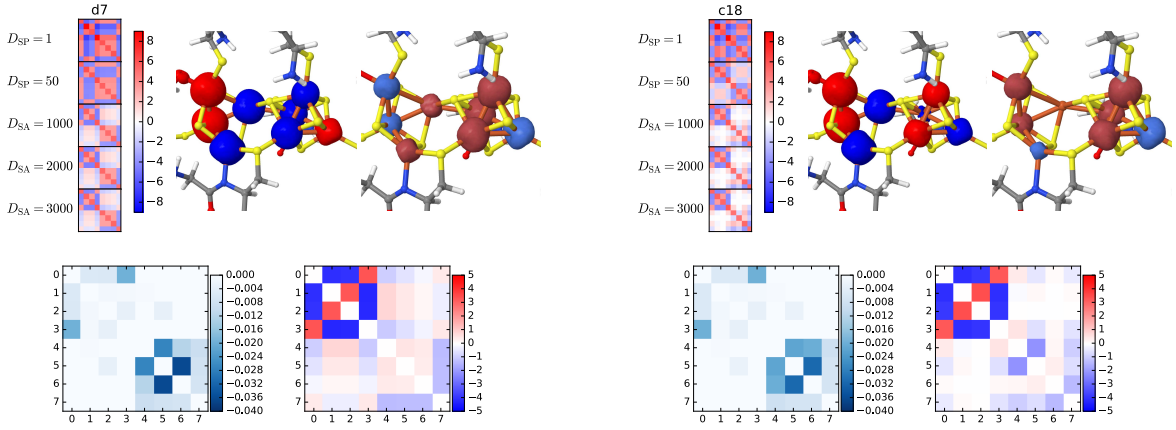

(1) d7: $(S_L, S_R) = (0.79, 3.88)$ (2) c18: $(S_L, S_R) = (1.55, 2.62)$

(3) c3: $(S_L, S_R) = (4.18, 1.92)$ (4) d15: $(S_L, S_R) = (0.80, 3.90)$

Supplementary Figure 41: Analysis of the lowest two $S = 4$ states of the P^{OX} cluster. First row: spin-spin correlation functions $\langle \vec{S}_A \cdot \vec{S}_B \rangle$ between the eight irons and spin-spin correlation density $\sigma_A(\vec{r}) = \langle \vec{S}_A \cdot \sum_B \vec{S}_B(\vec{r}) \rangle$ for the first iron atom. Second row: charge (left) and spin (right) fluctuations among different irons. The effective spins of the left cubane S_L and the right cubane S_R are computed from the expectation values of local spin-square operators $\langle \hat{S}_L^2 \rangle$ and $\langle \hat{S}_R^2 \rangle$ for the irons on the left and right cubanes, respectively.

Supplementary Table 22: Local populations and spin-spin correlation functions for Fe atoms of the lowest four spin isomers of the $S = 4$ state of the P^{OX} cluster. The results were obtained from DMRG with $D = 3000$ in the localized active orbital basis. The effective spin of each iron S_{Fe} was computed from the expectation value of the local spin-square operator $\langle \hat{S}^2_{Fe} \rangle$. The local S^z_{Fe} values are computed for the high-spin states ($M_S = S$).

					$\langle \vec{S}_A \cdot \vec{S}_B \rangle$							
no.	atom	N_{Fe}	S_{Fe}	S^z_{Fe}	Fe1	Fe2	Fe3	Fe4	Fe5	Fe6	Fe7	Fe8
d7	Fe1	6.24	1.88	-0.52	5.42	-4.33	-4.22	3.62	-1.81	-1.41	-1.10	1.10
	Fe2	6.15	1.90	0.44	-4.33	5.52	3.48	-4.49	1.52	1.18	0.93	-0.93
	Fe3	6.23	1.87	0.43	-4.22	3.48	5.38	-4.45	1.48	1.15	0.90	-0.90
	Fe4	6.08	1.97	-0.58	3.62	-4.49	-4.45	5.86	-1.99	-1.55	-1.21	1.21
	Fe5	6.32	1.85	1.64	-1.81	1.52	1.48	-1.99	5.26	3.23	3.25	-3.47
	Fe6	6.40	1.81	1.66	-1.41	1.18	1.15	-1.55	3.23	5.10	3.27	-3.48
	Fe7	6.28	1.87	1.74	-1.10	0.93	0.90	-1.21	3.25	3.27	5.36	-3.59
	Fe8	6.26	1.76	-1.33	1.10	-0.93	-0.90	1.21	-3.47	-3.48	-3.59	4.84
c18	Fe1	6.24	1.88	0.55	5.43	-4.18	-3.88	3.62	1.08	-0.09	1.03	-1.16
	Fe2	6.15	1.90	-0.16	-4.18	5.53	3.46	-4.19	-0.30	0.01	-0.30	0.33
	Fe3	6.23	1.88	0.00	-3.88	3.46	5.39	-3.96	0.02	-0.03	0.00	0.00
	Fe4	6.08	1.97	0.69	3.62	-4.19	-3.96	5.86	1.36	-0.12	1.30	-1.45
	Fe5	6.35	1.78	1.23	1.08	-0.30	0.02	1.36	4.95	-1.23	2.27	-2.64
	Fe6	6.40	1.77	0.73	-0.09	0.01	-0.03	-0.12	-1.23	4.90	1.59	-1.63
	Fe7	6.29	1.86	1.72	1.03	-0.30	0.00	1.30	2.27	1.59	5.33	-3.71
	Fe8	6.25	1.79	-1.37	-1.16	0.33	0.00	-1.45	-2.64	-1.63	-3.71	4.98
c3	Fe1	6.23	1.89	0.61	5.44	-2.84	-2.63	3.15	-1.44	1.19	1.13	-1.41
	Fe2	6.15	1.91	0.79	-2.84	5.57	3.53	-0.86	-1.88	1.54	1.47	-1.84
	Fe3	6.21	1.89	0.84	-2.63	3.53	5.44	-0.71	-1.98	1.63	1.55	-1.94
	Fe4	6.07	1.98	1.33	3.15	-0.86	-0.71	5.88	-3.15	2.59	2.47	-3.09
	Fe5	6.34	1.81	-1.35	-1.44	-1.88	-1.98	-3.15	5.08	-3.41	-2.61	3.14
	Fe6	6.41	1.76	1.51	1.19	1.54	1.63	2.59	-3.41	4.84	2.81	-3.57
	Fe7	6.33	1.79	1.60	1.13	1.47	1.55	2.47	-2.61	2.81	5.02	-3.78
	Fe8	6.18	1.90	-1.50	-1.41	-1.84	-1.94	-3.09	3.14	-3.57	-3.78	5.52
d15	Fe1	6.24	1.88	-0.54	5.42	-4.32	-4.21	3.62	-1.78	-1.49	1.19	-1.22
	Fe2	6.15	1.90	0.46	-4.32	5.52	3.48	-4.49	1.50	1.26	-1.00	1.02
	Fe3	6.23	1.87	0.45	-4.21	3.48	5.37	-4.44	1.47	1.23	-0.98	1.01
	Fe4	6.08	1.97	-0.60	3.62	-4.49	-4.44	5.86	-1.95	-1.64	1.30	-1.34
	Fe5	6.32	1.85	1.62	-1.78	1.50	1.47	-1.95	5.27	3.22	-3.60	3.34
	Fe6	6.38	1.80	1.59	-1.49	1.26	1.23	-1.64	3.22	5.05	-3.65	3.27
	Fe7	6.33	1.75	-1.32	1.19	-1.00	-0.98	1.30	-3.60	-3.65	4.83	-3.40
	Fe8	6.17	1.92	1.83	-1.22	1.02	1.01	-1.34	3.34	3.27	-3.40	5.61

6.4.4 Excited states

The lowest four excited states of the lowest four spin isomers (d7, c18, c3, and d15) were computed in a state-averaged manner with $D = 2000$ starting from the converged ground state solutions. They are characterized in Supplementary Figs. 42 and 43.

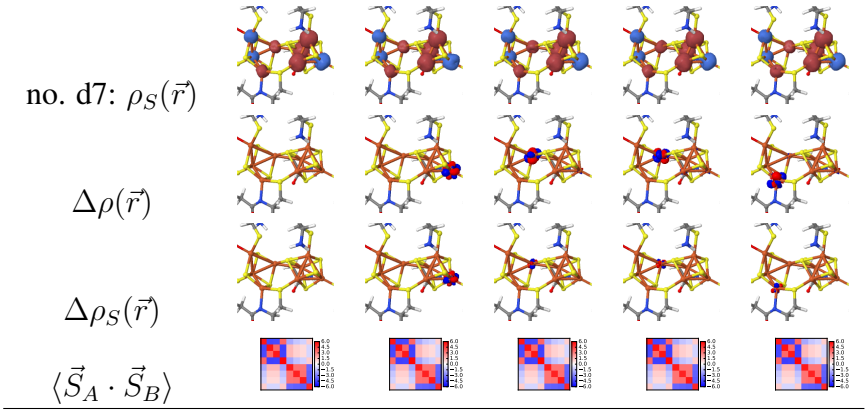

Supplementary Figure 42: Spin densities $\rho_S(\vec{r})$, density differences $\Delta\rho(\vec{r})$, spin density differences $\Delta\rho_S(\vec{r})$, spin-spin correlation functions $\langle \vec{S}_A \cdot \vec{S}_B \rangle$, and relative energies ΔE (in kcal/mol) for the lowest five states of the lowest four spin isomers with $S = 4$ of the P^{OX} cluster. Numbers in parentheses are relative energies computed at $D = 3000$ for the lowest two spin isomers (d7 and c18).

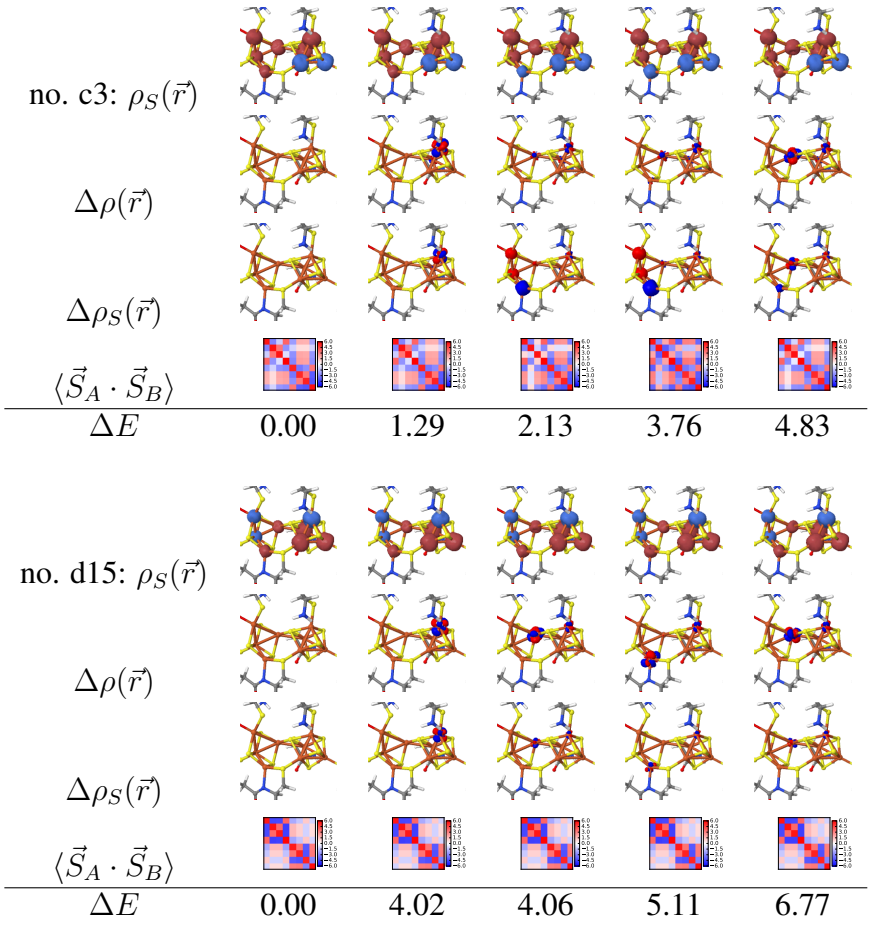

Supplementary Figure 43: Spin densities $\rho_S(\vec{r})$, density differences $\Delta\rho(\vec{r})$, spin density differences $\Delta\rho_S(\vec{r})$, spin-spin correlation functions $\langle\vec{S}_A\cdot\vec{S}_B\rangle$, and relative energies ΔE (in kcal/mol) for the lowest five states of the lowest four spin isomers with $S = 4$ of the P^{OX} cluster.

References

[1] Münck, E. *et al.* Nitrogenase. viii. mössbauer and epr spectroscopy. the mofe protein component from azotobacter vinelandii op. *Biochim. Biophys. Acta, Protein Struct.* **400**, 32–53 (1975).

[2] Zimmermann, R. *et al.* Nitrogenase x: Mössbauer and epr studies on reversibly oxidized mofe protein from azotobacter vinelandii op nature of the iron centers. *Biochim. Biophys. Acta, Protein Struct.* **537**, 185–207 (1978).

[3] Huynh, B. *et al.* Nitrogenase xii. mössbauer studies of the mofe protein from clostridium pasteurianum w5. *Biochim. Biophys. Acta, Protein Struct.* **623**, 124–138 (1980).

[4] Surerus, K. K. *et al.* Mössbauer and integer-spin epr of the oxidized p-clusters of nitrogenase: Pox is a non-kramers system with a nearly degenerate ground doublet. *J. Am. Chem. Soc.* **114**, 8579–8590 (1992).

[5] Tittsworth, R. C. & Hales, B. J. Detection of epr signals assigned to the 1-equiv-oxidized p-clusters of the nitrogenase mofe-protein from azotobacter vinelandii. *J. Am. Chem. Soc.* **115**, 9763–9767 (1993).

[6] Rupnik, K. *et al.* P+ state of nitrogenase p-cluster exhibits electronic structure of a [fe4s4]+ cluster. *J. Am. Chem. Soc.* **134**, 13749–13754 (2012).

[7] Mouesca, J.-M., Noodleman, L. & Case, D. Analysis of the 57fe hyperfine coupling constants and spin states in nitrogenase p-clusters. *Inorg. Chem.* **33**, 4819–4830 (1994).

[8] Kim, J. & Rees, D. Structural models for the metal centers in the nitrogenase molybdenum-iron protein. *Science* **257**, 1677–1682 (1992).

[9] Chan, M. K., Kim, J. & Rees, D. The nitrogenase femo-cofactor and p-cluster pair: 2.2 a resolution structures. *Science* **260**, 7 (1993).

[10] Peters, J. W. *et al.* Redox-dependent structural changes in the nitrogenase p-cluster. *Biochemistry* **36**, 1181–1187 (1997).

[11] Pansini, F., Neto, A. & Varandas, A. Extrapolation of hartree–fock and multiconfiguration self-consistent-field energies to the complete basis set limit. *Theor. Chem. Acc.* **135**, 261 (2016).

[12] Tao, J., Perdew, J. P., Staroverov, V. N. & Scuseria, G. E. Climbing the density functional ladder: Nonempirical meta–generalized gradient approximation designed for molecules and solids. *Phys. Rev. Lett.* **91**, 146401 (2003).

[13] Grimme, S., Ehrlich, S. & Goerigk, L. Effect of the damping function in dispersion corrected density functional theory. *J. Comput. Chem.* **32**, 1456–1465 (2011).

[14] Weigend, F. & Ahlrichs, R. Balanced basis sets of split valence, triple zeta valence and quadruple zeta valence quality for h to rn: Design and assessment of accuracy. *Phys. Chem. Chem. Phys.* **7**, 3297–3305 (2005).

[15] Neese, F. The orca program system. *Wiley Interdiscip. Rev. Comput. Mol. Sci.* **2**, 73–78 (2012).

[16] Klamt, A. & Schüürmann, G. Cosmo: a new approach to dielectric screening in solvents with explicit expressions for the screening energy and its gradient. *J. Chem. Soc., Perkin Trans. 2* 799–805 (1993).

[17] Cao, L. & Ryde, U. Influence of the protein and dft method on the broken-symmetry and spin states in nitrogenase. *Int. J. Quantum Chem.* **118**, e25627 (2018).

[18] Keable, S. M. *et al.* Structural characterization of the p1+ intermediate state of the p-cluster of nitrogenase. *J. Biol. Chem.* **293**, 9629–9635 (2018).

[19] Sharma, S., Sivalingam, K., Neese, F. & Chan, G. K.-L. Low-energy spectrum of iron-sulfur clusters directly from many-particle quantum mechanics. *Nat. Chem.* **6**, 927–933 (2014).

[20] Veryazov, V., Malmqvist, P. Å. & Roos, B. O. How to select active space for multiconfigurational quantum chemistry? *Int. J. Quantum Chem.* **111**, 3329–3338 (2011).

[21] Guo, S., Watson, M. A., Hu, W., Sun, Q. & Chan, G. K.-L. N-electron valence state perturbation theory based on a density matrix renormalization group reference function, with applications to the chromium dimer and a trimer model of poly (p-phenylenevinylene). *J. Chem. Theory Comput.* **12**, 1583–1591 (2016).

[22] Angeli, C., Cimiraglia, R., Evangelisti, S., Leininger, T. & Malrieu, J.-P. Introduction of n-electron valence states for multireference perturbation theory. *J. Chem. Phys.* **114**, 10252–10264 (2001).

[23] Jorge, F., Canal, N. A., Camiletti, G. & Machado, S. Contracted gaussian basis sets for douglas-kroll-hess calculations: Estimating scalar relativistic effects of some atomic and molecular properties. *J. Chem. Phys.* **130**, 064108–064108 (2009).

[24] Presti, D., Stoneburner, S. J., Truhlar, D. G. & Gagliardi, L. Full correlation in a multiconfigurational study of bimetallic clusters: Restricted active space pair-density functional theory study of [2fe-2s] systems. *The Journal of Physical Chemistry C* (2019).

[25] Corliss, C. & Sugar, J. Energy levels of iron, fe i through fe xxvi. *Journal of Physical and Chemical Reference Data* **11**, 135–241 (1982).

[26] Sayfutyarova, E. R. & Chan, G. K.-L. A state interaction spin-orbit coupling density matrix renormalization group method. *J. Chem. Phys.* **144**, 234301 (2016).

[27] Ohki, Y., Sunada, Y., Honda, M., Katada, M. & Tatsumi, K. Synthesis of the p-cluster inorganic core of nitrogenases. *J. Am. Chem. Soc.* **125**, 4052–4053 (2003).

[28] Liu, W. Ideas of relativistic quantum chemistry. *Mol. Phys.* **108**, 1679–1706 (2010).

[29] Saue, T. Relativistic hamiltonians for chemistry: a primer. *ChemPhysChem* **12**, 3077–3094 (2011).

[30] Peng, D. & Reiher, M. Exact decoupling of the relativistic fock operator. *Theor. Chem. Acc.* **131**, 1081 (2012).

[31] Pipek, J. & Mezey, P. G. A fast intrinsic localization procedure applicable for abinitio and semiempirical linear combination of atomic orbital wave functions. *J. Chem. Phys.* **90**, 4916–4926 (1989).

[32] Sun, Q. *et al.* Pyscf: the python-based simulations of chemistry framework. *Wiley Interdiscip. Rev. Comput. Mol. Sci.* (2017).

[33] Chan, G. K.-L., Keselman, A., Nakatani, N., Li, Z. & White, S. R. Matrix product operators, matrix product states, and ab initio density matrix renormalization group algorithms. *J. Chem. Phys.* **145**, 014102 (2016).

[34] Li, Z. & Chan, G. K.-L. Spin-projected matrix product states: Versatile tool for strongly correlated systems. *J. Chem. Theory Comput.* **13**, 2681–2695 (2017).

[35] Sharma, S. & Chan, G. K.-L. Spin-adapted density matrix renormalization group algorithms for quantum chemistry. *J. Chem. Phys.* **136**, 124121 (2012).

[36] Chan, G. K.-L. & Head-Gordon, M. Highly correlated calculations with a polynomial cost algorithm: A study of the density matrix renormalization group. *J. Chem. Phys.* **116**, 4462–4476 (2002).

[37] Olivares-Amaya, R. *et al.* The ab-initio density matrix renormalization group in practice. *J. Chem. Phys.* **142**, 034102 (2015).

[38] White, S. R. Density matrix renormalization group algorithms with a single center site. *Phys. Rev. B* **72**, 180403 (2005).

[39] Rissler, J., Noack, R. M. & White, S. R. Measuring orbital interaction using quantum information theory. *Chem. Phys.* **323**, 519–531 (2006).

[40] Barcza, G., Legeza, Ö., Marti, K. H. & Reiher, M. Quantum-information analysis of electronic states of different molecular structures. *Phys. Rev. A* **83**, 012508 (2011).

[41] Kurashige, Y., Chan, G. K.-L. & Yanai, T. Entangled quantum electronic wavefunctions of the mn4cao5 cluster in photosystem ii. *Nat. Chem.* **5**, 660–666 (2013).

[42] Becke, A. D. Density-functional exchange-energy approximation with correct asymptotic behavior. *Phys. Rev. A* **38**, 3098 (1988).

[43] Perdew, J. P. Density-functional approximation for the correlation energy of the inhomogeneous electron gas. *Phys. Rev. B* **33**, 8822 (1986).

[44] Becke, A. D. Density-functional thermochemistry. iii. the role of exact exchange. *J. Chem. Phys.* **98**, 5648–5652 (1993).

[45] Lee, C., Yang, W. & Parr, R. G. Development of the colle-salvetti correlation-energy formula into a functional of the electron density. *Phys. Rev. B* **37**, 785 (1988).

[46] Stephens, P., Devlin, F., Chabalowski, C. & Frisch, M. J. Ab initio calculation of vibrational absorption and circular dichroism spectra using density functional force fields. *J. Phys. Chem.* **98**, 11623–11627 (1994).